STATIC SYNCHRONOUS GENERATOR WITH SLIDING DROOP CONTROL FOR DISTRIBUTED GENERATION IN MICROGRIDS

Bruno Wanderley França

Tese de Doutorado apresentada ao Programa de Pós-graduação em Engenharia Elétrica, COPPE, da Universidade Federal do Rio de Janeiro, como parte dos requisitos necessários à obtenção do título de Doutor em Engenharia Elétrica.

Orientador: Mauricio Aredes

Rio de Janeiro

Julho de 2016

STATIC SYNCHRONOUS GENERATOR WITH SLIDING DROOP CONTROL FOR DISTRIBUTED GENERATION IN MICROGRIDS

Bruno Wanderley França

TESE SUBMETIDA AO CORPO DOCENTE DO INSTITUTO ALBERTO LUIZ COIMBRA DE PÓS-GRADUAÇÃO E PESQUISA DE ENGENHARIA (COPPE) DA UNIVERSIDADE FEDERAL DO RIO DE JANEIRO COMO PARTE DOS REQUISITOS NECESSÁRIOS PARA A OBTENÇÃO DO GRAU DE DOUTOR EM CIÊNCIAS EM ENGENHARIA ELÉTRICA.

Examinada por:

_____

Prof. Mauricio Aredes, Dr.-Ing.

_____

Prof. Antônio Carlos Ferreira, Ph.D.

_____

Prof. Luís Guilherme Barbosa Rolim, Dr.-Ing.

_____

Prof. Walter Issamu Suemitsu, Dr. Ing.

_____

Prof. Vitor Hugo Ferreira, D.Sc.

_____

Prof. Luiz Antonio de Souza Ribeiro, D.Sc.

RIO DE JANEIRO, RJ - BRASIL

JULHO DE 2016

França, Bruno Wanderley

Static Synchronous Generator with Sliding Droop Control for Distributed Generation in Microgrids/ Bruno Wanderley França. – Rio de Janeiro: UFRJ/COPPE, 2016.

XIV, 110 p.: il.; 29,7 cm.

Orientador: Mauricio Aredes

Tese (doutorado) – UFRJ/ COPPE/ Programa de Engenharia Elétrica, 2016.

Referências Bibliográficas: p. 101-111.

1. Static Synchronous Generator. 2. Distributed Generation. 3. Microgrids. I. Aredes, Mauricio. II. Universidade Federal do Rio de Janeiro, COPPE, Programa de Engenharia Elétrica. III. Título.

Dedico este trabalho à minha amada avó, Noêmia Rabello da Costa.

“Os loucos abrem os caminhos que depois emprestam aos sensatos” Carlo Dossi.

AGRADECIMENTOS

À minha mãe Katia Wanderley da Costa, à minha tia Darci Rodrigues da Rosa e ao Maurício Aredes. Vocês são a base da minha formação e tenho gratidão eterna por tudo que fizeram por mim.

À minha família, em especial aos meus irmãos Tiago e Rodrigo, meu tio João Pimenta e meus primos Vinicius e Marcelo. Ao meu avô Carlos Wanderley (in memoriam) e à minha avó Noêmia (in memoriam), quem eu dedico esse trabalho. Que Deus esteja sempre com vocês.

Ao meu irmão de vida, Leonardo, minha comadre Marta e meu afilhado Leozinho.

À minha namorada Camille.

Aos meus amigos do Laboratório de Eletrônica de Potência e Média Tensão (LEMT), em especial ao André Ramos de Castro pela ajuda no desenvolvimento das simulações, ao Antônio Felipe da Cunha Aquino pela ajuda nas análises dos resultados e ao Chris P. Tostado pela ajuda na revisão do texto.

Ao meu amigo Bruno Laurindo e à minha amiga Fernanda.

Ao meu orientador na Universidade de Tsinghua, professor 柴建云 (Chai Jianyun), e ao professor 刘德华 (Dehua Liu) por possibilitarem minha pesquisa durante meu intercâmbio acadêmico. 非常感谢我在清华大学的指导老师柴建云教授的支持与帮助以及清华大学中国-巴西气候变化与能源技术创新研究中心主任, 刘德华先生, 提供给我在中国留学和研究的机会. Ao Ilan E. Cuperstein pela sua amizade e pela ajuda durante meu período de instalação e adaptação na Universidade de Tsinghua.

Ao meu amigo Igor, um irmão que conheci na China, e que compartilhou comigo momentos especiais da minha vida.

Aos membros da banca pelas contribuições em minha tese.

À Universidade Federal do Rio de Janeiro e ao Programa de Engenharia Elétrica da COPPE/UFRJ.

À Capes, CNPq e Faperj pelo apoio financeiro.

Resumo da Tese apresentada à COPPE/UFRJ como parte dos requisitos necessários para a obtenção do grau de Doutor em Ciências (D.Sc.)

GERADOR SÍNCRONO ESTÁTICO COM CONTROLE DE DESLIZAMENTO DA CURVA DE DROOP APLICADO NA GERAÇÃO DISTRIBUÍDA EM MICRORREDES

Bruno Wanderley França

Julho/2016

Orientador: Maurício Aredes

Programa: Engenharia Elétrica

Este trabalho propõe um controle de deslizamento das curvas de *droop* (curvas de variação de carga com a frequência e variação de potência reativa com a tensão) utilizadas em unidades de Geração Distribuída (unidades de GD) controladas como Geradores Síncronos Estáticos (*Static Synchronous Generator* – SSG). Nesse sentido, o controle de deslizamento das curvas de *droop* visa o posicionamento adequado dessas curvas sem descaracterizar seu funcionamento básico como máquina síncrona virtual. Sendo assim, os controles da frequência e da tensão são realizados em microrredes com GD sem a necessidade de dispor de um sistema de comunicação. No modo conectado, as unidades de GD despacham potência ativa para a rede e realizam regulação de tensão, enquanto que a frequência é predominantemente imposta pelas grandes unidades de geração presentes na rede. Em modo ilhado, as unidades de GD realizam o compartilhamento de potência ativa e reativa, além de garantir regulação de frequência e tensão. O compartilhamento de potência ativa entre unidades de GD é comprometido entre unidades de geração com potências nominais distintas quando o controle SSG clássico é utilizado com curvas de *droop* estáticas. Essa desvantagem é mitigada com o controle proposto.

Abstract of Thesis presented to COPPE/UFRJ as a partial fulfillment of the requirements for the degree of Doctor of Science (D.Sc.)

STATIC SYNCHRONOUS GENERATOR WITH SLIDING DROOP CONTROL FOR DISTRIBUTED GENERATION IN MICROGRIDS

Bruno Wanderley França

July/2016

Advisor: Maurício Aredes

Department: Electrical Engineering

This work proposes a control that slides the droop curves of Static Synchronous Generators (SSG). With this new feature, the SSG is able to perform additional functionalities without mischaracterizing the primary behavior as a virtual synchronous machine. Thus, adequate frequency and voltage control is achieved in a microgrid involving distributed generation (DG), without the need of a communication-system. In grid-connected microgrids, DG units mainly perform active-power supply and voltage regulation, whereas the system frequency is mainly imposed by the principal generation units (higher rotating kinetics) connected in the grid. Contrarily, in islanded microgrids, the DG units have to perform active-power sharing between all DG units, reactive-power sharing, as well as to ensure frequency control and voltage regulation. An accurate active-power sharing between DG units with different nominal powers is not possible if classic SSG controller and static droop curves are employed. This drawback is overcome with the proposed controller.

CONTENTS

LIST OF FIGURES

ABBREVIATIONS AND ACRONYMS

AC	Alternating Current
CHP	Combined Heat and Power
CPS	Centralized Power System
CSC	Current-Source Converter
CUPS	Custom Power Systems
DC	Direct Current
DG	Distributed Generation
DFIG	Doubly-fed induction generator
DPS	Distributed Power System
DSP	Digital Signal Processor
DR	Distributed Resource
EMF	Electromotive Force
EPS	Electric Power System
ESS	Energy Storage Systems
FACTS	Flexible Alternating Current Transmission Systems
GESS	Generation and Energy Storage Systems
HVAC	High Voltage Alternating Current
HVDC	High Voltage Direct Current
IBS	Intelligent Bypass Switch
IGBT	Insulated Gate Bipolar Transistor
LV	Low Voltage
PCC	point of common coupling
PI	Proportional-Integral
PLL	phase-locked loop
pu	per unit
PV	photovoltaic
R&D	Research and Development
SHVDC	Synchronverter High Voltage Direct Current
SIN	Brazilian National Grid (in Portuguese)
STATCOM	Static Synchronous Compensator
SG	Synchronous Generator

SSG	Static Synchronous Generator
SVC	Static VAR Compensator
THD	Total Harmonic Distortion
VSC	Voltage-Source Converter
VSM	Virtual Synchronous Machine
VISMA	Virtual Synchronous Machine
WAMS	Wide-Area Monitoring Systems

Chapter 1 – Background and motivation

This chapter presents the thesis overview. The motivation and main goals are also discussed.

Introduction

The global effects of the massive usage of carbon-based fuels are leading to trends of change in energy production and consumption profile, which are characterized by seeking clean alternatives of energy generation and by optimizing energy consumption efficiency [1]. The efforts to achieve the latter are focused on losses reduction with technological enhancement of the electrical products and public awareness to tackle energy waste.

The electric energy generation and consumption profile in the past decades has usually been composed of a few major power plants and large consumer centers, e.g. large urban centers and industrial parks. The literature refers to this configuration as a Centralized Power System (CPS). The transmission system is also an important component in this scenario, since the power plants and the consumption centers can be positioned far from each other.

In the modern power systems, the massive connection of renewable energy sources and other types of non-traditional electrical devices, such as those based on power electronics, are changing the traditional way of operating the power system. The renewables comprise both utility-scale power plants and residential or community-local generation. They are sited according to the geographic disposal of resources and are mainly characterized by an intermittent availability, which ranges from long-term intermittency, i.e. seasonal, to short-term intermittency.

In this way, the power system configuration is being modified with the growth of the distributed connection of energy sources into the conventional CPS. If the distributed generation (DG) becomes a significant portion of the total power delivered, the power system will be then featured as a Distributed Power System (DPS). However, this is not a simple profile change. In this scenario, the influence of each component on the whole system is increased and, consequently, the traditional infrastructure of control and protection of these components is not suitable for ensuring the system feasibility and reliability. As the penetration and relevance of DG grows higher, so does the demand for an improved technological infrastructure.

Recent standards and studies have promoted DG feasibility. Their main goal is to support the transition from CPS to DPS as well as to anticipate and overcome its challenges. The development of equipment connected in a DPS has to worry not only

about the features to which the equipment is intended to fulfill, but also about its operating impact on the Electric Power System (EPS), mainly regarding other equipment and subsystems connected at the vicinity.

The grid-connection of renewable sources is usually performed through power electronic converters as the front-end devices. These devices are suitable since they are controlled by microprocessors, providing operational flexibility. A desirable mode of controlling the front-end converter – usually composed of a Voltage-Source Converter (VSC) – is to emulate a Virtual Synchronous Machine (VSM), because with this control method, besides the power dispatch, it is capable of contributing to the system stability through the frequency and voltage regulation control.

The parallel connection of multiple VSC-based distributed generators is an important issue in a DPS. There are some restrictions when increasing the number of parallel units, such as undesired inner-loop currents, harmonic currents and the need of communication systems to perform power sharing between DGs [2]. The VSM emulation is a well-known control method for parallel-connected converters. Similar concepts nominate this control method as Synchronverter [3], Virtual Synchronous Machine (VISMA or VSM) [4] and Static Synchronous Generator (SSG) [5].

This control method has been distinguished as a convenient solution due to the typical usage of synchronous machines in the traditional generation systems. Therefore, renewables would be integrated into the existing power system in the same way as the traditional power plants [3]. This reduces the impact of DGs in the existing CPS or in future DPS, and avoids the necessity of a deep transformation in terms of the system operation and control. Moreover, the conventional infrastructure developed along the past years for the synchronous generators, e.g. power apparatus, auxiliary equipment and control techniques, can be applied to a power converter emulating virtual synchronous machine since it works harmoniously with the rotational, electromechanical, synchronous machines.

This work thoroughly investigates the effectiveness of the controller presented in the paper “Static synchronous generators for distributed generation and renewable energy” [5]. For sharing performance in islanded mode of operation of microgrids, it has been verified that a communication system has to be provided to ensure the active-power sharing of DG units with different setpoints. The role of this communication system is to properly adjust the slope and no-load parameters of the droop curves. Moreover, the

SSG performance in dynamic and steady-state conditions is compromised if conventional (static) droop curves are employed as in [5]. The inertia effect emulated by the SSG control is impaired in case of flat slope of the droop curve, which is adopted to achieve reduced frequency deviation in steady-state condition. Conversely, suitable slope of the droop curve, when adopted to ensure the inertia emulation, can lead to increase frequency deviation in steady-state.

The main contribution of this work is an enhanced structure of the controller presented in [5] that keeps the synchronous performance from the original structure and overcomes the aforementioned drawbacks.

Research goals and objectives

This work proposes a control structure for DG units operating continuously as SSG, in islanded or grid-connected microgrids. In order to guarantee the SSG performance, the controller presented in [5] is used as the basis of the new controller. With this new controller the DG units operate with suitable performance in dynamic and steady-state condition. The operation of such units is according to required functionalities established for both modes of operation (islanded and grid-connected). The functionalities are determined considering the present standards and trends for DG in DPS. However, the control structure has to allow future insertions or modifications of these functionalities since they will certainly be improved with the development of the DG in DPS.

Islanding detection and communication systems are not required to ensure the proper functioning of DG units, although the proposed controller is compatible with hierarchical inputs if provided. These features aim to obtain an enhanced controller for DG units in accordance with future trends in distributed power generation, communication systems, and supervisory technologies in DPS like Wide-Area Monitoring Systems (WAMS).

In summary, the following goals will be pursued:

- Study the future trends on the electric power system with distributed resources. In this sense, the rise of new grid architectures such as microgrids, new standards, and changes to the overall control of EPS are highlighted as a path of changing from a CPS to a DPS;

- Propose suitable functionalities to be applied in DG units, which would contribute to a flexible and feasible power grid with a wide range of emerging technologies and fast technological development profile. This includes power electronic devices, multi-directional power flow, power quality commitment, deep penetration of smart grid concepts, etc;
- Investigate the drawbacks of the controller presented in [5] that prevent the SSG from fulfilling the aforementioned functionalities. The main drawbacks are related to the sharing performance in islanded mode and the mismatch between inertia emulation and reduced frequency deviation in steady-state.
- Develop a controller that enables the SSG controller of [5] to overcome these drawbacks. Validate the new controller in relation to these drawbacks and also in relation to the proposed functionalities.

Outline of the thesis

After this chapter, in Chapter 2, the EPS is described with focus on the main characteristics that distinguish a CPS from a DPS. The DPS is discussed in the context of the rise of microgrids, the standards concerning the DG connection in present EPS (IEEE standards), and the hierarchical architectures proposed in recent studies addressing the growth of distributed resources in EPS.

In Chapter 3 the Static Synchronous Generator is studied. First, a model of the synchronous generator that satisfies the desired characteristics to be reproduced by the front-end devices of DG units is described. Next, the main controller of the Static Synchronous Generator is presented in detail, with the equations and control loop analysis, along with special functionalities that can be incorporated to such a controller.

Chapter 4 introduces the contributions of this thesis. The proposed functionalities; the drawbacks of the conventional (static) droop method; the proposed enhancement of the SSG controller, and; the sliding droop control is introduced through a comprehensive study of each topic.

The validations of the claims made in Chapter 4 are found in Chapter 5. In this chapter, analyses are performed through two approaches: simulation and experimental analysis. The simulation analysis investigates the SSG performance in stand-alone conditions and a microgrid scenario, and the experimental analysis is performed in an

experimental bench containing two DG units, which enables tests in islanded and grid-connected modes. Finally, Chapter 6 provides the conclusions and provides suggestions for future works.

List of publications

Some results of this work have been published previously in the following papers:

[6] B. W. França, A. R. de Castro, and M. Aredes, "Wind and photovoltaic power generation integrated to power grid through dc link and synchronverter," in *2015 IEEE 13th Brazilian Power Electronics Conference and 1st Southern Power Electronics Conference (COBEP/SPEC)*, Nov. 29 2015-Dec. 2 2015, pp. 1-6.

[7] E.L. van Emmerik, B.W. França, and M. Aredes, "A synchronverter to damp electromechanical oscillations in the Brazilian transmission grid," in *Industrial Electronics (ISIE), 2015 IEEE 24th International Symposium on*, 3-5 June 2015, pp. 221-226.

[8] EL van Emmerik et al., "Synchronverter to damp multiple electromechanical oscillations," in *Advances in Power and Energy Engineering*.: CRC Press, #mar# 2016, pp. 617-622--. [Online]. http://dx.doi.org/10.1201/b20131-102

There is a manuscript in reviewing process with the following title:

B. W. França, J. Chai, and M. Aredes, " Synchronverter with Sliding Droop Control for Distributed Generation in Microgrids," in *Power Electronics, IEEE Transactions on*.

Moreover, other papers with related topics were published by the author:

[9] B.W. Franca, L.F. da Silva, M.A. Aredes, and M. Aredes, "An Improved iUPQC Controller to Provide Additional Grid-Voltage Regulation as a STATCOM," *IEEE Transactions on Industrial Electronics*, vol. 62, no. 3, pp. 1345-1352, 2015.

[10] J.A.M. Neto, L. Lovisolo, B.W. Franca, and M. Aredes, "Robust positive-sequence detector algorithm," in *IECON '09. 35th Annual Conference of IEEE Industrial Electronics, 2009.*, 2009, pp. 788-793.

[11] Bruno W França et al., "Performance analysis and technical feasibility of an iUPQC in industrial grids," *Journal of Power and Energy Engineering*, vol.

2, no. 04, p. 500, 2014.

[12] Maynara A Aredes, Bruno W França, and Maurício Aredes, "Fuzzy adaptive P&O control for MPPT of a photovoltaic module," *Journal of Power and Energy Engineering*, vol. 2, no. 04, p. 120, 2014. [Online]. http://www.scirp.org/journal/PaperInformation.aspx?PaperID=44866

Chapter 2 - Electric Power systems with Distributed Resources

This chapter presents the main aspects of the electric power system and its future trends with the growth of distributed generation.

Centralized Power System (CPS)

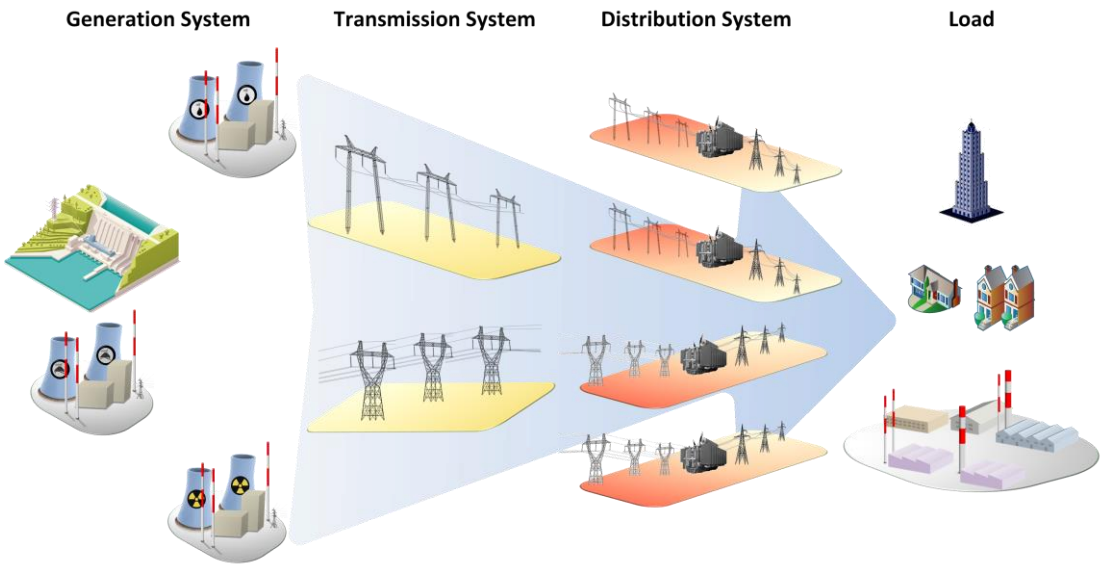

Fig. 1: Centralized Power System outlook.

The current configuration of the electric power systems is mostly characterized by a Centralized Power System, as depicted in the illustration of Fig. 1. This is based on a simple structure with unidirectional power flow, indicated by the blue arrow, from large power plants to the final customers, which are interconnected through transmission and distribution power systems. These components (generation, transmission and distribution) have specific roles in the electric power system (EPS). The electric power is predominantly generated by synchronous generators driven by steam or hydro turbines [13]. The transmission systems are responsible for the energy transportation through long distances and are characterized by high voltage transmission lines in both alternating current (HVAC) and direct current (HVDC). Finally, the distribution systems are usually characterized by a radial architecture and aim to deliver the power to the final customers (end-user).

Due to the flexibility of alternating current (ac) systems in comparison with the direct current (dc) systems, most power systems are purely composed of ac subsystems. Only in specific cases is the use of dc power system justified. For instance, an HVDC transmission system is more competitive in transmitting bulk power over long distances, in a point-to-point configuration (not a meshed grid).

The importance of each component on the EPS reliability and stability depends on the amount of power flow contained therein. The unidirectional power flow, along with

the grid embranchment, results in a power ramification from one component to the next along the network. As a result, failures in the generation and transmission components have significant impact on the final use of the energy, whereas a meshed distribution grid can be more selective in isolating a faulty area and thus avoiding its effect on other consumers in the vicinity.

Control and protection of the generation and transmission systems ensure the overall reliability. As an example, coordinated protection as applied in transmission systems is a selective procedure to isolate the faulty equipment that avoids the fault propagation to upstream components. However, this kind of protection is feasible due to the unidirectional configuration of CPS and may not be effective if the transmission system is within an environment that requires a bidirectional power flow.

The growth of the energy demand promotes the necessity of upgrading the EPS. In a CPS scenario, this is possible through grid expansion, e.g. with new power plants, transmission systems, distributed networks etc. Note that there is a connection between these components, since it is not possible to individually upgrade one of them without affectiong the possibility of overload condition in the others. In this way, a project for expanding a conventional EPS has to cover the viability, time and costs of all the components belonging to the network at which the power flow is understood. Thus, the CPS expansion is critically impacted by the complexity of its execution steps.

The advent of power electronic devices and renewable resources may reduce the complexity of the CPS expansion. Some of these devices aim to enhance the power capability of the grid by optimizing its usage, such as Flexible Alternating Current Transmission Systems (FACTS) that provides variable reactive power support and power flow control along the power corridors [14]. Other devices can provide complementary ways for the power generation, distribution and delivery by the addition and management of energy resources in different points of the grid [15], such as Energy Storage Systems (ESS) [16], [17], [18] and renewables such as wind powered and photovoltaic (PV) generators. There is also power quality equipment applied to distribution systems, well-known as Custom Power Systems (CUPS). However, the large-scale application of these elements, specially the renewables, may lead to a mischaracterization of the traditional CPS profile.

Distributed Power System (DPS)

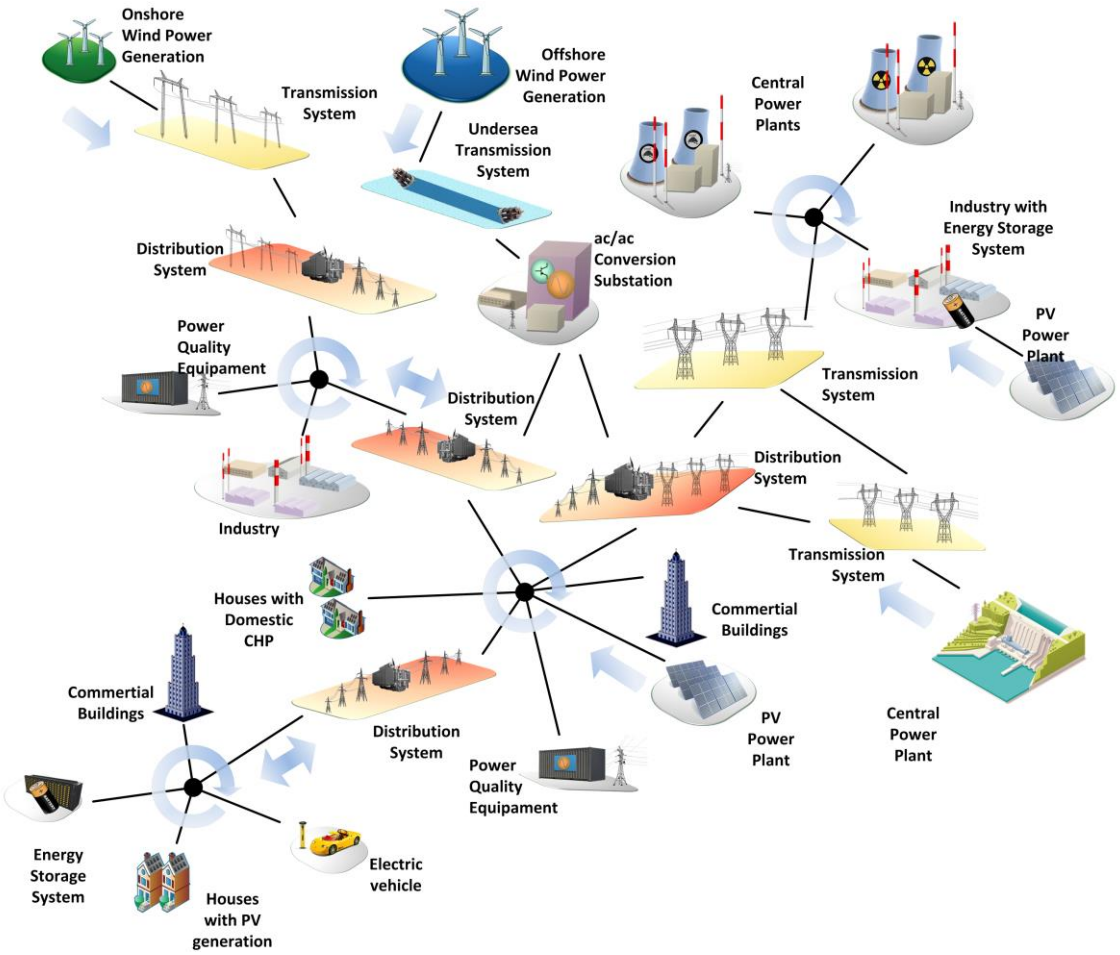

Fig. 2: Example of a Distributed Power System outlook.

The Distributed Power System is characterized by many generators spread into the grid in which each one generates a relatively small portion of the total power demanded by consumers. These generators are also classified as Distributed Generation (DG) and are a subset of a Distributed Resource (DR). Therefore, DRs or distributed energy resources (DERs) are defined in [19] as "*sources of electric power that are not directly connected to a bulk power transmission system*", which includes both generators and energy storage technologies.

At first sight, it is possible to realize that DGs increase the resource availability and the operational flexibility of the whole electric network. Moreover, the proximity of generation and consumption improves the power quality and the power reliability, while reducing the losses in the transmission system over long distances. However, despite the obvious benefits, other important aspects have to be highlighted. Indeed, a deep

transformation in the traditional EPS characteristics is necessary and it is boosted by DR growth and by the DPS establishment. The changes in infrastructure have to be evaluated. They are required for ensuring the proper operation of the system throughout its modernization.

In contrast to the CPS, it is hard to predict the overall power flow in a DPS due to its fast dynamic generation profile and the different possible pathways in which the power flow can be established. It is possible to realize in the example of Fig. 2, where the grid architecture is meshed differing from the traditional CPS (compare with Fig. 1). The consumer profile is also affected by the growth of local generation in sites where before there was a pattern of energy consumption. In this way, the power flow can be reversible, from the consumer area with DGs into the transmission system. Note that both traditional concepts of source and load can be applied to such a grid configuration, depending on the power availability and local demand.

Fig. 2 depicts an example of a DPS outlook. The arrangement of the grid components is clearly different from that configuration presented in a CPS. There are still some elements in this system that do not exist in traditional EPS, such as the energy storage systems, power quality equipment, etc. It is important to integrate, harmonize and control these elements to ensure the system reliability. The roles of each one have to be properly defined and the control structure must drive forward the operating compatibility between the individual and the hierarchical controls. This may result in smart interfaces between the controllers of distinct levels of the EPS with additional control loops and synchronization procedures. In other words, as the EPSs are being modified from traditional CPS to modern DPS, the philosophy of the control system has to follow from centralized to distributed approach, with the active participation of several grid components.

Microgrids

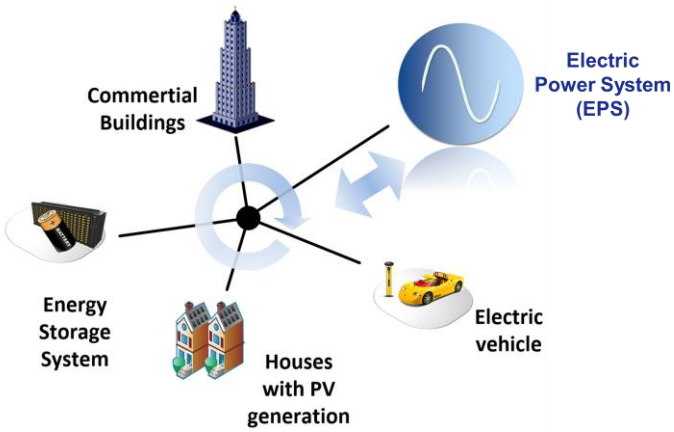

Fig. 3: Example of a microgrid.

The concept of microgrid is a promising solution to the challenge of DPS viability [20]. Indeed, the appearance of microgrids can be seen as a transition stage from the currently CPS dominated approach to the DPS approach. An example of this system is illustrated in Fig. 3. It is basically a subsystem composed of a limited quantity of distributed resources, loads and other types of power conditioners. Moreover, it is a local network that provides operational benefits due to a customizable level of independence from the main grid. In a microgrid, critical disturbances such as those related to frequency and voltage regulation, and also power quality issues as harmonics, have to be solved inside the microgrid and thus, avoiding its propagation into the main grid.

Microgrids have two possible modes of operation: the grid-connected mode where the microgrid is connected to the grid; and the islanded mode where the microgrid should operate isolated from the grid, in a standalone type of operation. The grid-connected mode enables the bidirectional power flow between the microgrid and the grid, as illustrated by the bidirectional blue arrow in Fig. 3. The complete microgrid can be represented as a "single component" of the grid. The islanded mode is suitable for the microgrid reliability since this mode enables the microgrid to operate stably without being affected by disturbances in the grid. The power flow inside the microgrid is represented by the circular arrow in Fig. 3. This power flow exists when there are power resources feeding local loads internally in the microgrid. It is important to highlight that in islanded mode the available resources provided by the DRs must be enough to power the loads and ensure frequency and voltage control inside the isolated microgrid. If all

the loads cannot be fed, the major controller of the microgrid has to shut down ordinary loads in order to ensure the power balance and to continue supplying critical loads.

The microgrid concept is defined by many institutions around the world and it is presented in established works, such as [21], [22], [23] and [24]. Some common concepts are summarized in the following notes.

The U.S. Department of Energy briefly defines microgrids as: *"localized grids that can disconnect from the traditional grid to operate autonomously and help mitigate grid disturbances to strengthen grid resilience"* [25].

Another example is the well-known white paper published by the Consortium for Electric Reliability Technology Solutions (CERTS) [23]. In this approach the microgrid is emphasized as a power and heat provider. Moreover, it is highlighted that the majority of the microsources are power electronics based devices. According to the document, the microgrid is as a single aggregated system, and the islanded mode of operation has to be ensured even if problems arise in the main power grid. After problems are solved, the microgrid must be reconnected. It is also important to achieve smooth transition between modes of operation to ensure the proper functioning of the entire system. A distinct point established in the CERTS approach is the employment of combined heat and power (CHP) technology as part of the microgrid concerns. In this sense, the microgrid has to allow the usage of the wasted heat from the power generation process for optimizing the overall efficiency of the resources.

The EU funded project "MICROGRIDS – Large Scale Integration of Micro-Generation to Low Voltage Grids" originated the European microgrid concept, which defines microgrids *"as an LV distribution system to which small modular systems are to be connected"* [20]. According to this concept, the microgrid is defined as a low voltage (LV) system with physical proximity between the power generation and consumption. It is connected at the EPS through a MV/LV substation, but can be operated in islanded mode. The achievement of suitable operation in islanding mode is not a simple task and involves R&D investments. These investments are justified by the microgrids' benefits, such as ensuring power reliability of critical loads, reducing the power demand in peak times, providing alternatives on the electricity commodity market, etc.

Another distinguishing aspect of the microgrids is the return of the dc system approach. As most DRs use power electronic converters as a front-end device, many studies have evaluated the feasibility of microgrid implementation through dc network

[26], [27], and [28]. Moreover, PV power generation is currently one of the most promising renewable generation system, and then, as its generation is in dc, the implementation of a dc microgrid can be cost-effective in case of high penetration of PV on it. Other examples of technologies with the same profile are fuel cells and energy storage systems (ESS), which currently are not as developed as the PV technology, but will stimulate further developments in dc microgrids.

The dc microgrids have some technical advantages when compared with ac microgrids such as the absence of reactive power, fewer problems with harmonics, unbalanced voltages and currents, and is easier to synchronize them. The studies of dc microgrids are related to the following subjects.

- Stability analysis [26];
- Renewable integration, dispatch control and load sharing [28];
- Generation and storage management [29], [30];
- Protection system [31], [32], [33];
- Controllers of dc-dc power electronic converters [34].

However, motors as well as loads with different voltage levels would require special power electronic converters to be used in dc microgrids, which can raise the costs of a microgrid implementation. On the other hand, the advent of microgrids in the actual context leads to implementation of them in ac power grids and, therefore, the infrastructure of these networks are suitable to be utilized by or to become ac microgrids. Maturated protection devices technology for ac systems exists, but further developments have to be carried out to comply with dc systems.

A more complex approach is the hybrid microgrids [35], [36], [37], [38], [39], and [40]. This approach can be seen as a solution to conveniently integrate ac and dc systems and to achieve the best cost-effective microgrid scenario. The arrangement of these systems depends on their sources (in ac and/or dc), their loads (in ac and/or dc), and their buses (in ac and/or dc). The interconnection between ac and dc elements is performed through interface power converters, which can provide unidirectional or bidirectional power flow according to the operational demand of the interconnected subsystems.

Some documents in the current literature provide actual examples of microgrid implementation for ac, dc and hybrid microgrids [2], [35], [41], and [42].

IEEE Standards for interconnecting DR with EPSs (IEEE Std 1547 series)

The IEEE 1547 is a series of standards for interconnecting DRs with EPSs. Presently, the active versions are the listed in Table I.

TABLE I
IEEE 1547 ACTIVE VERSIONS

Standard	Publication Year
IEEE Standard for Interconnecting Distributed Resources with Electric Power Systems [19]	2003
IEEE Standard for Interconnecting Distributed Resources with Electric Power Systems - Amendment 1 [43]	2014
IEEE Standard Conformance Test Procedures for Equipment Interconnecting Distributed Resources With Electric Power Systems [44]	2005
IEEE Application Guide for IEEE Std 1547, IEEE Standard for Interconnecting Distributed Resources with Electric Power Systems [45]	2008
IEEE Guide for Monitoring, Information Exchange, and Control of Distributed Resources Interconnected With Electric Power Systems [46]	2007
IEEE Guide for Design, Operation, and Integration of Distributed Resource Island Systems with Electric Power Systems [47]	2011
IEEE Recommended Practice for Interconnecting Distributed Resources with Electric Power Systems Distribution Secondary Networks [48]	2011
IEEE Guide for Conducting Distribution Impact Studies for Distributed Resource Interconnection [49]	2013

These standards consider the interconnection of DRs in an area EPS at primary or secondary distribution voltages through a single point of common coupling (PCC). They include the interconnection of a single DR unit in an area EPS, as well as the interconnection of local EPS with multiple DR units in an area EPS. The standards address limited aggregated capacity of a DR installation up to 10 MVA. Hence, microgrids that fit in the context aforementioned may be backed in the IEEE 1547.

Synchronous machines, induction machines and static power converters are the DR generators treated as power conversion technologies and, consequently, these are the front-end devices of the generation systems. The synchronous machines are suitable for power supplying during EPS outage and their power factor are easily controlled. The

same is not true for induction machines. There is a derivation of the latter, known as doubly-fed induction generator (DFIG) that is able to control the reactive power through the use of power electronic converters to drive the rotor field current, which can also provide some support for frequency stability by allowing variable speed generation.

Some aspects related to the electric parameters and the system conditions for proper connecting DR units in an area EPS are summarized below:

- **Voltage regulation**

In the first version of the standard, DR units were forbidden to perform voltage regulation at the PCC. In case of allowing DR voltage regulation by an EPS operator, it was not according to [19]. If the voltage regulation is performed simultaneously by DR units and grid voltage regulators, a conflict between controllers can provoke undesirable inner current circulation, although multiple voltage regulators can be coordinated in a same area EPS. By setting adequate time responses in the controllers, overvoltages can be avoided and reasonable active and reactive power dispatches in DR units can be achieved.

The operational benefits of providing voltage regulation, active and reactive power control by DRs are evident. If well-coordinated, those benefits improve the system reliability, robustness and power quality. The prohibition of active participation of the DR in the voltage regulation has been revoked in [43] to consent with the coordinated operation of the area EPS and DR operators. The allowable range of an Area EPS service-voltage is defined by Range A of [50] that is shown in Table II. The DR shall not cause this voltage to go outside the allowable range.

TABLE II
VOLTAGE RANGE A: ANSI C84.1 – 2011 [50]

Range A	Minimum voltage (pu)	Maximum voltage (pu)
$120 - 600\ V$ Systems	0.95	1.05
Above $600\ V$ and less than $46\ kV$ Systems	0.98	1.05

In fact, several situations involving a non-coordinated DR operation may lead to voltage deviations in unacceptable levels. These situations are caused by changing the active and reactive power profile. The active power delivered by DRs can increase the voltage level in the vicinity of the PCC due to a reduction of the current flowing from

the utility to the loads, and thus reducing the voltage drop in the feeder of the power utility. The reactive power drained or injected by DRs has the same effect as that of a Static Synchronous Compensator (STATCOM), where reactive power supply (capacitive) results in voltage rise and reactive power drain (inductive) results in voltage drop.

Along with the allowable range of an Area EPS service-voltage, the operating voltage of DR devices is limited in a range from 0.88 to 1.10 pu of the nominal voltage. In the case of voltages outside of the ANSI limits (Table II) but within the operating voltage range, the DR control has to work towards restoring the voltage within ANSI limits or it may be disconnected. DR de-energizing in response to abnormal voltages is required within the clearing times presented in Fig. 4. The clearing times in this figure are according to the amendment [43] that includes the default settings and the adjustable setting limits through mutual agreement between the EPS and DR operators. The base voltages are the nominal system voltages stated in [50].

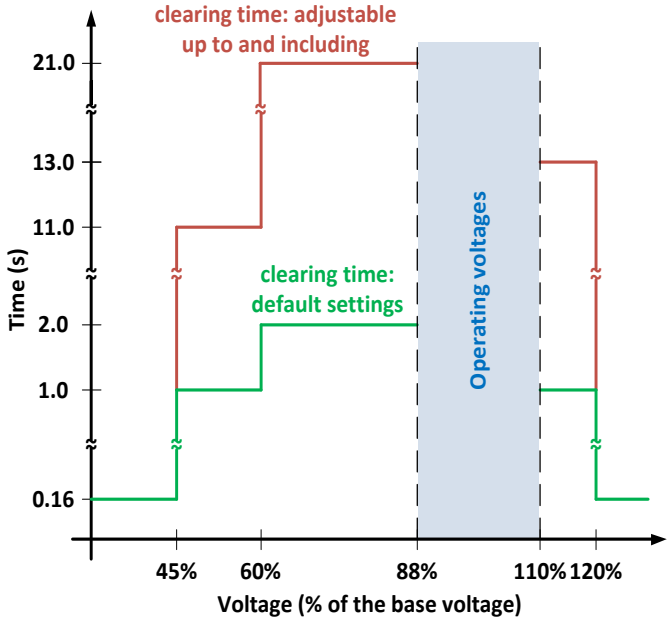

Fig. 4: Interconnection system default response to abnormal voltages [43].

- **Synchronization**

The DR synchronization has to comply with the limits of voltage fluctuation (±5% of the prevailing voltage level) and achieve reduced flicker disturbance. Furthermore, test procedures are necessary to ensure the interconnection of the systems only if the frequencies, voltages, and phase angles are within the allowable limits. The limits are established to three different ranges, in kVA, (0 - 500, 500 - 1500, and 1500 - 10000).

For instance, for the lowest power range, up to 500 kVA, the maximum differences that are allowable during synchronization are: $\Delta f = 0.3\,Hz$, $\Delta V = 10\%$ and $\Delta\phi = 20°$.

Similarly to the previous criteria for voltage regulation, DR shall cease to energize an area EPS in case of critical frequency deviations, which must shut down with settled clearing time. The clearing times in Fig. 5 are according to the default settings in amendment [43], but adjustable clearing times are also permitted under mutual agreement between the EPS and DR operators. These adjustable clearing times can reach increased values up to 300 seconds.

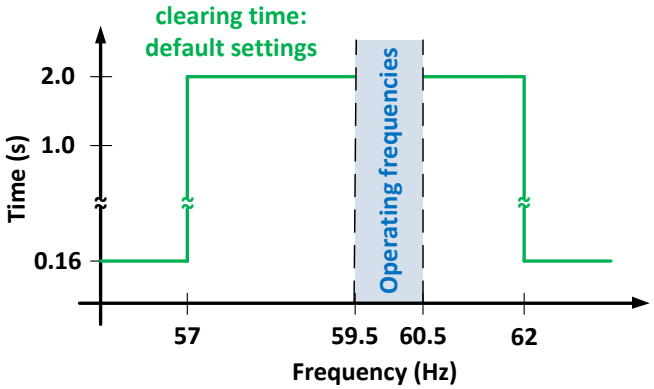

Fig. 5: Interconnection system default response to abnormal frequencies [43].

- **General aspects**

It is important to highlight that other issues, such as installation, protection, and monitoring, have to be regarded for achieving suitable operation of DR. These aspects are presented in [19] over the general requirements, covered in the subjects: Integration with Area EPS grounding, Monitoring provisions, Isolation device, Protection from electromagnetic interference, Surge withstand performance, and Paralleling devices. Further explanations about these aspects are well discussed in [45]. Moreover, standards related to DR concerns may change along with the progress of the knowledge and technology of the area, which are encouraged by the growing penetration of DR in the electric systems.

The IEEE 1547 standard does not allow DR units to remain operational under islanding mode, fault condition, and area EPS reconnection. Clearly, this restriction is in contrast to the trends in microgrid approaches. However, it is understood here as a provisory, but necessary, approach to enable the DR penetration in the area EPS, which is still characterized by a CPS configuration. In a well-established DPS, the protection devices and the hierarchical controllers may carry out the system reliability even under

occurrences of major grid outages, preventing harmful conditions and managing the whole system to become operational and capable to be restored. This includes the DR operation towards the system reliability in abnormal scenarios.

Hierarchical controllers applied to DPS and microgrids

The increasing portion of DR affects several aspects of power systems, such as its power management, protection and controllability (i.e. frequency control and voltage regulation). In terms of the physical structure, depending on the type, amount and placement of these resources in a distribution-network facility, the power capacity of this network may not be able to withstand the upgrowth of the power flow and its effect on a multidirectional pattern. Therefore, enforcements in transmission and/or distribution power lines and the usage of FACTS and/or power quality devices may be needed.

Hierarchical control architecture is a convenient approach to contribute to the increasing penetration of DRs in power systems [2], [27], [28], [35], [42], [51], [52], [53], [54], [55], [56], and [57]. The main purpose is to provide a systematic and consistent structure that controls the power system in an orderly manner, regarding all spheres of concerns. In other words, hierarchical control architecture is being considered in DPS and microgrid scenarios to coordinate each active grid component, ensuring the overall reliability of the system.

Different approaches of hierarchical controllers can be found in the literature. The differences are related to the management architecture (centralized or decentralized), the microgrid system (ac, dc, or hybrid), and the strategies adopted in general. The latter can be understood as control strategies that will compose each hierarchal level to ensure power management, coordination of elements, regulation (voltage and frequency), protection etc. Some specific concerns of these structures will be detailed through different approaches highlighted here.

First, in [28] a general hierarchical architecture was proposed for ac and dc microgrids. It was based on the traditional dispatch controllers that are present in CPS, which have been extensively used to perform power dispatching in ac power systems, and the international standard ANSI/ISA-95. Therefore, this approach is similar to most other approaches, and the general structure permits the implementation of different control strategies. The general hierarchical structure is composed of primary, secondary and tertiary control levels.

The primary control level is local and mainly responsible for ensuring power sharing between DR units. ESS must be regarded in this context, and a special controller should be available according to the state of charge (SoC) of the storage elements. The control methods employed to perform power sharing can be categorized according to the usage (or absense) of a communication system [58]. Some advantages and disadvantages of implementing a hierarchical control system with or without a communication system are listed in Table III and Table IV, respectively. Master-slave [59], [60], average load sharing [61] and circular chain control [62], [63] are examples of such control methods based on communication systems.

CERTS [23] is in compliance with the non-use of a communication system to ensure the basic operation of microsources in microgrids [42], which constitutes the principle of "plug-and-play" functionality. In this context, the "plug-and-play" functionality is featured by the ability of inserting a new microsource in a microgrid without the need of changing any parameter or configuration of other units already in operation. The droop control is the control method capable of covering "plug-and-play" functionality, and for this reason it has been claimed as the controller employed at the primary control level. It is mirrored on the behavior of synchronous machines and will be deeply discussed in the next chapters. It is important to emphasize that control methods with communication systems are able to simultaneously perform power sharing and voltage/frequency regulation. Therefore, these controllers do not fit the architecture addressed in [28] and only the droop control is considered there.

TABLE III
ADVANTAGES AND DISADVANTAGES OF POWER SHARING CONTROL METHODS BASED ON COMMUNICATION SYSTEM

Advantages
✓ Provides accurate power sharing and voltage/frequency regulation
✓ The controller is easier to be implemented
Disadvantages
× DG unit operation is in an non-autonomous pattern
× Increased cost and complexity
× Reduced reliability and robustness
× High overcurrent during startup (Master of MS control)

TABLE IV
ADVANTAGES AND DISADVANTAGES OF POWER SHARING CONTROL METHODS NOT-BASED ON COMMUNICATION SYSTEM

Advantages
✓ Plug-and-play functionality ✓ Improved reliability and robustness ✓ Well-known behavior from conventional Power Systems
Disadvantages
× Must deal with some frequency/voltage deviation as a mean of "communication link" to perform power sharing × Reactive power sharing is not ensured between DG units located far from each other

Another drawback addressed on the primary control level is the grid-forming ability [64]. This is particularly relevant in case of islanded mode of operation. Depending on the implemented PWM control strategy, a power-electronics converter can be controlled to behave as a controlled voltage source or as a controlled current source. On the other hand, the power converter can be characterized as Voltage-Source Converter (VSC) if it contains a dc-voltage source, or as Current-Source Converter (CSC) if it contains a dc-current source.

Current PWM control is typically applied in DGs as mean of ensuring power reference tracking. The dynamic performance of power tracking is better if current PWM control is implemented. Usually, it uses a phase-locked-loop (PLL) to synchronize the power electronic converter with the grid and a current reference is generated from the desired power injection. However, during islanded mode of operation this type of controller cannot sustain the microgrid at a stable frequency and voltage point of operation.

Voltage PWM control is more suitable for DGs in microgrid application in several aspects. A key point is its capability to provide virtual inertia, ride-through capability and power-quality enhancement to DPS and microgrids. Hence, this work will consider the voltage PWM control to implement the concept of primary control (droop control) in a power converter emulating a virtual synchronous machine.

Some works define the behavior of a power converter as an exchangeable, controlled current source and controlled voltage source, according to the microgrid mode of operation, that is, a DG unit has to operate as a "current source" during grid-

connected mode of operation, whereas it has to operate as a "voltage source" during islanded mode of operation. Unfortunately, this exchangeable controller needs an auxiliary state-machine control method to detect the transitions between islanding and grid-connected modes [65], and [66]. Islanding detection can be easily implemented if a communication channel exists. If there is no communication, a kind of local detection method has to be implemented. The former has the same drawbacks of a non-autonomous pattern and increased costs and complexity, similarly as mentioned for the case of power sharing control methods based on a communication system (Table III).

The communication link has to be fast to ensure the dynamic of changing from voltage- to current-control methods. The need of an islanding detector itself has many issues. Islanding detectors can be subdivided into two groups, the passive- and the active-local methods. The passive-local method uses local measurements at the PCC, whereas the active-local method is based on the injection of noise signals into the power system and the analysis of system response. The main drawback of the passive method is the failure to detect islanding in some specific conditions, e.g. if the microgrid generation and consumption are quite equivalent. On the other hand, the active method has questionable usage as the idea of inserting a disturbance into the grid can cause a power quality problem if the growth of DG becomes more and more significant.

This work is in compliance with the idea of using a unique, current controller or voltage controller for each DG unit as a means of avoiding the need of fast and precise islanding detection to ensure the power system reliability. Clearly, in this case the major installed power of DG units in a microgrid has to behave as a controlled voltage source to sustain frequency and voltage stability during the islanding mode of operation. The problem of determining the portions of installed current and voltage behaving DG units is itself a hard task, which is outside the scope of this work.

The secondary control level of the hierarchical control system aims to coordinate DG units in order to reach frequency and voltage restoration, as well as to perform synchronization of the microgrid during transitions from islanded to grid-connected mode. Consequently, it has been featured with a certain dependency on a data communication system between units (decentralized control) [67] or between units and a centralized microgrid controller [68].

An example of a centralized overview is shown in Fig. 6. In this scheme, the voltage is measured at the microgrid bus and the signals of voltage amplitude (V_{MG}) and

frequency (ω_{MG}) are obtained through a positive-sequence detector and transmitted to the secondary control via low-bandwidth communication link. These signals are compared with references, which can be provided by the tertiary control (ω_{ref}, V_{ref}) or be stated as constants (ω_{ref}, V_{ref}), to feed PI controllers. If the microgrid is operating in grid-connected mode, the reference is provided by the tertiary control according to the desired power exchange between the grid and the microgrid. Otherwise, the references are the nominal values of the islanded microgrid that are constants. The outputs are the frequency and voltage deviations $\delta\omega$ and δV. Note that the frequency deviation can be added with a synchronization deviation signal ($\Delta\omega_{sync}$) for synchronization procedures during transition from islanded to grid-connected mode. By receiving theses deviations, the primary control of each DG is able to contribute harmoniously to the frequency and voltage restoration.

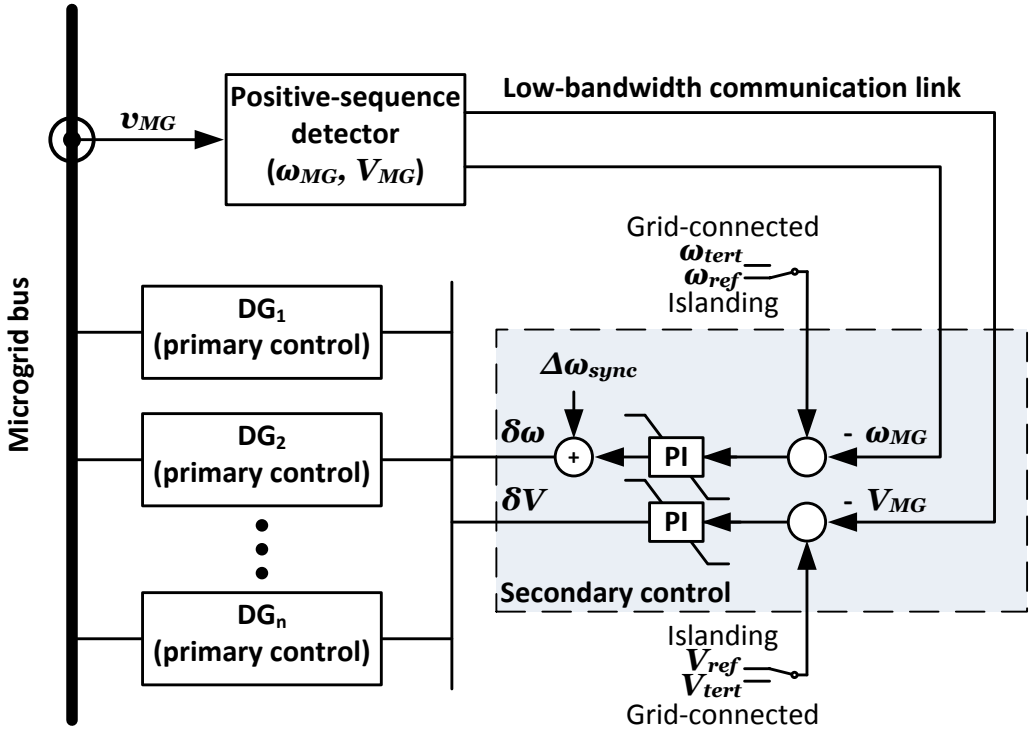

Fig. 6: Example of secondary control level, adapted from [28].

In practice, the secondary control level is always acting on the system, and the voltage and frequency are always varying around the reference values due to the dynamics of loads and connected generators. This oscillation is more significant if a high number of intermittent sources, like PV and wind power, exist. Recent studies have been done to evaluate the impact of these resources not only on the performance of the secondary control, but also in specific security issues such as the coordination of

frequency threshold to disconnect each type of DG under loss of load or generation as a mean of avoiding the system collapse [69]. Sometimes these studies lead to retrofit programs in the existing DG units.

An interesting approach of decentralized hierarchical control is introduced in [52], where an Energy Management System (EMS) is proposed with the elements of the EPS treated as family members. This kind of architecture is seen as a promising strategy to be applied in scenarios with deep penetration of intermittent renewables, as wind generation, and stochastic ESSs, such as electric vehicles, which are important elements in the current EPS of China. EMS Family architecture is decentralized and provide partial-autonomous and partial-interactive/coordinated patterns for each EMS family member. The elements of the grid are treated as EMS family members in order to establish theirs roles in the EPS, and to ensure intelligence everywhere. In other words, for each family member (or element of the EPS), the individual responsibilities (autonomous operational functions) and the common responsibilities (common operational functions) are defined. The family architecture is organized with the definition of the hierarchy for the common responsibilities and the interconnection of these members (organizational network provision).

The tertiary control level concerns the economic aspects used to determine the power dispatch [28]. Fig. 7 depicts an example of this control structure together with the synchronization control loop. The reference of the optimum dispatch is provided to the controller as the active and reactive power references (P_{ref} and Q_{ref}). These references are compared with the active and reactive power flow between the grid and the microgrid, and therefore PI controllers provide the tertiary frequency and voltage references to be used to feed the secondary control level (see Fig. 6). The synchronization control loop looks to the grid and microgrid voltages to keep them synchronized and ready to be reconnected, that is, to allow the transition between islanding to grid-connected mode, acting continuously in the deviation signal, $\Delta\omega_{sync}$, as suggested in Fig. 5. The control structure of this part is similar to a PLL controller [14].

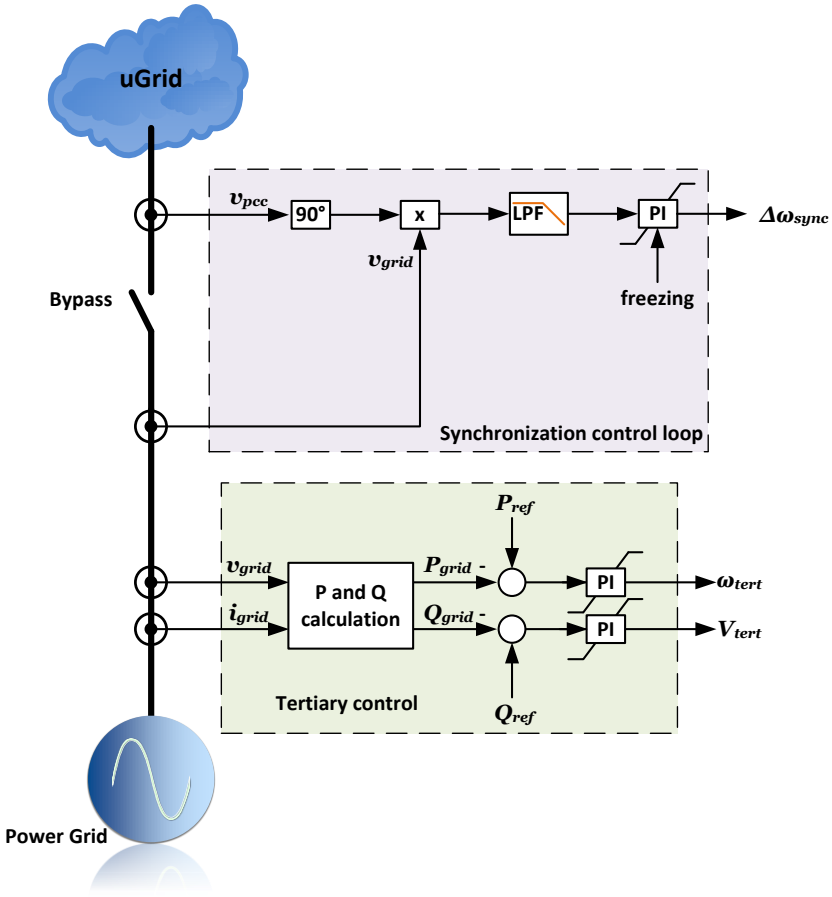

Fig. 7: Example of tertiary control level and synchronization control loop, adapted from [28].

Chapter 3 - Static Synchronous Generator (SSG)

In this chapter the SSG is explained through the model of synchronous machines, the presentation of the SSG control structure and some additional functionalities that can be explored.

The idea of controlling a power electronic converter as a virtual synchronous generator was introduced in contemporaneous papers such as [4], [70] and [5]. The main purpose of such control method is to provide a solution for the negative impacts caused by the deep penetration of power electronic devices into the power grid. The grid changes provoked by these devices have major impact on the system's safety, stability, and power quality, by strongly affecting electric parameters such as frequency and voltage. Moreover, the converter operation as a virtual synchronous machine is a convenient control method that allows it to actively contribute to the system's resilience. A patent application with the subject *"Control of a Voltage Source Converter using Synchronous Machine Emulation"* was filed in 2008 [71] and another with the subject "Static Synchronous Generators" was filed in 2009 [72].

In [4], the Virtual Synchronous Machine (VISMA or VSM) was proposed as a solution approach for embedding the behavior of a synchronous machine along with the advantages of using a Voltage-Source Converter as the power circuit. The basic concept of VSM considers a primary source and/or a storage system at the dc side of the power converter, as illustrated in Fig. 8. As a result, the VSM could be employed as a "motor" or a "generator", with a full four-quadrant range of operation.

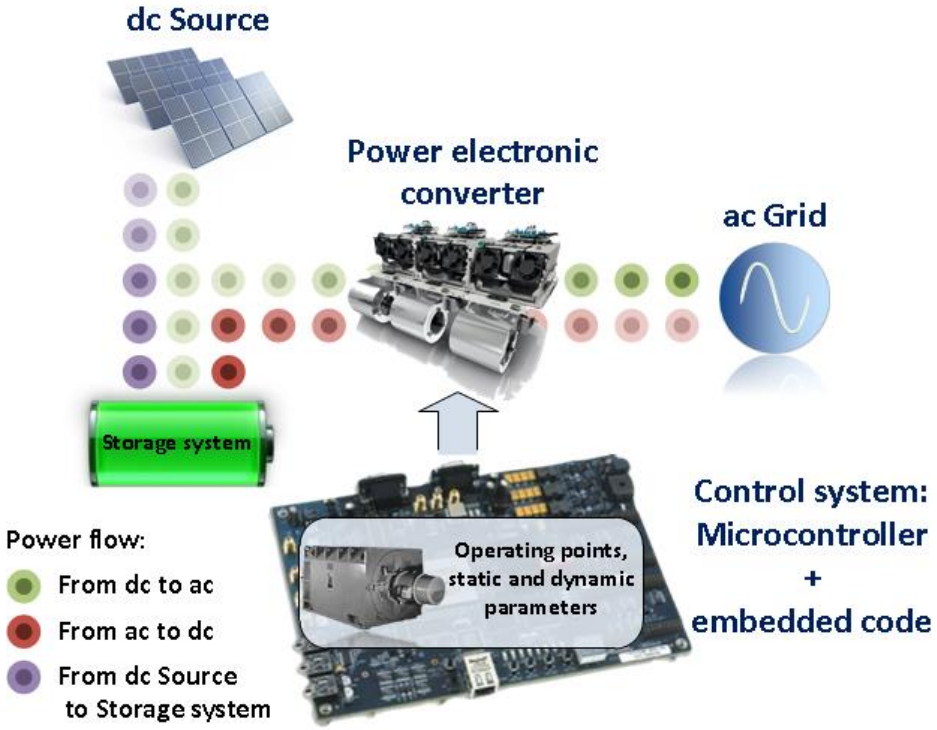

Fig. 8: Basic concept of the Virtual Synchronous Machine.

The electromagnetic and mechanical parameters of a synchronous machine are used to model and to mimic its dynamic and static properties in real time. Since they are parameters inside the VSM digital controller they can change or be adaptive along the VSM operation to achieve enhanced performance. This concept introduces a novel perspective on power-electronics devices controlled as virtual synchronous generators, since the opportunity of varying in real time the machine parameters ensures an enhanced performance that could not be accomplished by actual rotating machines with fixed parameters given inherently in the constructive design of the machine.

The equipment referred to as a Static Synchronous Generator (SSG) was pointed out in [5] as a promising control method that enables a deep penetration of renewables into the grid. This statement is based on the intuitive assumption that the power converter should be used as the front-end device of renewables and be operated as a "conventional" synchronous machine, performing the power delivery of a renewable resource in the same way as conventional power generators. In this work, the SSG controller is developed through the theoretical analysis and modeling of the synchronous machines. Many other studies were developed based on this main structure as in [73], [74], [75] and [76]. The same authors renamed this equipment to Synchronverter in [3] and kept this nomenclature thereafter.

The aforementioned control methods are different from conventional controllers of power-electronics converters in grid-connected mode of operation. Up to now, in this mode of operation, power converters have been employed with conventional controllers, which force them to behave as controlled current sources, that is, they simply behave as "grid followers", without contributing to the frequency and voltage stability of the entire power system. In this way, the priority is to achieve accurate performance in injecting the desired active- and reactive power into the grid [77], [78]. A phase-locked loop (PLL) controller or similar method is used to track the system frequency and phase angle of the voltage at the PCC. These parameters are important to ensure that the injected currents are properly synthesized according to the desired active- and reactive power references (power orders). Hence, this traditional way for controlling power converters leads to a "grid-follower" device, without any active contribution to the power frequency control and voltage stability of the whole power system.

The proper operation of conventional controllers relies on the voltage compliance at the PCC. In case of frequency disturbance, phase shifting, or even in power outage, the

PLL may lose accuracy and the power injection will be compromised. Furthermore, if the power grid does not have reasonable strength, the transitory response of the converter can lead to increasing the system perturbation and then collapsing the system. Contrarily to conventional controllers used for the front-end converters, the SSG controller does not need a PLL circuit to track the power frequency and phase angle, since the virtual synchronous machine control method itself constitutes a kind of PLL with several advantages and flexibilities, as introduced in [79].

The frequency- and voltage-drooping mechanisms provide synchronous machines with a natural stable condition for the parallelism with other synchronous machines in large power systems [80], [81]. The parallelism of several large synchronous machines in a power system makes it a stiff system in terms of power frequency, which can be seen as an "infinite bus" with constant frequency and voltage at a point of coupling of a microgrid. In this case, the active and reactive power injected by a relatively small generator or a microgrid is easily controlled through a proper positioning of the droop curves, which are varied respectively by the governor set point of the (virtual) turbine and the field current of the (virtual) machine excitation apparatus. In case of parallelism between two or a limited number of generators, the droop curves of each generator plus the whole amount of loads dictate the power sharing and the resultant frequency and voltage values.

The dynamic response of synchronous generators is naturally stable under grid-connection and transient conditions. During the grid-connection of a synchronous generator, the difference between the frequencies of the grid and the generator results in opening the torque angle just after closing the circuit-breaker. The consequent induced torque acts in opposite direction of the angle opening. As a result, the generator speed varies in the sense of achieving the synchronous speed and the torque angle reaches a stable point of operation.

The transient stability is directly related to the inertial energy stored in the rotating mass of the machine rotor. Generators with high inertia are desirable as they contribute to increase the margin of stability. Contrarily, the increasing number of renewables connected to the power system tends to weaken the grid inertia, since most of renewables employ "grid-follower" controllers to the power converters as the front-end interface. In other words, the high penetration of grid-follower generation makes invalid the traditional assumption that the grid inertia of an EPS is sufficiently high enough to

guarantee the system control and stability [82], [83]. If the converter is controlled as an SSG, virtual rotational inertia is provided in the same sense as a real rotational machine, contributing to the increase of the equivalent grid inertia. This concept can also be applied to implement control strategies to energy storage or load shedding systems.

EPS with reduced inertia is sensitive to fast variation of active power, which is a usual peculiarity of intermittent renewables such as solar and wind power generations. The major impact lies on the frequency deviation, which is also sensitive to failures and power outages. The clearing time (see Fig. 5) is the period that the power system has to recover from a frequency disturbance. The protection system has to shut down loads or generators if the reaction time is not sufficient to restore the system frequency within the operating limits before the clearing time has elapsed [84]. Hence, the grid stability can be evaluated for a given disturbance according to its reaction time and clearing time. The grid can be considered stable if the reaction time is lower than the clearing time.

Synchronous Generator Model

Synchronous generator models can be widely found in the literature, as in [80], [85] and [86]. The degree of detail depends on the purpose of modeling and here some simplifications are assumed. The goal in this model is to identify the principal characteristics of the synchronous generators and their influences on the electric system. This includes electrical and mechanical parts. The characteristics will be then employed in the controller of the Static Synchronous Generators. This assumption leads to studies of the synchronous generators in EPS as found in [85] and reproduced on [5], where emphasis is given on the operational behavior and its overall concerns, without detailing the analysis on low-impact phenomena. In other words, the synchronous generator model developed here adopts every assumption that leads to the simplification of the structure and equations, but still reproducing all the main characteristics that are deemed relevant to the EPS and thus should be reproduced by an SSG.

The model is applicable in both transient and steady-state conditions. The saturation is neglected, thus considering only linear magnetic circuits and disregarding the induced currents in the rotor (damper winding and iron). The mechanical structure is simplified assuming an idealized generator with just one pair of poles in the virtual rotor [87]. For the electric part of the model, the armature and field (rotor) windings are thus

represented as concentrated coils in Fig. 9, where R_S and L are resistance and self-inductance of the armature coils assumed identical for each phase; R_f and L_f are the resistance and self-inductance of the field coil; M represents the mutual inductances between each adjacent armature coils; v_a, v_b, v_c and v_f are the armature and field voltages at the terminals; i_a, i_b, i_c and i_f are the armature and field currents, respectively. The armature coils are thus regarded as identical and they are connected in wye (star) connection. The field coil is rotating in the counter-clockwise direction and the mutual inductances can be expressed according to the rotation angle θ as:

$$\begin{aligned} L_{af} &= M_f cos\theta \\ L_{bf} &= M_f \cos(\theta - 120°) \\ L_{cf} &= M_f \cos(\theta - 240°) \end{aligned} \tag{3.1}$$

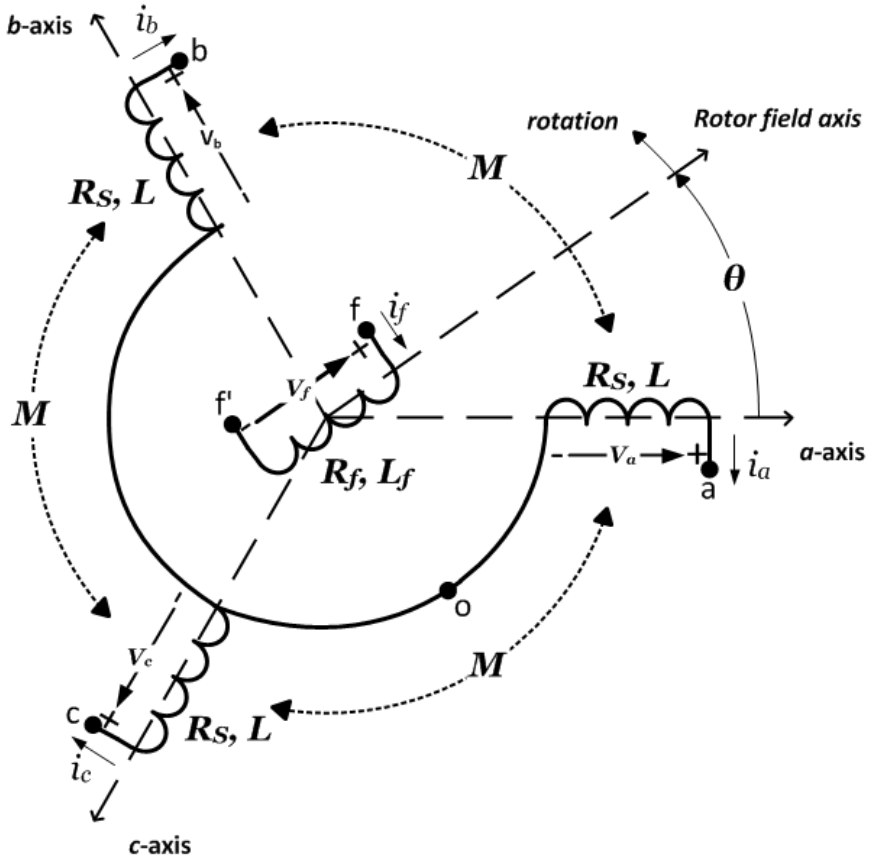

Fig. 9: Generalized model of a three-phase synchronous generator, adapted from [85] and [5].

Therefore, the flux-linkage (represented by λ) is established considering the current of the own coil, the currents of the others coils and ($i_a + i_b + i_c = 0$):

$$\begin{aligned} \lambda_a &= Li_a - M(i_b + i_c) + L_{af} i_f = L_s i_a + L_{af} i_f \\ \lambda_b &= Li_b - M(i_c + i_a) + L_{bf} i_f = L_s i_b + L_{bf} i_f \end{aligned} \tag{3.2}$$

$$\lambda_c = Li_c - M(i_a + i_b) + L_{cf}i_f = L_s i_c + L_{cf}i_f$$

$$\lambda_f = L_f i_f + L_{af}i_a + L_{bf}i_b + L_{cf}i_c$$

Where the inductance $L_S = L + M$. Armature flux linkage equations can be rewritten as:

$$\lambda = \begin{bmatrix}\lambda_a \\ \lambda_b \\ \lambda_c\end{bmatrix} = L_S \begin{bmatrix}i_a \\ i_b \\ i_c\end{bmatrix} + M_f i_f \begin{bmatrix}cos\theta \\ \cos(\theta - 120°) \\ \cos(\theta - 240°)\end{bmatrix} \tag{3.3}$$

Finally, the voltages are determined at the terminals of the armature and field windings. For the armature coils:

$$i = \begin{bmatrix}i_a \\ i_b \\ i_c\end{bmatrix}; v = \begin{bmatrix}v_a \\ v_b \\ v_c\end{bmatrix}$$

$$v = -R_S i - \frac{d\lambda}{dt} = -R_S i - L_S \frac{di}{dt} + e \tag{3.4}$$

$$e = \begin{bmatrix}e_a \\ e_b \\ e_c\end{bmatrix} = M_f i_f \frac{d\theta}{dt} \begin{bmatrix}sin\theta \\ \sin(\theta - 120°) \\ \sin(\theta - 240°)\end{bmatrix} - M_f \frac{di_f}{dt} \begin{bmatrix}cos\theta \\ \cos(\theta - 120°) \\ \cos(\theta - 240°)\end{bmatrix} \tag{3.5}$$

$$v_f = R_f i_f + \frac{d\lambda_f}{dt} \tag{3.6}$$

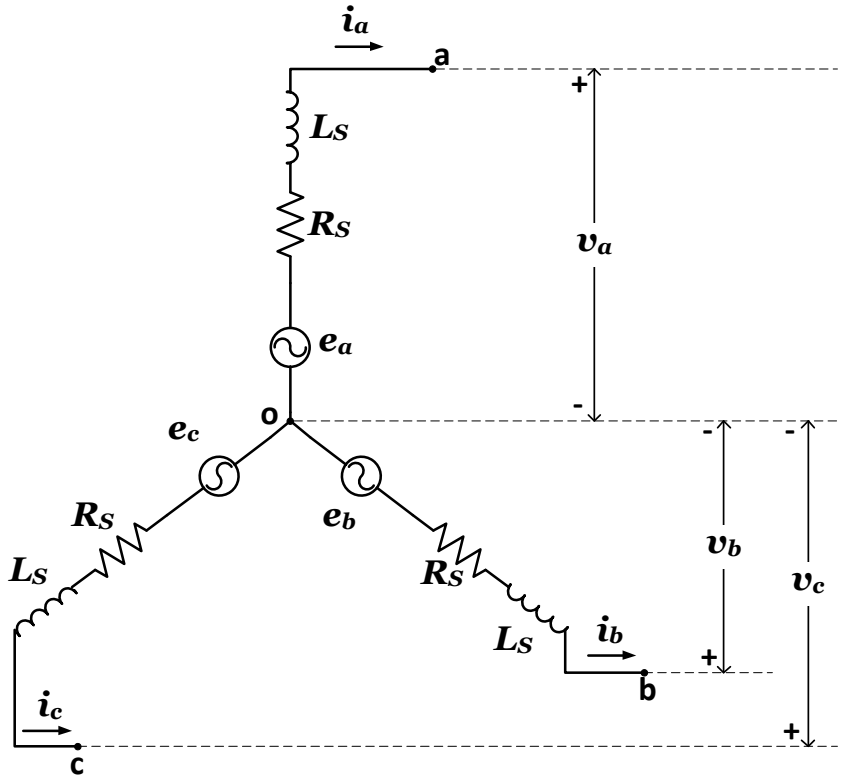

Fig. 10: Electric circuit of the synchronous generator model.

The voltage e is the generated electromotive force (emf) also known as no-load voltage, open-circuit voltage, synchronous internal voltage, or generated voltage [85].

Hereafter, it will be referred to as the generated voltage. It is convenient to consider the field current i_f controlled by a dc current source as well as to neglect the second part of eq. (3.5). Therefore, the generated voltage becomes:

$$e = \begin{bmatrix} e_a \\ e_b \\ e_c \end{bmatrix} = M_f i_f \frac{d\theta}{dt} \begin{bmatrix} sin\theta \\ \sin(\theta - 120°) \\ \sin(\theta - 240°) \end{bmatrix} \tag{3.7}$$

The electric circuit of the synchronous generator model is represented as shown in Fig. 10.

For the mechanical characteristics of the synchronous generators, the principal expression that governs the machine comprises the inertia J, the mechanical torque T_m, the electromagnetic torque T_e, and the damping factor D_p:

$$J \frac{d\omega}{dt} = T_m - T_e - D_p \omega \tag{3.8}$$

It is important to highlight that the angular velocity ω is defined regarding the simplification adopted of a two-pole machine. Hence, the mechanical and the electrical angles are equal. This means that hereafter the rotor speed is equal to the electrical angular velocity and both will be referenced just as ω:

$$\omega = \frac{d\theta}{dt} \tag{3.9}$$

The electromagnetic torque (T_e) can be obtained from the instantaneous active power transferred across the air-gap (P) by dividing it by the rotor speed [87]. According to Fig. 10:

$$P = e_a i_a + e_b i_b + e_c i_c = e^T \cdot i = M_f i_f \omega \begin{bmatrix} sin\theta \\ \sin(\theta - 120°) \\ \sin(\theta - 240°) \end{bmatrix}^T \cdot \begin{bmatrix} i_a \\ i_b \\ i_c \end{bmatrix} \tag{3.10}$$

Thus:

$$T_e = \frac{P}{\omega} = M_f i_f \begin{bmatrix} sin\theta \\ \sin(\theta - 120°) \\ \sin(\theta - 240°) \end{bmatrix}^T \cdot \begin{bmatrix} i_a \\ i_b \\ i_c \end{bmatrix} \tag{3.11}$$

Finally, the reactive power has to be calculated as it plays an important role in the EPS issues. According to [5], it can be calculated by defining a voltage e_q, which is delayed from the generated voltage e by $\pi/2$:

$$e_q = M_f i_f \omega \begin{bmatrix} \sin(\theta - 90°) \\ \sin(\theta - 210°) \\ \sin(\theta - 330°) \end{bmatrix} = -M_f i_f \omega \begin{bmatrix} cos\theta \\ \cos(\theta - 120°) \\ \cos(\theta - 240°) \end{bmatrix} \quad (3.12)$$

$$Q_{e_q} = e_{q_a} i_a + e_{q_b} i_b + e_{q_c} i_c = {e_q}^T \cdot i = -M_f i_f \omega \begin{bmatrix} cos\theta \\ \cos(\theta - 120°) \\ \cos(\theta - 240°) \end{bmatrix}^T \cdot \begin{bmatrix} i_a \\ i_b \\ i_c \end{bmatrix} \quad (3.13)$$

The voltage e_q for the reactive power calculation is not considered a widespread solution. It reproduces the reactive power at the output of the generated emf, and, indeed, at this point the reactive power has low importance for the EPS. Conversely, the reactive power at the terminals of the generator is the parameter usually considered for the synchronous control and it differs from eq. (3.12) due to the L_S inductance. Moreover, in practical circumstances the reactive power at the terminal of the machine is easier to calculate since the current and voltage can be measured. Hence, the reactive power considered here can be calculated in the abc-reference frame [14] as:

$$Q = (v_{ab} i_c + v_{bc} i_a + v_{ca} i_b)/\sqrt{3} \quad (3.14)$$

Static Synchronous Generator Model

The goal of the Static Synchronous Generator model is to embed the principal characteristics of a synchronous machine performance into the main controller of a power electronic converter. It is not interesting to reproduce all the effects that should be found in actual machines. For instance, the losses intrinsically present on actual synchronous machines (e.g. magnetic, electric and mechanical losses) are not useful to be reproduced by the power converter since in a primary assessment those do not aggregate any benefits to the SSG performance.

The main controller considered here was firstly proposed in [5], which basically reproduces the synchronous generator model previously presented in this chapter. Therefore, the power circuit and the main controller of the SSG are shown in Fig. 11. The power circuit is composed of a dc/ac power electronic converter (inverter) with a switching filter. The switching filter is an LC filter, where R_S and L_S are the resistance and inductance of the commutation inductor, respectively. Note that the ac voltage and current as well as the parameters of the inductor depicted in Fig. 11a lead to an intuitive correlation of this power circuit with the electric circuit of Fig. 10. A design criterion can be established with respect to the capacitor by setting its value to tune the resonant

frequency of the passive filter at the switching frequency [5]. However, detailed design criterions can be employed instead, to achieve reduced THD values at the terminal voltage [88], [89].

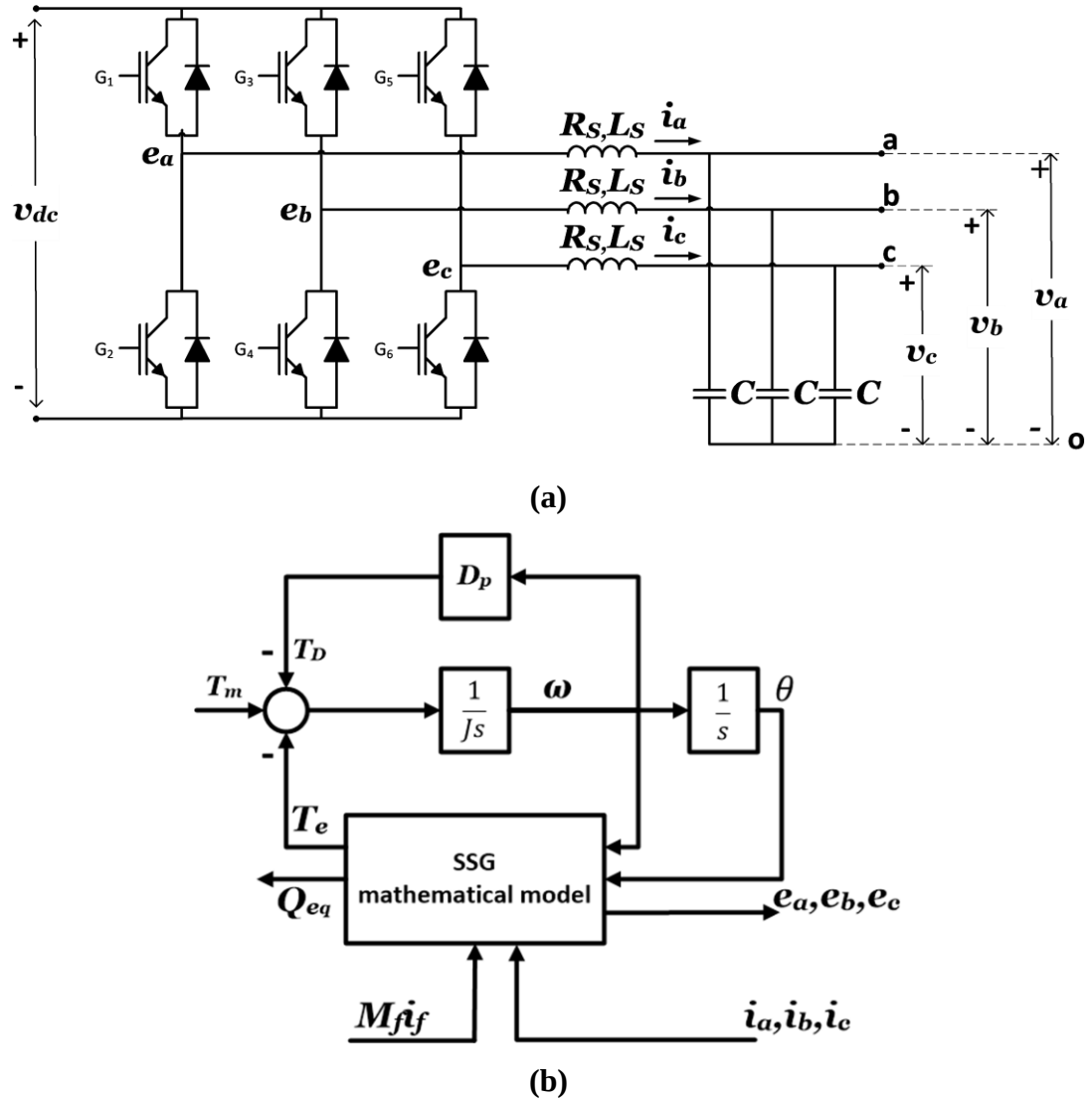

Fig. 11: Static Synchronous Generator, adapted from [5]: a) power circuit, b) main controller.

The SSG main controller (Fig. 11b) emulates the characteristics described in the Synchronous Generator Model. The inputs are the measured currents i_a, i_b and i_c; the virtual mechanical torque T_m, and the virtual flux-linkage $M_f i_f$. The SSG mathematical model is composed of the three equations that provide the virtual electromagnetic torque T_e, eq. (3.11); the reactive power Q_{e_q}, eq. (3.13); and the virtual generated voltages e_a, e_b and e_c, eq.(3.7).

The upper loop of the controller ensures the proper emulation of the mechanical characteristics of a synchronous generator by reproducing the mechanical expression

defined in eq. (3.8). The inertia J is implemented as an integral gain. In actual machines the inertia cannot be changed because it is a physical parameter that depends on the constructive arrangement and the weight of the material. However, in the SSG the inertia can vary as it is a numeric parameter in the control loop. Indeed, the parameter J is an integral gain in the control loop that emulates the inertia through the angular speed variation. In this way, this gain is deemed as virtual inertia [90], [91]. The damping factor D_p emulates the mechanical droop torque T_D due to friction, windage and other mechanical losses caused by the prime mover speed. In an ideal synchronous generator these effects can be disregarded. However, the damping factor is an important tool that can be employed as a frequency drooping coefficient to provide frequency drooping control, as will be discussed later.

The main control of Fig. 11 ensures the inverter behavior as a virtual synchronous machine. Additional controllers should be employed to provide the active and reactive power control. These controllers have to be properly designed to avoid the mischaracterization of the synchronous machine performance. Fig. 12 shows the SSG controller with P and Q control loops. In this controller the set point of active power P_{set} is used to calculate the virtual mechanical torque T_m. In stable conditions the deviation of the angular frequency is negligible and the mechanical torque can be calculated by using the reference frequency ω_{ref} as

$$T_m = \frac{P_{set}}{\omega_{ref}} \ , \tag{3.15}$$

assuming the simplification adopted for a two-pole machine (one pair of poles, $p = 1$). The frequency-droop control is composed of the control loop that generates the drooping torque T_D, which can be expressed by:

$$T_D = \left(\omega_{ref} - \omega\right) \cdot D_p \ , \tag{3.16}$$

$$D_p = -\frac{\Delta T}{\Delta \omega} \ . \tag{3.17}$$

The D_p constant is used here as a frequency droop coefficient, ΔT is the change in the total torque acting on the virtual rotor, and $\Delta\omega$ is the change in the frequency deviation. The frequency droop mechanism is characterized by the speed drop (ω diminish, then $\Delta\omega > 0$) when increasing the electromagnetic torque (T_e increase, then $\Delta T < 0$), and thus eq. (3.17) has a minus sign to make D_P positive (negative slope effect [3]). The angle θ is generated from ω to feed the SSG mathematical model, and has to be limited up to 2π with a reset procedure in practical implementations to avoid

numerical overflow. In this way, the mechanical expression defined in eq. (3.8) is adapted with the droop control loop as:

$$J\frac{d\omega}{dt} = T_m - T_e + D_p(\omega_{ref} - \omega) \tag{3.18}$$

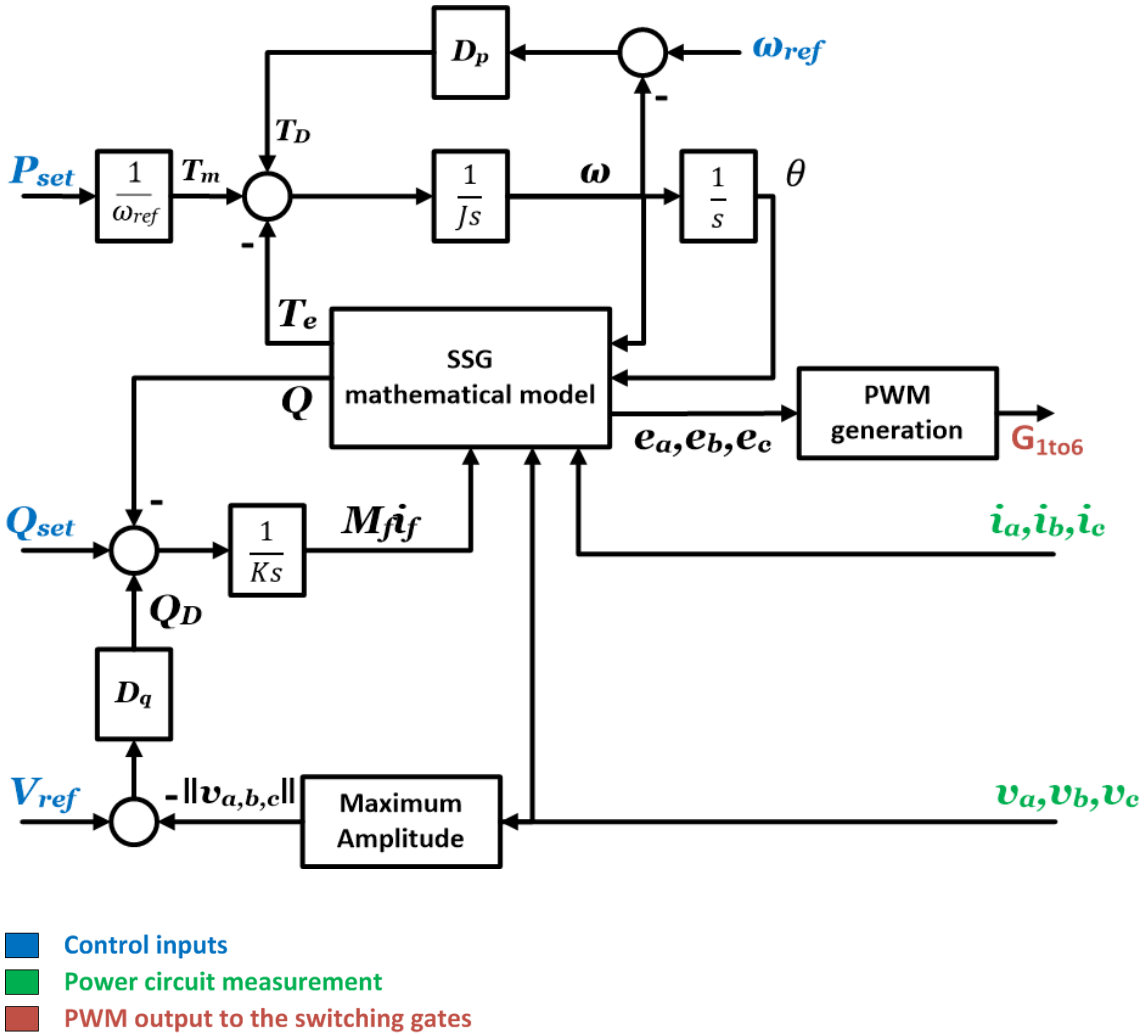

Fig. 12: Classic SSG controller with P and Q control loops, adapted from [5].

The reactive power control loop controls the amplitude of the voltages e_a, e_b, e_c by providing the signal $M_f i_f$, which corresponds to the magnetic flux of a virtual excitation winding on the SSG mathematical model (see eq. (3.7)). The voltage-droop control is composed of the control loop that generates the reactive power Q_D, which is expressed by:

$$Q_D = (V_{ref} - V_{pcc}) \cdot D_p \tag{3.19}$$

$$D_p = -\frac{\Delta Q}{\Delta V} \tag{3.20}$$

Where the D_q constant is the voltage droop coefficient, ΔQ is the change of reactive power and ΔV is the change of voltage amplitude. The minus sign in eq. (3.20) has the

same purpose to make D_q positive (negative slope effect). It is important to highlight that the equation used to calculate the reactive power Q in this approach is different from Q_{e_q} in eq. (3.13), which is the calculation employed in the SSG mathematical models of [5] and [3]. Eq. (3.13) uses only the measured current and the generated voltage to estimate the reactive power at the switches' terminals (i.e. the electrical point indicated by the voltages e_a, e_b and e_c in Fig. 11a). Despite the simplicity of using the internal variables $M_f i_f$ and ω, the reactive power Q_{e_q} may differ significantly from the reactive power at the terminals (a, b and c at Fig. 11a) in case of increased values of the inductance L_S or when the concept of virtual impedance control is applied. For instance, in Fig. 12, the virtual impedance control would be located in between the voltage references e_a, e_b and e_c and the PWM control block. Here, the same calculation proposed in the Synchronous Generator Model, eq. (3.14), and in [73], is employed to calculate Q in the SSG controller of Fig. 12, which provides the instantaneous reactive power at the converter's terminals.

The reference signals of the generated voltages are used to feed the PWM generation block. In this block a simple PWM controller such as that found in [14] is employed to determine the pulses at the gates of the power semiconductors. For the general purposes of the SSG, there is no need of employing special PWM technique as the reference voltages correspond to the synchronous internal voltages [5] and [3].

Special functionalities, peripheral controllers and some applications of SSGs

One of the main advantages of the SSG in comparison with actual synchronous generators is the ability to dynamically change its virtual parameters, which is not feasible in actual machines due to obvious reason of physical dependency (constructive characteristics). This leads to the possibility of enhancements in many areas not previously envisioned. Some possible benefits of such ability will be discussed here.

The virtual inertia was already pointed out here as a possible solution to avoid the lack of grid inertia with the high penetration of power electronic converters as front-end interface of renewable generation. Moreover, enhanced performance [90] and special functionalities may be available as the virtual inertia is not unchangeable. First, it is necessary to observe the maximum virtual inertia that can be emulated, according to the

hardware configuration of the DG unit. Indeed, it is related to the stored energy of the generation system. For instance, a capacitor bank will be considered as the storage element since it is the most used short-term storage element. The energy equivalence between the kinetic energy in a synchronous rotor (E_k) at nominal speed (ω_n) and the static energy in a capacitor bank (E_C) at nominal voltage level (V_{dc}) determines the maximum inertia (J_{max}) that can be mimicked by the SSG. Therefore, it is stated as [92], [6]:

$$E_k = \frac{1}{2} J_{max} {\omega_n}^2 \tag{3.21}$$

$$E_C = \frac{1}{2} C {V_{dc}}^2 \tag{3.22}$$

$$J_{max} = \frac{C {V_{dc}}^2}{{\omega_n}^2} \tag{3.23}$$

where C is the capacitance of the dc bank. The moment of inertia normalized in terms of per unit inertia constant H is more convenient and, considering the base power S_{base}, eq. (3.23) can be expressed as:

$$\mathrm{H}_{max} = \frac{\mathrm{E_k}}{S_{base}} = \frac{E_C}{S_{base}} \tag{3.24}$$

$$\mathrm{H_{max}} = \frac{\mathrm{C{V_{dc}}^2}}{2\ \mathrm{S_{base}}} \tag{3.25}$$

Hence, if the virtual inertia is configured in a value higher than the obtained in eq. (3.23) and eq. (3.25), according to the hardware configuration, the SSG will not be able to faithfully reproduce the effect of this inertia since the energy stored is not enough to do it. It is important to highlight that depending on the generation type (wind, solar, fuel cell etc.) special control strategies can be adopted to increase the maximum stored energy and, consequently, provide more inertia to the system [93].

An application of the virtual inertia is presented in [94] and [91] for stability purposes and enhanced dynamic performance in tracking the steady-state frequency. The control concept has a simple comprehension in physical aspects. The goal is to control the SSG with increased inertia in such periods that it can contribute to the stability of the power system. In contrast, the SSG will be controlled with decreased inertia to achieve fast dynamic response. An enhancement of this approach leads to the negative virtual-inertia concept. Instead of just reducing the virtual inertia, the negative value of the virtual inertia is capable of reaching the steady state with an even faster

performance. Note that this is not possible with a real machine. Theoretically, it can be interpreted as an instantaneous exchange of the poles of the machine with selective values of inertia, which results in a controlled attempt to reverse the rotor turn in order to achieve fast deceleration.

The virtual impedance is a control method used for many purposes such as to ensure the P-ω/Q-V droop effectiveness, to equalize harmonic load sharing or achieve reduced voltage THD, to improve the converter's performance in microgrid scenarios, and to provide fault ride through capability, soft start etc. It can be used as a peripheral controller of the SSG without mischaracterizing the synchronous operation.

The droop control method is an important approach to enable parallelism of power electronic converters and to perform power sharing [95]. There are two possibilities to implement this control method in a power electronic converter: through classical P-ω/Q-V droop curves, or through the Q-ω/P-V droop curves. Considering that the change in frequency along the power system is far less than the change in voltage amplitude, it is advantageous to implement the control method using classical P-ω/Q-V droop curves in order to ensure the active-power sharing in a large range of operation.

The effectiveness of the droop control method depends on the X/R ratio of the line impedance [96]. For the classical P-ω/Q-V droop curves, the P-ω relation is effective only if $X/R \gg 1$. According to Fig. 13 and disregarding the physical (real) impedance of the SSG, the active and reactive power at the infinite bus can be stated as:

$$\mathrm{P} = \frac{EV}{Z}\cos(\Theta - \phi) - \frac{V^2}{Z}cos\Theta \tag{3.26}$$

$$\mathrm{Q} = \frac{EV}{Z}\sin(\Theta - \phi) - \frac{V^2}{Z}sin\Theta \tag{3.27}$$

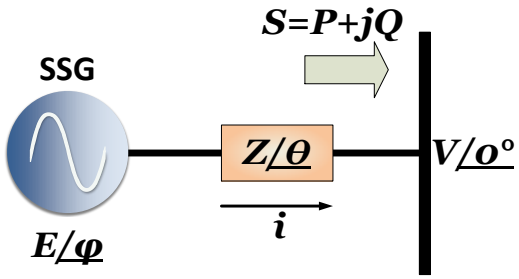

Fig. 13: SSG connected at an infinite bus, adapted from [96].

In transmission networks $X \gg R$ ($\Theta \approx 90°$), and eq. (3.26) and (3.27) can be simplified as:

$$\mathrm{P} = \frac{EV}{X}\sin\phi \tag{3.28}$$

$$\mathrm{Q} = \frac{EV\cos\phi - V^2}{X} \tag{3.29}$$

This is what actually led to the classical approach of the P-ω/Q-V droop curves. Therefore, in an SSG connected to the grid via inductive transmission line, the classical P-ω/Q-V droop curves can be employed without the need of additional impedance. However, the DG generation in microgrids is connected in distribution networks, where it is possible to have $X \ll R$ ($\Theta \approx 0°$), and eq. (3.26) and then (3.27) can be simplified as:

$$\mathrm{P} = \frac{EV\cos\phi - V^2}{R} \tag{3.30}$$

$$\mathrm{Q} = -\frac{EV}{R}\sin\phi \tag{3.31}$$

In this case, the classical approach of P-ω/Q-V droop curves is no longer as effective and, consequently, the predominant effect is interchanged and Q-ω/P-V droop curves become more effective. This interchange can be seen in the major influence of the angle ϕ in the reactive power, eq. (3.31), and the amplitude of the voltages E and V in the active power control, eq. (3.30). Here, using the classical P-ω/Q-V droop curves requires that inductance be installed in series with the Z impedance in order to restore or to impose the inductive predominance of the line impedance. The virtual impedance concept can be employed in the converter controller as a solution to avoid costs of installing this additional inductance. It is important to highlight that the magnitude of Z is limited due to the total power transfer capacity [97], which means that if the magnitude of the virtual impedance is too high, then the active and reactive power flow is limited (see denominator of eq. (3.26) and (3.27)).

Other functionalities are available with the use of virtual impedance [98]. The integration of power electronic devices into the electric power system brings many benefits. However, harmonic contents are generated by these devices, and it becomes a critical power-quality drawback if the quantity of the installed power electronic devices is increased. The virtual impedance concept can be improved as a control function in order to reduce the negative impacts of these drawbacks. In this way, DRs with specific

virtual-impedance design are able to equally share the harmonic contents and achieve reduced voltage THD [96].

The main controller of the Static Synchronous Generator proposed in [5] can be enhanced with additional controllers in order to perform complementary functionalities. For instance, the conventional SSG controller is enhanced in [76] to operate in wind power systems, or in [75] to faithfully reproduce the behavior of synchronous machines. Moreover, the SSG controller can be employed together with other power electronic applications as proposed in: [73] to operate a rectifier to mimic a synchronous motor; [74] to control a STATCOM to mimic a synchronous condenser, and; [99] to control HVDC transmission systems. In this way, the SSG controller has become a control methodology for inverter-based equipment that aims to behave as smart synchronous devices. In some applications, the nomenclature SSG is not suitable since the equipment is not working as a generator. In this case, the synchronverter nomenclature is more appropriate. The following two examples of application of the synchronverter will be highlighted.

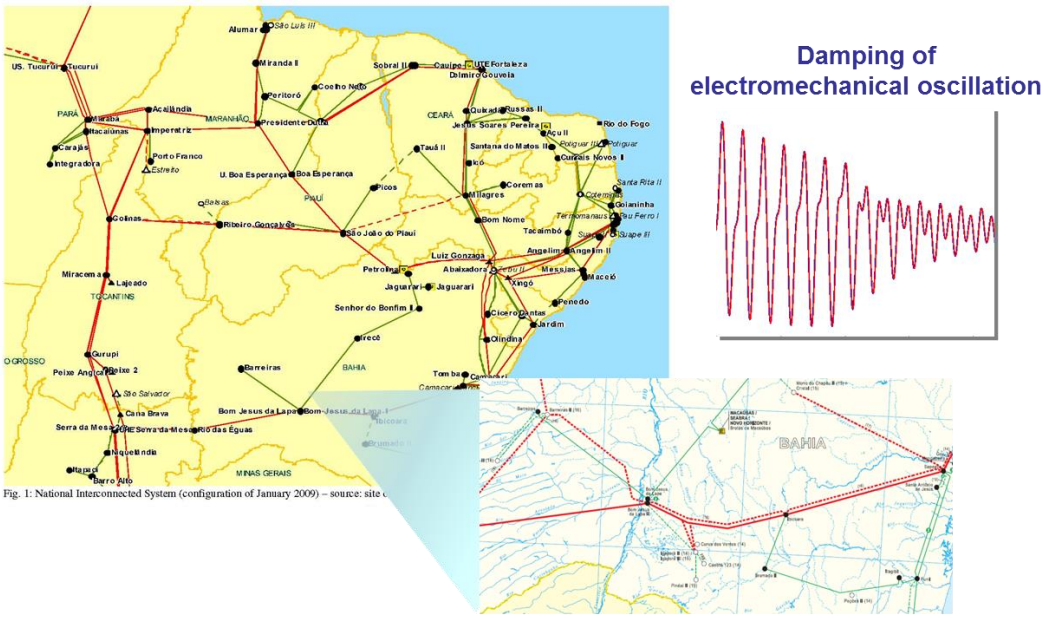

Fig. 1: National Interconnected System (configuration of January 2009) – source: site

Fig. 14: SSG as a SVC at Bom Jesus da Lapa substation, adapted from [8].

In [8], a synchronverter was employed to substitute an SVC in an important substation of the Brazilian EPS (Fig. 14). This substation is located in the central section of an important power corridor and the SVC has the role of damping electromechanical oscillations. The same controller used for the SVC was employed in the reactive-power control loop of the synchronverter. It was verified that the synchronverter is capable of performing the same functionality of the SVC. This is an

important finding since it demonstrates that FACTS can still perform its original functionalities while contributing to the grid inertia as would be the case using rotational synchronous machines.

The synchronverter was also evaluated as the ac/dc and dc/ac interfaces of an HVDC transmission system [99]. The system was named as synchronverter HVDC or SHVDC. At the beginning of the transmission system (ac/dc interface), the synchronverter behaves as a synchronous motor to draw power into the dc link, and at the end (dc/ac interface) the synchronverter operates as a synchronous generator (SSG) to deliver power into the EPS. This approach can be seen as strategic in multi-infeed scenarios, where the equivalent inertia has to be strengthened.

Chapter 4 - The Proposed SSG with Sliding Droop Control

In this chapter the proposed control method is introduced. First, the desired functionalities are presented. Then, the SSG with the proposed controller is explained together with the sliding droop control itself.

In the previous chapters the DG was discussed in several aspects. The transition in the EPS, from CPS to DPS, was introduced, as well as the trends of implementing hierarchical control structures in microgrids to allow their integration into the main power grid in a smooth manner, regarding the grid robustness and resilience. The droop and the SSG control methods were highlighted as suitable alternatives to work as the primary control level of a DG unit. In this case, no communication system is necessary to perform power sharing. A "plug-and-play" functionality for each DG unit can be assumed, and the power electronic converter behaves as a virtual synchronous machine.

In the classic droop control, the droop curves are static. The grid control (tertiary) defines the slope of the $P - \omega$ curve in order to achieve proportional active-power sharing. Moreover, when this classic droop control is associated with the SSG control method, the no-load frequency is dependent on the aforementioned slope and on the active-power dispatch, which compromises the active-power sharing for intermittent DG. In other words, the original controller of the SSG with static droop curves is not capable of ensuring power sharing between units with different active-power set points if there is no communication system to adjust the no-load position and the slope of the droop curves. This statement will be deeply investigated in this chapter and the new sliding droop control method will be introduced as a mean to overcome these issues. This subject is considered as the main contribution of this work. Hence, the proposed control method promotes the SSG as a suitable control method for DG in microgrids. Other complementary benefits will also be highlighted according to the proposed functionalities pointed out in this chapter.

Dynamic droop controls have been proposed in recent studies such as [100], [101] and [102]. In [100] the droop control method is used as a solution to avoid critical communication among UPS units, which are controlled as voltage sources in both islanded and grid-connected modes. The droop coefficient is controlled as a function of the State-of-Charge (SoC) of batteries, and thus the overall active power flow is according to the power demand and availability. However, it still needs a low bandwidth communication system to report the microgrid operation-mode and receive the active and reactive set points. The system counts with an Intelligent Bypass Switch (IBS) that plays an important role by detecting faults in the grid, by performing the microgrid disconnection, and by controlling the frequency and voltage deviations between grid and microgrid during resynchronizing procedures after the fault clearance.

The last functionality is performed by adjusting the set point of the UPS units. Although the controller is effective in active, reactive and harmonic sharing, it uses a complex structure that must be properly tuned regarding the system configuration, which implies an increased complexity when considering a large number of units in the same microgrid.

In [101] and [102] the reactive-power sharing is investigated for DGs connected in different buses and using $Q - V$ droop method, where the effects of mismatched line impedance can lead to the deterioration of sharing performance. Indeed, the insurance of the reactive-power sharing is a hard accomplishment since it is controlled through the measured voltage at the point of connection, which varies with the grid arrangement and power flow [67]. Another issue about the reactive-power sharing is that in some cases it is not mandatory or taken as priority.

Proposed SSG functionalities

In this work the SSG controller from [5] is employed as the main controller that ensures the virtual synchronous machine performance, and a sliding droop control is developed to achieve enhanced performance. With this sliding droop control, DG unit operates continuously as an SSG without changes in the controller, even during transitions between islanded and grid-connected mode. The novelty here is to realize active/reactive power sharing and frequency/voltage regulation without the need of any communication channel between DG units. As a result, the new sliding droop control aims to achieve negligible frequency/voltage deviation and to ensure the power sharing by itself, thus diminishing the demand for a communication channel. Its applicability is strengthened if there is no possibility to have a communication system to implement the microgrid or if the communication system is not cost-effective. In summary, the SSG connected in a microgrid should achieve the following goals:

In islanded mode of operation

- Perform suitable frequency and voltage regulation within a predictable margin of error;
- Share the active-power between all DG units proportionally to theirs set points;
- Share the reactive power between DG units.

In grid-connected mode of operation

- Inject active power according to its set points, which can be dictated by a tertiary control in case of an existing communication channel and energy management system, or by a local, maximum power point tracking (MPPT) in the primary source (renewable energy generation system);
- Inject reactive power according to the voltage set point to perform voltage regulation along the microgrid.

Despite the absence of a communication system, the voltage profile along the microgrid and the system frequency have to be kept at acceptable values, even during islanded mode of operation. With this proposed control method it is possible to ensure a reduced and predictable margin of error in both frequency and voltage regulation. The same cannot be obtained with the static droop curves due to the slope necessary to avoid increased power oscillation in frequency and voltage transients [51].

The goals chosen here are based on the pursued goals in current studies and on the present standards in the field [23]. However, the controller is suitable to be adapted to other requirements that may be added or even may substitute those proposed in this work. For instance, different requirements can be established for the active-power dispatch according to the kind of resource, generation costs, generation time (considering peak demand hours), operational rules etc. [103].

The principle of operation of the proposed control method consists in sliding the frequency and voltage droop curves to achieve the goals aforementioned. The pattern of sliding is pre-established in such manner that only the measurement of local variables is required. A previous knowledge or real time measuring of the grid impedance is not necessary and there is no need of an islanding detection method, since the controller is the same for both situations, i.e. during grid-connected or islanded modes of operation.

Static droop control method in the classic SSG

Here the applicability of the static droop control method, used in the classic SSG controller (Fig. 12), will be evaluated through the proposed functionalities and the present standard of IEEE 1547.

The hardware structure of Fig. 8 is adopted as the basic structure of the DG units. It is assumed that the primary energy resource and the storage element are managed by a specific controller that provides the active-power order (P_{set}) to the SSG (see P_{set} in Fig. 12) and ensures the dc-voltage regulation [104]. This controller will be named here as the controller of the generation and ESS, or simply GESS control. Therefore, P_{set} is provided by the GESS control according to the currently available resource. It represents the power that should be injected by the DG unit in grid-connected mode with the system frequency ($\omega \approx \omega_{ref}$) mainly imposed by the principal generators in the power grid. If the power dispatch in the microgrid is not equal to the sum of all P_{set} for every DGs, which is a common situation in islanded microgrids, then the exceeding power has to be stored or discharged by the GESS control. In this situation the mechanical torque (T_m) and the electromagnetic torque (T_e) are also different from each other.

In order to ensure that, in an islanded microgrid, each DG unit will dispatch power proportionally to its currently available resource (second functionality proposed on the islanded mode of operation), the ratio between T_e and T_m have to be the same for each unit. Thus,

$$\frac{T_{e1}}{T_{m1}} = \frac{T_{e2}}{T_{m2}} = \cdots = \frac{T_{en}}{T_{mn}} \tag{4.1}$$

has to be satisfied. The indexes $i = 1, 2, \ldots, n$ refer to the DG units connected at the microgrid.

The validity of eq. (4.1) will be checked with the classic droop concept through the active-power control loop of the SSG (upper side of Fig. 12) and the example depicted in Fig. 15, which presents the active-droop curve of two SSG connected in an islanded microgrid. $T - \omega$ curves were used instead of the $P - \omega$ curves to agree with eq. (4.1), but indeed they are correlative in this analysis. Fig. 15 ω_0 shows the no-load frequency.

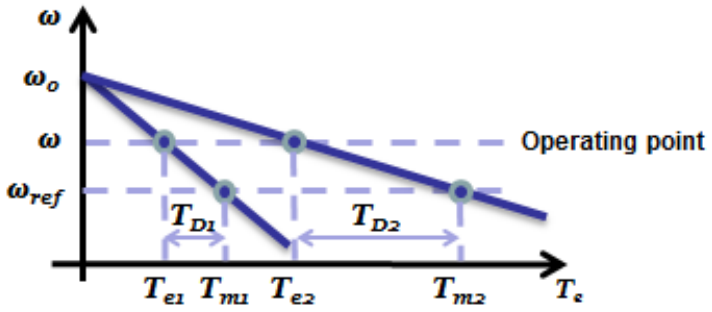

Fig. 15: Example of two droop curves ($T - \omega$).

In order to ensure the validity of eq. (4.1) independently of the operating point, if the classic droop control is adopted, the no-load frequency (ω_0) has to be the same for all DG units and the droop coefficient (D_{pi}) of each one has to be proportional to the mechanical torque (T_{mi}) [51]. These two requirements can be observed through the ω_0 position and the distinct slopes of the curves in Fig. 15.

The electromechanical equation of the classic SSG is given by:

$$T_m - T_e + D_p(\omega_{ref} - \omega) = J\frac{d\omega}{dt} \tag{4.2}$$

and in steady state $J\frac{d\omega}{dt} = 0$. Then, the no load frequency (ω_0) is calculated as:

$$\omega_0 = \omega_{ref} + \frac{T_{mi}}{D_{pi}}. \tag{4.3}$$

In an EPS with a communication system and hierarchical control, the tertiary controller determines the droop gains (D_{pi}) and the nominal output power (T_{mi}) under nominal frequency. This is the same as setting the no-load frequency to the same value for all DG units and ensuring that the D_{pi} gain is proportional to T_{mi} [51]. However, this is not the case in a DPS with no communication system and with intermittent renewable generations that continuously vary their available power reference values, T_{mi}.

Without a communication channel, D_{p_i} is fixed as the ratio of the nominal power, T_{eN}, and the maximum allowed frequency deviation $\Delta\omega_{max}$ ($D_{p_i} = T_{eN_i} / \Delta\omega_{max}$). Hence, the conventional droop control is not suitable to ensure power sharing in this situation. Eq. (4.3) leads to conclude that the power sharing is achieved only between those DG units that have the same ratio T_{mi}/T_{eN_i} (i.e., the same per unit mechanical torque). Consequently, according to Fig. 12, each active-power set point (P_{set_i}) has to be the same in proportion to their respective power basis, which is a very particular condition and almost never satisfied with intermittent renewable generation.

Another drawback of the conventional droop method is related to the magnitude of the frequency deviation. A solution to achieve reduced frequency deviation in an islanded microgrid might be accomplished by decreasing $\Delta\omega_{max}$, which corresponds to an increase in the gains D_{p_i}. However, this is not a good solution in grid-connected mode and can degenerate the performance of the SSG, as well as cause instability during transitions between isolated and grid-connected microgrid modes of operation.

The IEEE standard [45] in the amendment [43] determines that Distributed Resources (DR), which includes DG, shall be able to provide modulated power output as a function of frequency according to pre-established and field adjustable ranges of deviation. For instance, this requirement is intended to permit the area EPS operator to count on DR participation to support the grid robustness in local mode oscillations, and also to avoid undesired overcurrent and sag/swell voltages at the dc-link during transient disturbances. In this sense, fixed droop curves would not be suitable to achieve both reduced frequency deviation in islanded mode and modulated power output in grid-connected mode.

Proposed SSG main controller

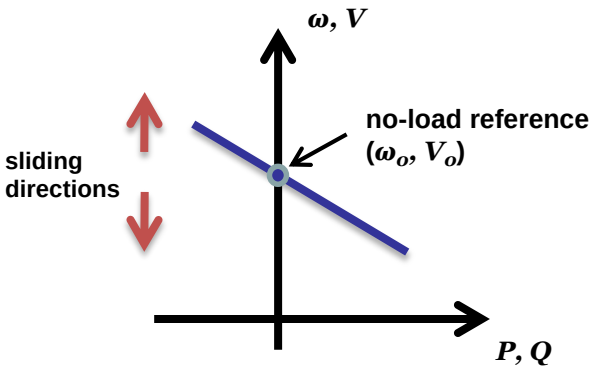

Fig. 16: Sliding droop control method.

The "sliding droop control" term is adopted here because the new control method will continuously vary the no-load reference values ω_0 and V_0 of the $P \times \omega$ and $Q \times V$ droop curves, as shown in Fig. 16. As a result, the droop curves will slide to be positioned at the best operating point, according to the proposed SSG functionalities. The per unit system is adopted to facilitate the control implementation in SSG with different power ratings. Fixed values of D_p and D_q droop coefficients can be applied independently from their power ratings. This ensures that the incremental torque T_D in

Fig. 12 is proportional to the power rating of each SSG, and the power sharing in steady state will be also proportional to their nominal powers, if they have the same per unit reference values ω_0 and V_0 in a given time interval.

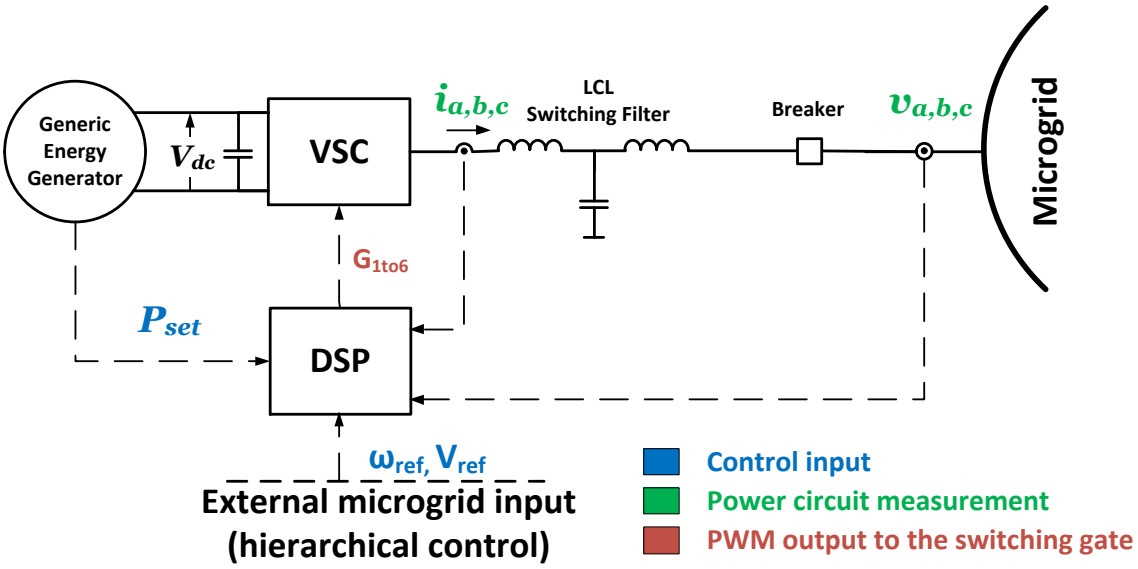

Fig. 17: Overall diagram of the hardware configuration used in the proposed controller.

The proposed controller is developed considering the power circuit and control structure as depicted in Fig. 17. The microcontroller with the embedded control code is represented by the Digital Signal Processor (DSP), which receives the measurements of the bus voltage ($v_{a,b,c}$) and the SSG current ($i_{a,b,c}$), along with the control inputs from the generic energy generator (P_{set}) and from a possible hierarchical controller of the microgrid (ω_{ref} and V_{ref}). It is important to highlight that if there is no hierarchical controller in the microgrid, these inputs can be replaced by constant reference values. The DSP outputs are the PWM gate pulses for the drivers of the power converter (VSC). The VSC is considered here as the conventional full-bridge three-phase IGBT converter (equal to the bridge on the left side of Fig. 11a) and the LCL-filter is used to filter the harmonic content produced by the VSC switching. An ordinary circuit breaker can be used to connect the SSG to the microgrid. The dc-link is composed of a capacitor bank with a voltage V_{dc} that is controlled by a GESS control. It is assumed that this GESS control manages the energy injected by the generic energy generator into the dc-link to maintain the dc voltage around its reference value, according to the power being injected by the SSG into the microgrid. It also passes continuously the power order, P_{set}, to the DSP, which gives the information about the maximum, or the desired, or even the ongoing available power generation. In other words, the active power set point P_{set} can be understood as a "maximum/desired" power that the SSG should deliver to

the microgrid or to the grid. This occurs only during periods when both the system voltage and frequency remain equal to their reference values.

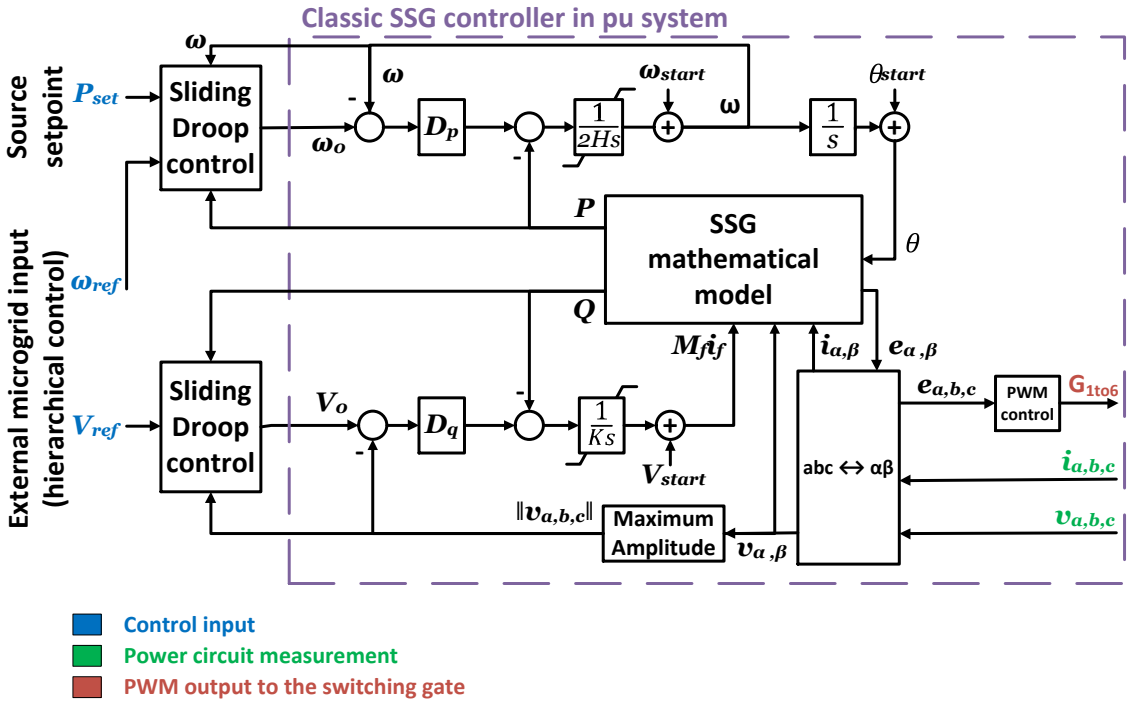

Fig. 18: Proposed controller.

The proposed control is shown in Fig. 18. The classic SSG control method is employed in the main part, which ensures the emulation of a virtual synchronous machine. Although the control structure of [5] is employed, here the whole control system is designed in per unit base (pu). Moreover, the αβ reference frame is adopted for reducing the processing efforts in the control code embedded in the DSP. Hence, regarding the simplification adopted of a two-pole machine (one pair of poles, $p = 1$) and transforming eq. (3.11), (3.7) and (3.13) into the $\alpha\beta$ stationary reference-frame it is found that:

$$e_{\alpha,\beta} = \begin{bmatrix} e_\alpha \\ e_\beta \end{bmatrix} = \omega M_f i_f \begin{bmatrix} sin\theta \\ -cos\,\theta \end{bmatrix} \tag{4.4}$$

$$\begin{bmatrix} T_e \\ Q \end{bmatrix} = \begin{bmatrix} \frac{e_\alpha}{\omega} & \frac{e_\beta}{\omega} \\ v_\beta & -v_\alpha \end{bmatrix} \begin{bmatrix} i_\alpha \\ i_\beta \end{bmatrix} \quad \omega \approx 1pu \;\; \dashrightarrow \;\; T_e \approx P \tag{4.5}$$

In a stable grid, the frequency is regulated nearby the nominal value ($\omega \approx 1pu$) and, thus, through (4.5) it is noted that the approximation $T_e = P$ is valid, where P is the instantaneous active power delivered by the DG unit disregarding the switching filter losses. Moreover, as the reactive power is controlled at the terminal voltages, $v_{\alpha,\beta}$ are

used instead of the generated internal voltages $e_{\alpha,\beta}$ (see eq. (3.13) and (3.14) as given in [5]).

The upper loop of the controller ensures the proper emulation of the mechanical characteristics of the synchronous generators. In the classical control loop this is done by reproducing the mechanical expression defined in eq.(3.18). By using the definition of the per unit inertia constant H:

$$H = \frac{E_k}{S_{base}} = \frac{\frac{1}{2}J\omega_n^2}{S_{base}} \ . \tag{4.6}$$

Equation (3.18) can be rewritten and rearranged as:

$$\frac{2S_{base}H}{\omega_n^2}\frac{d\omega}{dt} = T_m - T_e + D_p(\omega_{ref} - \omega)$$

$$2H\frac{d\frac{\omega}{\omega_n}}{dt} = \frac{T_m - T_e + D_p(\omega_{ref} - \omega)}{\frac{S_{base}}{\omega_n}} \tag{4.7}$$

Note that the term $\frac{S_{base}}{\omega_n}$ is the base torque and the term ω_n is the base frequency. Therefore, the mechanical expression defined in eq. (3.18) is equivalent to the per unit equation (4.8), where T_m, T_e, D_p, ω_{ref} and ω are parameters in per unit system.

$$2H\frac{d\omega}{dt} = T_m - T_e + D_p(\omega_{ref} - \omega) \tag{4.8}$$

In this work, the simplification $T_e = P$ is adopted regarding eq.(4.5), and the input P_{set} can also be directly related to the mechanical torque T_m. In this way, the terms related to torques, i.e. “electromagnetic torque” and “mechanical torque”, can still be used to keep the analogy with actual machines, in the same way that the active power terms can be used without characterizing misinterpretation of their physical meaning. The integrator gain is equal to $2H$ to deal with eq.(4.8), and $T_m + D_p(\omega_{ref} - \omega)$ is rearranged to employ the sliding droop control, replacing the classic droop control as will be discussed in the next subsection.

In the reactive-power control loop, all the parameters are also stated in per unit system by adopting the base power S_{base} and the base voltage.

Sliding droop control

The classical droop control loops are modified by including sliding droop curves in both the active- and reactive-power loops. The outputs of the sliding droop controls are

the varying frequency and voltage references at no-load (ω_0 and V_0) that feed the droop loops. If the microgrid is not provided with hierarchical control system and communication channels, ω_{ref} and V_{ref} variables can be fixed as 1.0 pu.

The sliding-droop control loops are depicted in Fig. 19. The control structures are similar for both active and reactive power loops. The start values ω_{start} and V_{start} can be obtained through an auxiliary positive-sequence detector [10], [105], and are useful to avoid higher transients during the startup of the SSG. If the grid is already powered before the startup of the SSG, the start values force the droop curves to stay in a position where the resulting injected powers P and Q would be ideally zero. These positions of droop curves are obtained by making $\omega_{start} = \omega_{grid}$ and $V_{start} = \|v_{a,b,c}\|$. Otherwise, if the grid is not powered, $\omega_{start} = \omega_{ref}$ and $V_{start} = V_{ref}$.

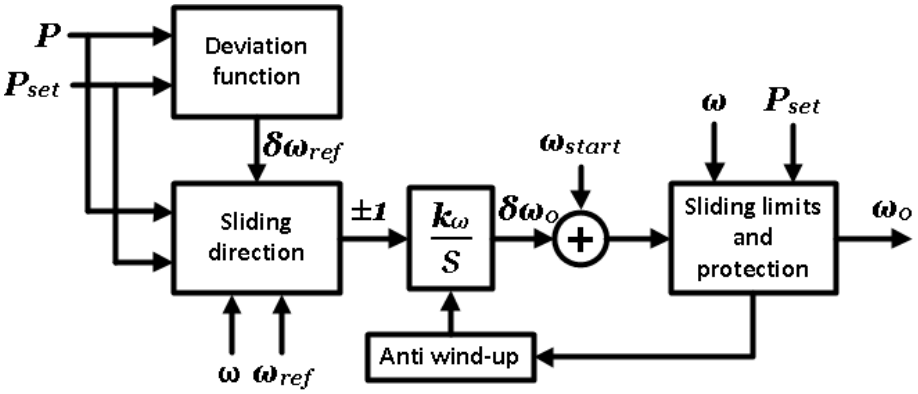

(a)

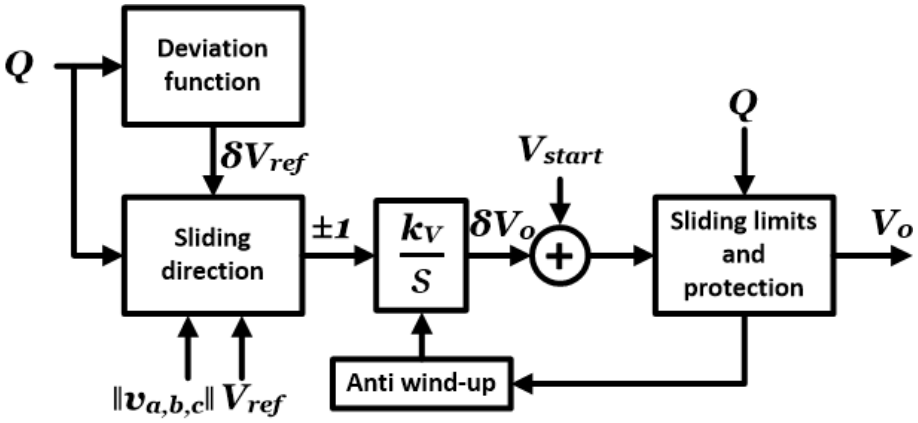

(b)

Fig. 19: Sliding droop control: a) active power, b) reactive power.

The main idea of the sliding droop control is to slide the droop curves in order to place them in such a position that tracks the frequency and the voltage in a reference that is the sum of the hierarchical-control (or fixed) references (ω_{ref} and V_{ref}) and the deviations $\delta\omega_{ref}$ and δV_{ref}. These deviations are determined through functions that

achieve optimum power sharing with reduced deviation according to the actual active and reactive powers of the SSG and their corresponding set points. In this work, Q_{set} will be set always zero.

The deviation function for the active power control is established as:

$$\delta\omega_{ref} = k_{S\omega}\left(1 - \frac{P}{P_{set}}\right), \quad for\ P \le P_{set}, and\ 0 < P_{set} \le 1, \tag{4.9}$$

where $k_{S\omega}$ is the maximum frequency deviation allowed in steady state. For the condition where $P > P_{set}$ the deviation function $\delta\omega_{ref}$ has no influence over the sliding direction control block. Hence, there is no reason to determine a frequency deviation under this condition. The sliding direction control block will determine if the droop curve slides up or down according to the following rule:

$$\begin{aligned} &if\ \omega > \left(\omega_{ref} + \delta\omega_{ref}\right)\ \ or\ \ P > P_{set} \quad \therefore\ slide\ down;\ output = -1 \\ &if\ \omega < \left(\omega_{ref} + \delta\omega_{ref}\right) \quad \therefore\ slide\ up;\ output = +1 \end{aligned} \tag{4.10}$$

Note that this controller does not depend on the D_P gain. In this way, reduced frequency deviation can be achieved in steady state by using a reduced $k_{S\omega}$ value, while suitable D_p value can be used to work properly in grid-connected mode, according to the requirements of the area EPS operator (see Fig. 18).

In steady state the frequency ω is the same for all DG units. Therefore, if there is enough available energy to feed the system, the rules in (4.10) guarantees that

$$\omega = \omega_{ref} + \delta\omega_{ref} \tag{4.11}$$

and, consequently, for DG units identified by indexes $i = 1,2,\dots,n$:

$$\delta\omega_{ref_1} = \delta\omega_{ref_2} = \cdots = \delta\omega_{ref_n}. \tag{4.12}$$

By substituting (4.9) in (4.12) and simplifying, it comes that

$$\frac{P_1}{P_{set1}} = \frac{P_2}{P_{set2}} = \cdots = \frac{P_n}{P_{setn}}, \tag{4.13}$$

which is analogue to the sharing condition stated in (4.1). Hence, the active-power setpoint does not interfere with power sharing when the proposed sliding droop controller is adopted. Moreover, the maximum frequency deviation $k_{S\omega}$ is also independent from the droop gain D_p.

Note that if the microgrid is operating in grid-connected mode, in steady state, the frequency ω in Fig. 18 is necessarily equal to the system frequency ω_{grid}. Therefore, if ω_{grid} is regulated and equal to ω_{ref}, in (4.11) it comes that $\delta\omega_{ref} = 0$ and in (4.9) this leads to $P = P_{set}$, that is, the delivered active power is equal to its setpoint and the

curve positioning is the same as depicted in Fig. 20. This ensures that all DG units will dispatch the active power setpoint in grid-connected mode, and thus no other deviation function is needed to achieve the active-power requirement of the DG operation in grid-connected mode. Moreover, it allows the grid-operator to indirectly control the DG participation on the active power dispatch by imposing a controlled frequency deviation. This frequency deviation will be exactly the deviation, $\delta\omega_{ref}$, which determines the ratio between the active-power dispatch and the available power. The gain k_ω of the integrator in Fig. 19a, as well as the sliding limits and protection block will be explained after the following description of the reactive-power sliding control.

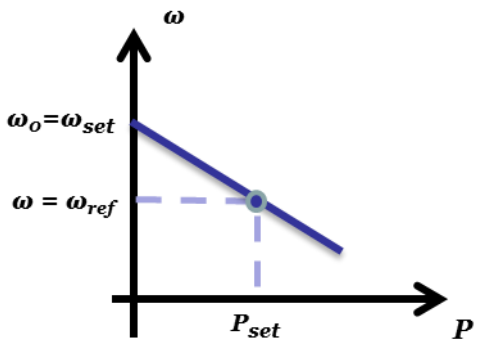

Fig. 20: Ideal active-droop curve positioning with regulated frequency.

Since the droop curves are used with fixed slope (D_p is constant) and in a pu system, ω_{set} (relative to P_{set} in Fig. 20) can be defined as:

$$\omega_{set} = \omega_{ref} + \frac{P_{set}}{D_p} \tag{4.14}$$

The proposed control method allows the D_p adjustment without compromising the frequency deviation in steady state, which is determined by $k_{S\omega}$. For instance, D_p can be set as

$$D_p = -\frac{\Delta \mathrm{P}}{\Delta \omega} = \frac{1pu}{\Delta\omega_{max}} \tag{4.15}$$

In this sense, by observing Fig. 18 with D_p set as eq. (4.15), the maximum allowed frequency deviation $\Delta\omega_{max}$ is the deviation between ω and ω_0 that causes $1\,pu$ of response in terms of mechanical torque (or control effort). This means that $\Delta\omega_{max}$ is related to the proportional response (primary response) of the DG units, which may be field adjustable and determined by the area EPS operator according to [43]. In practice, this adjustment can be done by both D_p or $\Delta\omega_{max}$.

Finally, the sliding droop control has to cover the special case when no active-power is available, that is, when $P_{set} = 0\,pu$. In this case, the no-load frequency has to be equal to ω in steady state, and thus the rule stated in (4.10) is substituted by (4.16).

$$\begin{aligned} if\ \omega_0 > \omega \ \ &\therefore\ slide\ down;\ output = -1 \\ if\ \omega_0 < \omega \ \ &\therefore\ slide\ up;\ output = +1 \end{aligned} \tag{4.16}$$

Now the same reasoning will be developed to the reactive power. The deviation function for the reactive power control is:

$$\delta V_{ref} = -k_{SV} Q, \tag{4.17}$$

where k_{SV} is the maximum voltage-amplitude deviation allowed. The gain k_{SV} can be tuned to ensure that negligible voltage deviation is achieved whenever the reactive power of the DG units is enough to regulate the voltage at the bus where the SSG is connected. The sliding direction control block has the following rule:

$$\begin{aligned} if\left(\left\|v_{a,b,c}\right\| > V_{ref} + \delta V_{ref}\right) \quad &\therefore\ slide\ down;\ output = -1 \\ if\left(\left\|v_{a,b,c}\right\| < V_{ref} + \delta V_{ref}\right) \quad &\therefore\ slide\ up;\ output = +1 \end{aligned} \tag{4.18}$$

This rule has a similar purpose as that of (4.11), i.e., this comparison aims to track $\left\|v_{a,b,c}\right\|$ in steady state as:

$$\|v_{a,b,c}\| = V_{ref} + \delta V_{ref}, \tag{4.19}$$

which leads to (4.20) and (4.21), in case of several DG units connected at the same ac bus.

$$\delta V_{ref_1} = \delta V_{ref_2} = \cdots = \delta V_{ref_n}. \tag{4.20}$$

$$Q_1 = Q_2 = \cdots = Q_n. \tag{4.21}$$

Hence, the reactive power sharing is ensured to those DG units.

The setpoint of the reactive power is neglected since it is considered always zero ($Q_{set} = 0\,pu$). Therefore, the ideal positioning of the reactive-droop curve in grid-connected mode and with regulated voltage-amplitude is presented in Fig. 21. The same analysis that leads to equation (4.14) can be done for expressing V_{set}. Thus, since the droop curves are used with fixed slope (D_q is constant) and in pu system, V_{set} (relative to Q_{set} in Fig. 21) can be defined as:

$$V_{set} = V_{ref} + \frac{Q_{set}}{D_q} = V_{ref}\ , \quad (Q_{set} = 0) \tag{4.22}$$

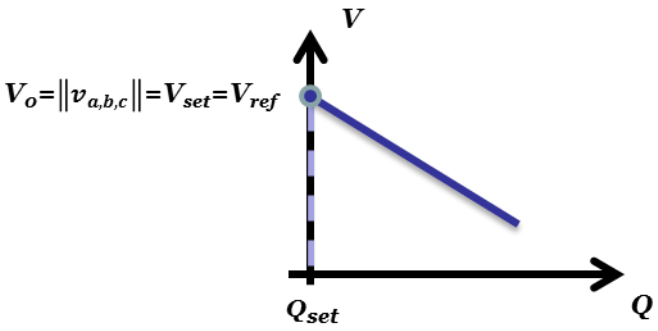

Fig. 21: Ideal reactive-droop curve positioning with regulated voltage-amplitude.

The proposed control method allows the D_q adjustment without compromising the amplitude deviation of the voltage in steady state, which is determined by k_{SV}. For instance, D_q can be set as:

$$D_q = -\frac{\Delta \mathrm{Q}}{\Delta \mathrm{V}} = \frac{1pu}{\Delta V_{max}} \tag{4.23}$$

Once again, the maximum deviation ΔV_{max} is the amplitude deviation that causes the DG unit response equal to $1\,pu$ of reactive-power injection (inductive or capacitive) into the grid. In this way, the same considerations can be ensured for field adjustment in accordance with [43].

For the reactive-power sharing, the sliding droop control has to ensure SSG operation without overload condition. This condition would be reached if the generated reactive power is not enough to perform voltage regulation within the desired limits. In this case, the no-load voltage has to be controlled in order to guarantee the reactive-power injection within the nominal power in steady state, and thus the rule stated in (4.18) is substituted by (4.24).

$$\begin{aligned} &if(Q > 1.0\,pu) \quad \therefore slide\ down\ (-1) \\ &if(Q < -1.0\,pu) \quad \therefore slide\ up \quad (+1) \end{aligned} \tag{4.24}$$

The integration gains k_ω and k_V in Fig. 19 are responsible to determine the speeds that the curves slide, and then can be tuned according to typical time responses of hierarchical secondary controllers. Since the inputs of these integrators are logic variables (+1 or –1), the integration gains k_ω and k_V determine the $\delta\omega_0$ and δV_0 sliding speed, in pu/s, respectively.

The sliding limits and protection block avoids undesirable behaviors that can arise during a faulty power system, which can be derived from the sliding curves outside the

limits. In other words, under abnormal situations, these control blocks prevents the placement of the droop curves in areas that degrade the proper functioning of the DG units. The anti wind-up control block interrupts the integration effect whenever the sliding limits and protection block acts.

Although this sliding limits and protection block is presented in the sliding droop controller, in this work, abnormal situations such as those found in the aforementioned faulty power system will not be investigated. Therefore, further enhancements should be performed in the future with thorough studies focusing on several distinct scenarios. The strategic position of this block in the arrangement of the controller should be highlighted. With this strategic position the droop curves are always protected against erroneous placement since the values of the no-load parameters are supervised.

In this work, the sliding limits and protection block was designed specifically to deal with overload condition for the active-power control, and to avoid erroneous droop curve positioning for the reactive-power control. In overload conditions the no-load frequency cannot slide below the limit in which ω would achieve the allowed maximum frequency deviation $\Delta\omega_{max}$ for the active-power setpoint. This means that the no-load frequency is limited above the value $\omega_{0_{min}}$ calculated in (4.25).

$$\omega_{0_{min}} = (\omega_{ref} - \Delta\omega_{max}) + \frac{P_{set}}{D_p} \tag{4.25}$$

For the reactive power, the sliding limits and protection block avoids the droop curve placement beyond the maximum deviation established by ΔV_{max}, for both limits above and under the reference value. This is done by limiting the no-load voltage between the limits calculated in (4.26). This is a redundant protection since the sliding-direction control block already acts against the overload condition.

$$\begin{aligned} V_{0_{max}} &= V_{ref} + \Delta V_{max} \\ V_{0_{min}} &= V_{ref} - \Delta V_{max} \end{aligned} \tag{4.26}$$

Chapter 5 – Validation and performance analysis of the sliding droop control

In this chapter the proposed sliding droop control is analyzed through simulation and experimental tests.

In the last chapter the functionalities of DG units controlled as an SSG with the proposed sliding droop control were introduced. This chapter attempts to evaluate the performance of such units, in order to confirm the compliance with the desired functionalities. In this work, the proposed control method was investigated through simulation analysis and experimental results. Different scenarios were set to validate all features described in the last chapter.

The simulation analyses were done using the PSCAD/EMTDC program. This program is capable of simulating multi-phase power systems. It also permits that a C code is used as the control code of a simulated power-electronic device. This is an important tool, since the control code can be employed posteriorly in the experimental test bench as is or with minor changes. In order to control multiple DG units with a unique control code, a specific protocol was configured. All units use the same control code, but a constructor was built with the stored variables to keep the individual processing of each unit, without interfering with the others.

The experimental results were obtained through two 3.5 kVA prototypes. They were connected in the same bus, which can operate in both islanded and grid-connected modes.

This chapter provides the details about the simulation scheme and analyses for both the stand-alone and microgrid scenarios and defines the experimental bench as well as the results of the performance tests.

Simulation analysis

The DG units were modeled in PSCAD/EMTDC with the same configuration of the experimental prototypes. The same values of the power-circuit components were adopted as well. Moreover, for simplicity, all DG units use the same model in all simulation cases. This model is depicted in Fig. 22.

In Fig. 22a, the general overview is shown as it is seen in the power grid schemes. It is composed of: the Power Electronic Converter block; a signal-output port used to plot the inner variables of the controller (up to fifteen variables of the control code); an input/output (I/O) block; the dc-link interconnection, which is connected with an ideal dc source that emulates an ideal GESS control; and the three-phase ac output with the measurement apparatus.

Fig. 22b shows the power-circuit components contained inside the Power Electronic Converter block, which are: the full-bridge three-phase power electronic converter itself; the switching filter; and the circuit-breaker. As the SSG controller is in per unit system, the component values are also depicted in per unit system. The inductors of the switching-frequency filter (LCL configuration) are modeled with their inner resistances, obtained through measurements in the experimental prototypes.

Finally, in Fig. 22c the blocks for data processing are shown. These blocks are also located inside the Power Electronic Converter block. Basically, these blocks normalize the signals in the same condition they are received in the DSP input-ports of the actual prototype. Therefore, a unique control code can be written to be used in both simulation and experimental prototype. The control code is processed using the normalized signals and the output signals are given back to the power-circuit components.

The parameter values are presented in Table V. In this table the same values of the power-circuit components (found in Fig. 22) are listed along with the control parameters set on the control code. Note that the sliding speed of the $\mathrm{Q}-\mathrm{V}$ curve was tuned much faster than typical dynamic profile of real secondary-controllers, in order to fit the results within a shorter simulation time. This was necessary due to data-storage constraints within the digital simulator.

TABLE V
DG UNIT PARAMETERS

Parameter	**Value**
Power rating (installed capacity of the power-circuit)	$\sqrt{P_N^2 + Q_N^2} = \ 1.4142\ pu$
Switching-frequency LCL filter	$L = 0.142pu, R_L = 0.002pu$ $C \ = \ 47.0pu$ $L = 0.067pu, R_L = 0.001pu$
Time constants H and K	14.4 s and 16.7 s
D_p and D_q, defined as in (4.15) and (4.23)	$200.0pu$ and $10.0pu$
Maximum deviations allowed $\Delta\omega_{max}$ and ΔV_{max}	$0.005pu$ and $0.1pu$
Sliding speeds k_ω and k_V	$5 \cdot 10^{-4}\ pu/s\ and\ 1 \cdot 10^{-2} pu/s$
$k_{S\omega}$ and k_{SV}	$2.5 \cdot 10^{-4}$ pu and $5 \cdot 10^{-2}$ pu

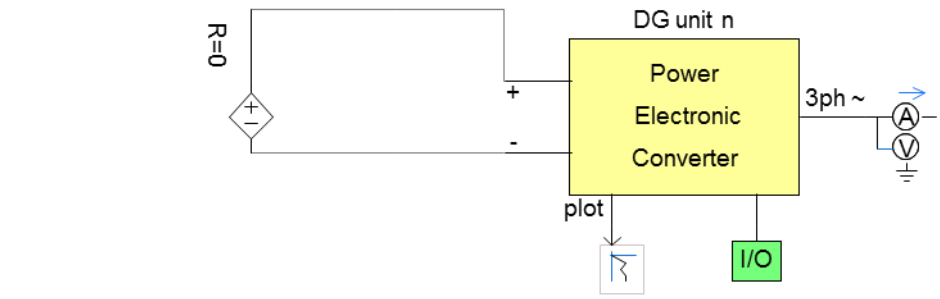

(a)

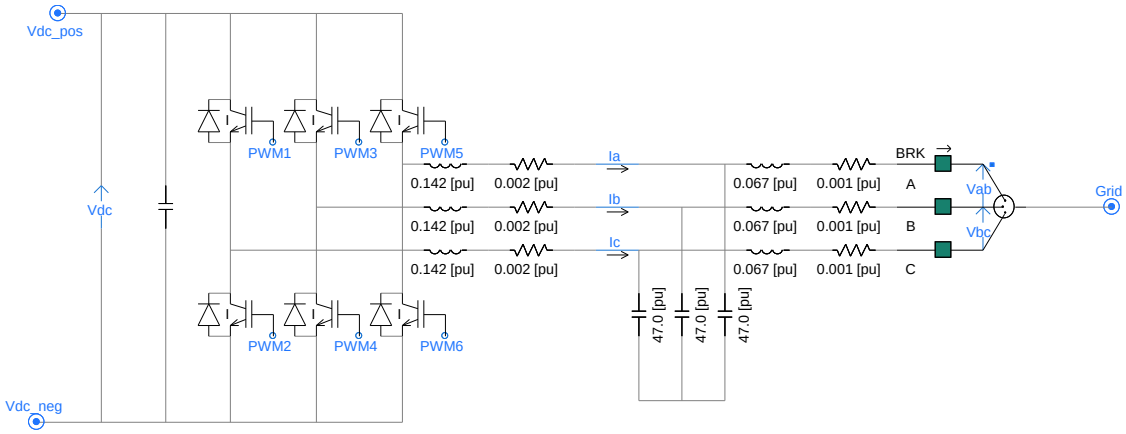

(b)

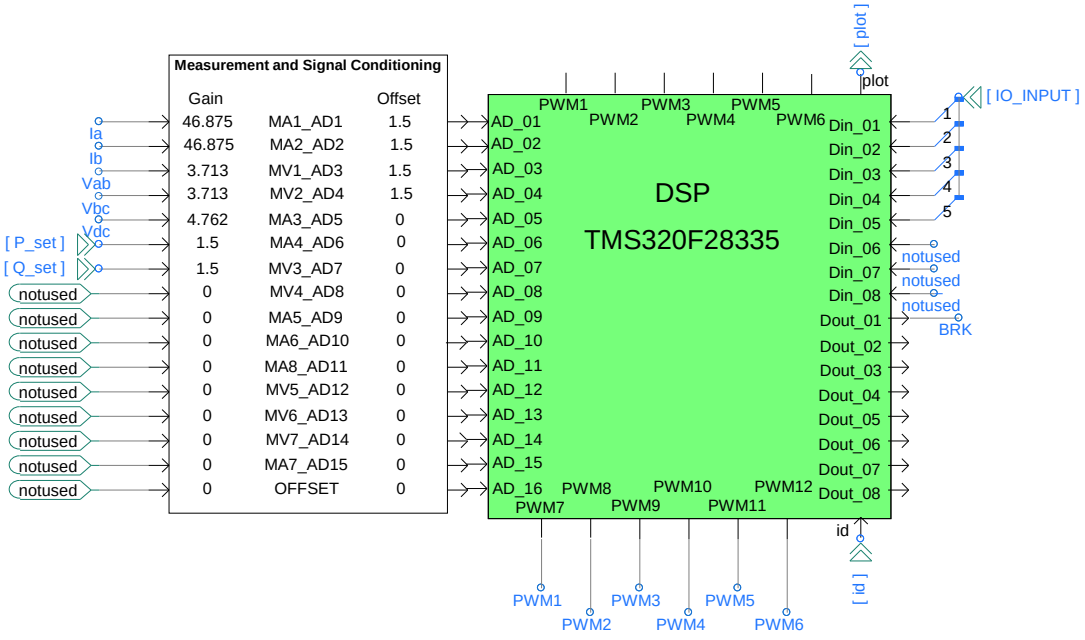

(c)

Fig. 22: DG unit scheme modeled in PSCAD/EMTDC: a) General overview; b) hardware configuration (power circuit); c) hardware configuration (data processing).

Case 1: Stand-alone characteristics

Here the main characteristics of the SSG with the proposed sliding droop controller are studied in stand-alone operation. In this way, some different scenarios are proposed. In scenario 1, normal operation and overload condition are analyzed; in scenario 2, the dynamic responses of the SSG are evaluated for the two possible transitions of the microgrid operation mode (grid-connected to islanded mode and vice-versa); scenario 3 verifies the effects produced by unbalanced and harmonic loads; in scenario 4, the SSG performance is investigated regarding the influence of the virtual inertia, the slope of the droop curve, and the sliding droop control on the dynamic response.

- **Scenario 1: isolated microgrid and overload analysis**

Fig. 23 depicts the grid overview for this scenario. The system events are presented in Table VI.

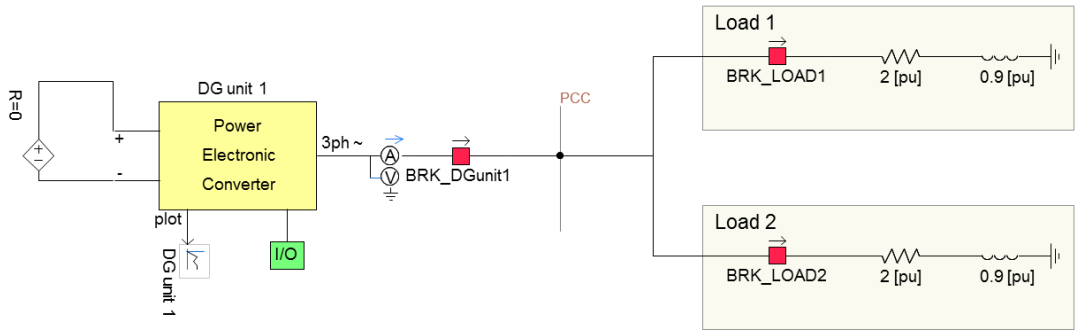

Fig. 23: SSG in stand-alone operation: scenario 1.

TABLE VI
SCENARIO 1: SYSTEM EVENTS

Event	Time
Load 1 connected (BRK_LOAD1 closed)	Initial condition
DG unit 1 starts up with $P_{set} = 0.5\ pu$	1.14 s
Load 2 connection	30.0 s

From the initial condition until $t = 30.0\ s$, only Load 1 was connected at the PCC. In this way, the system was operating under normal conditions, as can be seen in Fig. 24, with the active-power under the P_{set} limit and the reactive-power under the maximum limit ($1\ pu$). The system is in overload condition after $t = 30.0\ s$, because load 2 is connected, which increases the active-power, thus exceeding the P_{set} limit.

As the reactive-power is always lower than $1\ pu$, the SSG is always capable of providing the reactive-power demand. Hence, the voltage is regulated within the maximum voltage-amplitude deviation allowed (see k_{SV} value and the rms voltage, V_{rms} in Fig. 27, measured by the voltmeter at the PCC).

The same is not true for the frequency. In Fig. 26 the behavior of the sliding droop control can be observed through the frequency ω and the no-load frequency (ω_0) positioning. When the SSG control starts, ω_0 is in its starting position ($\omega_0 = \omega = \omega_{ref} = 1pu$ for black-start operation), and then the frequency drops according to the inertia H. Before the frequency stabilizes according to the D_p slope, the sliding droop control increases ω_0 until the frequency reaches the desired position, determined by the deviation function $\delta\omega_{ref}$ (compare the frequency deviation in Fig. 26 and the output of the deviation function in Fig. 28).

During the overload period, the order is to slide down the droop curve independently of $\delta\omega_{ref}$, since $P > P_{set}$. Therefore, the sliding limits and protection block prevent droop curve placement below the minimum value of the no-load frequency $\omega_{0_{min}}$ stated in (4.25). Note that in this case the frequency deviation obtained in ω indicates that the load demand is higher than the available power ($\omega < \omega_{ref} - \Delta\omega_{max}$). In real application this information should be used to perform protection against abnormal frequency in accordance with pre-stablished clearing time, as explained in Chapter 2. The clearing time has to be properly chosen concerning the capacity of the GESS to support overload condition.

Regarding the proposed functionalities inChapter 4, this scenario validates the performance of suitable frequency and voltage regulation within a predictable margin of error. In steady-state normal operation, the frequency and voltage deviations were within the maximum values allowed, dictated by $k_{S\omega}$ and k_{SV}.

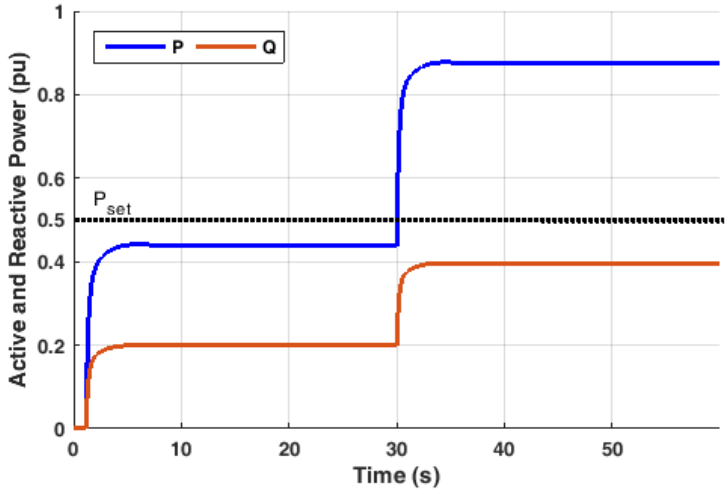

Fig. 24: Case 1, scenario 1: active and reactive power.

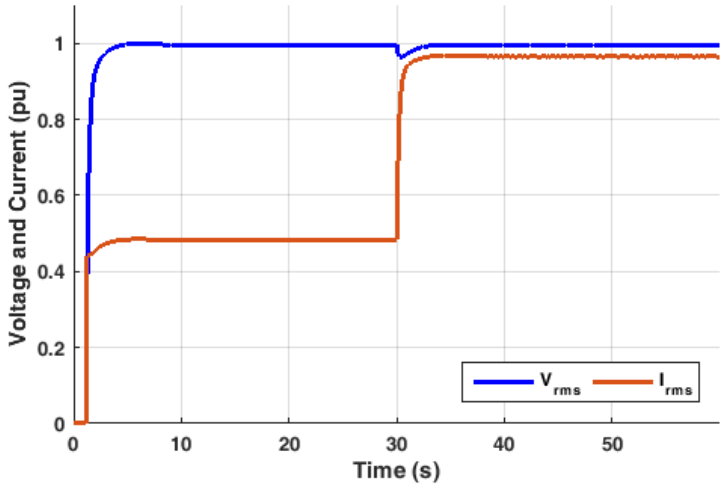

Fig. 25: Case 1, scenario 1: voltage and current.

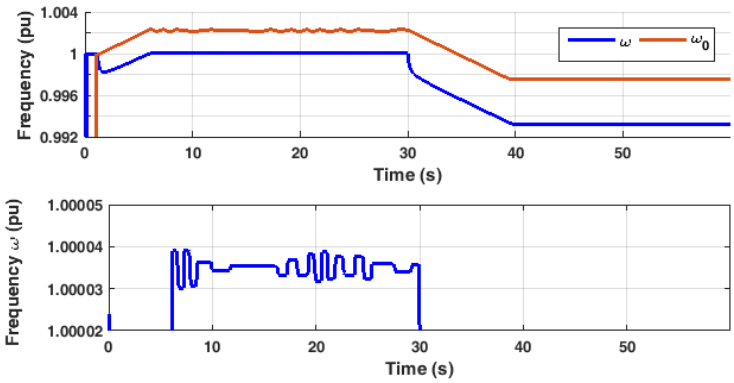

Fig. 26: Case 1, scenario 1: frequencies ω and ω_0.

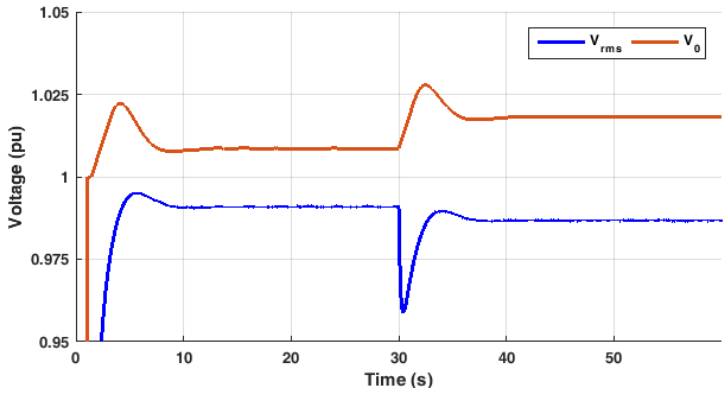

Fig. 27: Case 1, scenario 1: voltages V_{rms} and V_0.

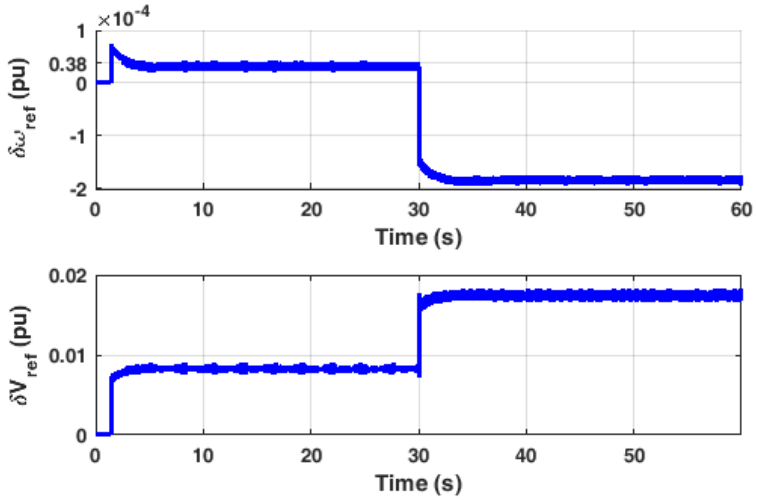

Fig. 28: Case 1, scenario 1: deviation functions $\delta\omega_{ref}$ and δV_{ref}.

- **Scenario 2: transition between microgrid operation-modes**

Fig. 29 depicts the grid overview for this scenario, which is composed of one DG unit, an ideal source representing the grid, and a fixed RL load. Two different simulations are carried out, one for each transition. In the first simulation the microgrid starts in grid-connected mode, and the islanding operation occurs at $t = 30.0s$. The opposite happens in the second simulation, where the microgrid starts in islanded mode and the grid-connection is also realized at $t = 30.0s$. The active-power setpoint is always $P_{set} = 1.0pu$.

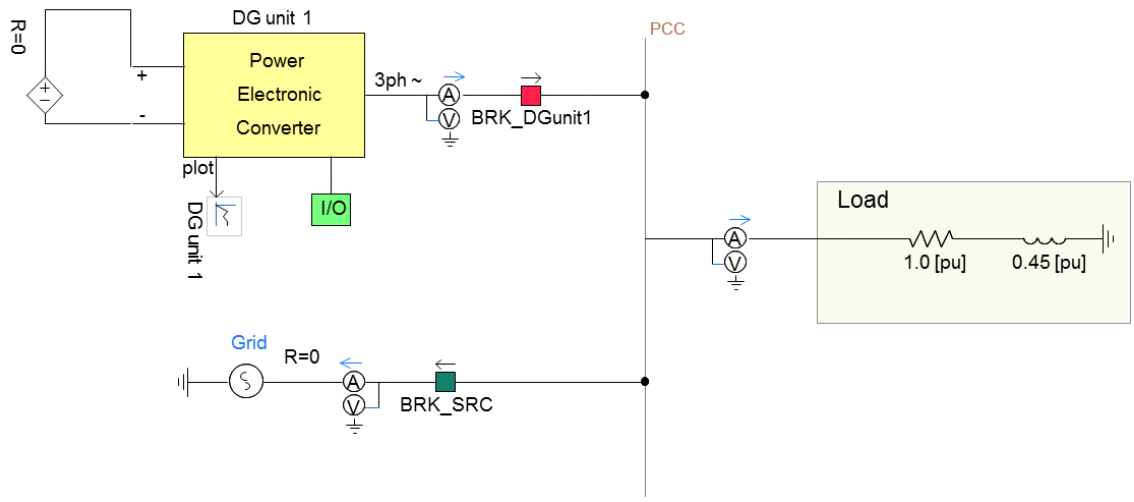

Fig. 29: SSG in stand-alone operation: scenario 2.

The following figures are similar to those obtained in the previous scenario. Fig. 30 depicts the active and reactive powers. Note that in grid-connected mode the DG unit dispatches the active power equal to the setpoint, P_{set}. This covers the proposed functionality of active-power injection according to its setpoint, since the total available power is dispatched to the microgrid. The sliding droop control reaches ω_0 at the maximum deviation ($\Delta\omega_{max}$) in grid-connected mode ($\omega_0 = \omega_{ref} + \Delta\omega_{max}$), and the curve positioning, detailed through ω_0 in Fig. 32, reproduces the ideal situation illustrated in Fig. 20. As the voltage amplitude is imposed and regulated by the ideal source, the reactive power is equal to zero in steady-state.

In Fig. 31 the smooth startup in grid-connected mode can be verified through the current profile during this period. After the startup procedure, the current increases along with the power dispatch. The voltage drop during the islanding transition has the dynamic dictated by the K factor (see Fig. 18), with reduced disturbance. The sliding droop control allows the voltage regulation, in steady state, within the limit of k_{SV}, as depicted in detail in Fig. 33.

The same smooth transition is verified in the frequency dynamic, as shown in Fig. 32. Consequently, those smooth transitions reflect on the current profile verified in Fig. 31 at $t = 30.0s$. Moreover, Fig. 32 shows that the frequency is regulated within the limits of $k_{S\omega}$ throughout the simulation. According to Fig. 34, both frequency and voltage deviations, in steady state, follow the deviation functions $\delta\omega_{ref}$ and δV_{ref}.

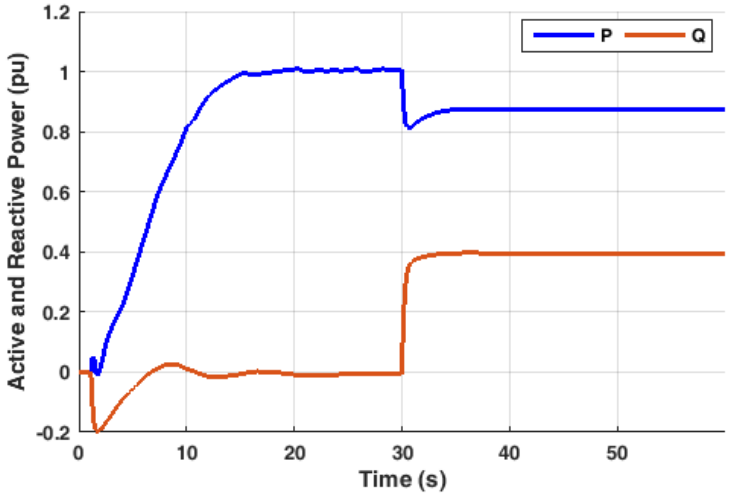

Fig. 30: Case 1, scenario 2, from grid-connected to islanded mode: active and reactive power.

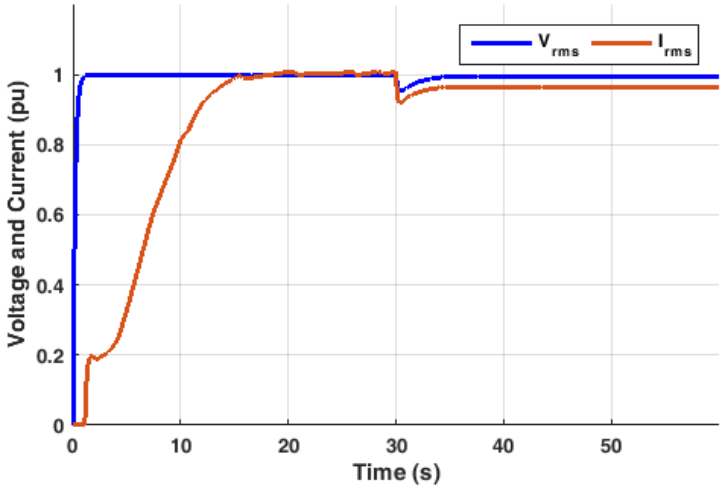

Fig. 31: Case 1, scenario 2, from grid-connected to islanded mode: voltage and current.

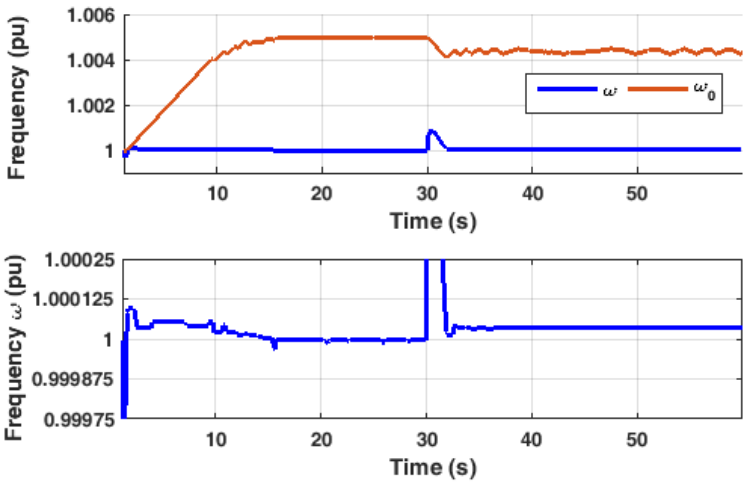

Fig. 32: Case 1, scenario 2, from grid-connected to islanded mode: frequencies ω and ω_0.

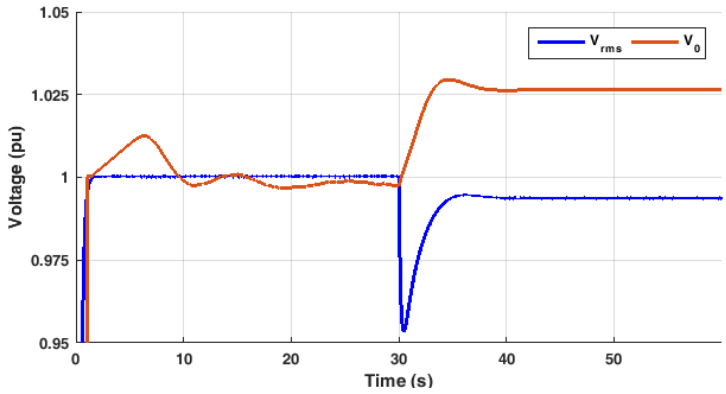

Fig. 33: Case 1, scenario 2, from grid-connected to islanded mode: voltages V and V_0.

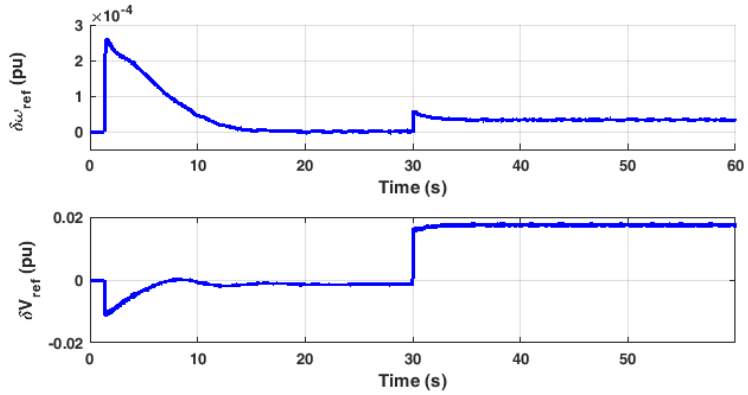

Fig. 34: Case 1, scenario 2, from grid-connected to islanded mode: deviation functions $\delta\omega_{ref}$ and δV_{ref}.

Fig. 35 to Fig. 39 show the results of the second simulation. The same analysis can be done for the smooth transition between modes. Here, an important observation should be highlighted. The voltages in the microgrid and in the grid were configured to be in phase at the moment of the circuit-brake closing (BRK_SRC in Fig. 29). At this moment, the deviations of frequency and voltage-amplitude between the grid and the microgrid were given by $\delta\omega_{ref}$ and δV_{ref}, respectively. These deviations are much lower than the maximum allowed values for synchronization procedures, which is a result of the proposed control. An example of these limits was pointed out in Chapter 2 ($\Delta f = 0.3\,Hz$, $\Delta V = 10\%$ and $\Delta\phi = 20°$). In case of a non-smooth response due to increased deviations, special controllers can be employed during the reclosing of the microgrid to the grid, such as the use of dynamic virtual inertia and dynamic virtual impedance. However, these issues are out of the scope of this work.

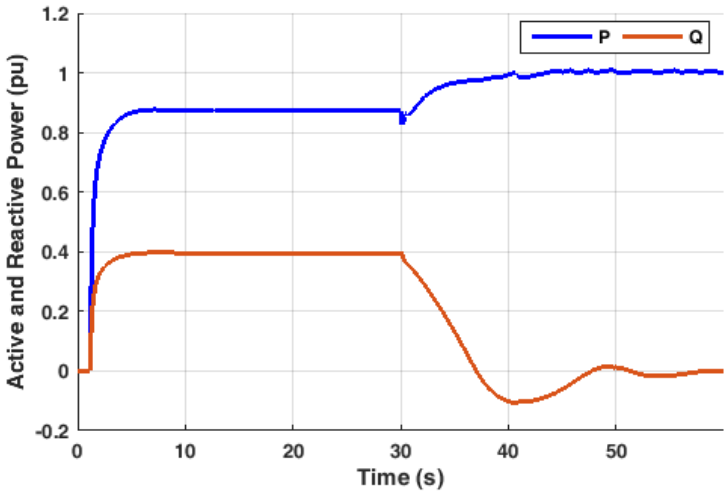

Fig. 35: Case 1, scenario 2, from islanded to grid-connected mode: active and reactive power.

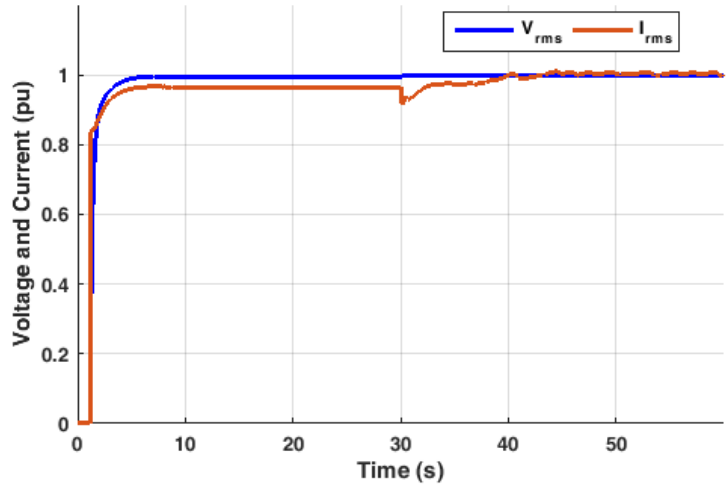

Fig. 36: Case 1, scenario 2, from islanded to grid-connected mode: voltage and current.

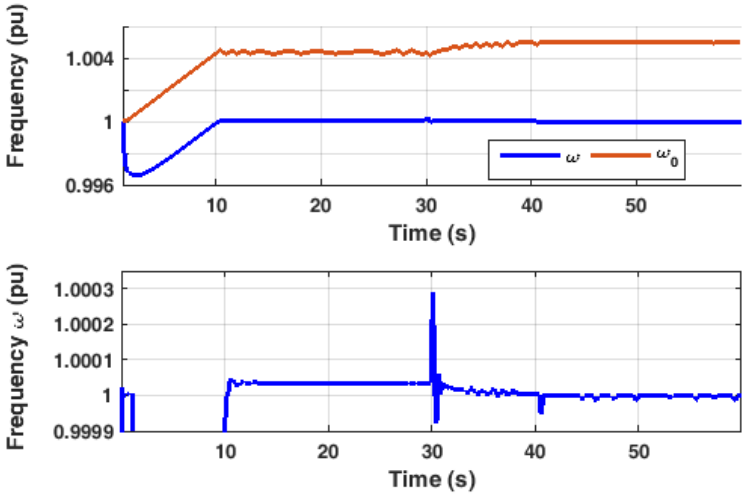

Fig. 37: Case 1, scenario 2, from islanded to grid-connected mode: frequencies ω and ω_0.

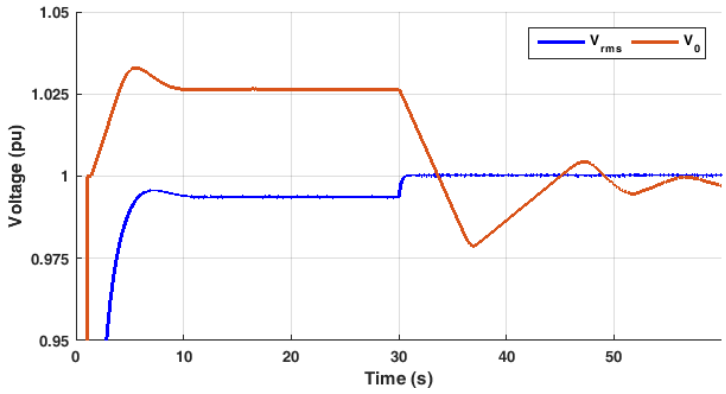

Fig. 38: Case 1, scenario 2, from islanded to grid-connected mode: voltages V_{rms} and V_0.

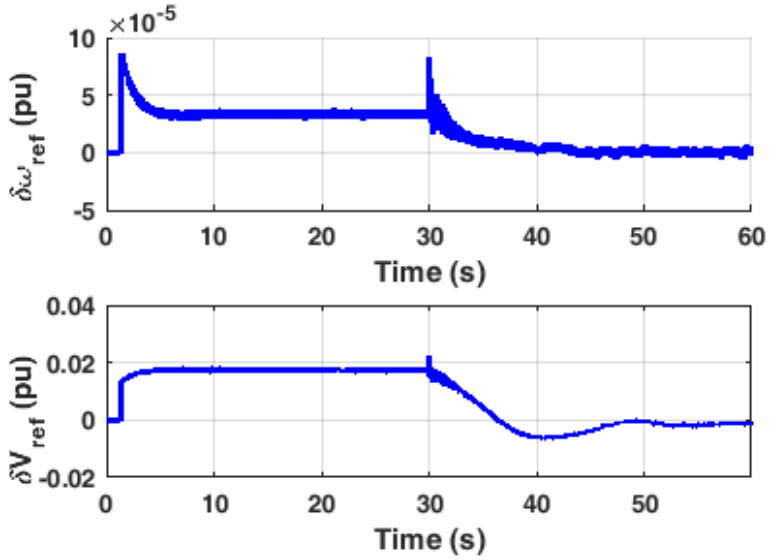

Fig. 39: Case 1, scenario 2, from islanded to grid-connected mode: deviation functions $\delta\omega_{ref}$ and δV_{ref}.

- **Scenario 3: unbalanced and harmonic loads**

Although the proposed functionalities in Chapter 4 do not mention any criterion regarding unbalanced and harmonic loads, it is important to evaluate the maintenance of these functionalities when the DG unit is feeding such loads. This importance is even more relevant in the microgrid scenario due to the increased number of these loads in LV networks. Therefore, the scenario depicted in Fig. 40 is composed of the DG unit, an unbalanced load (Load 1) that is connected during the first 30.0 seconds of the simulation, and a harmonic load (Load 2) that is connected during the last 30.0 seconds of the simulation. The active-power set point is always $P_{set} = 1.0pu$.

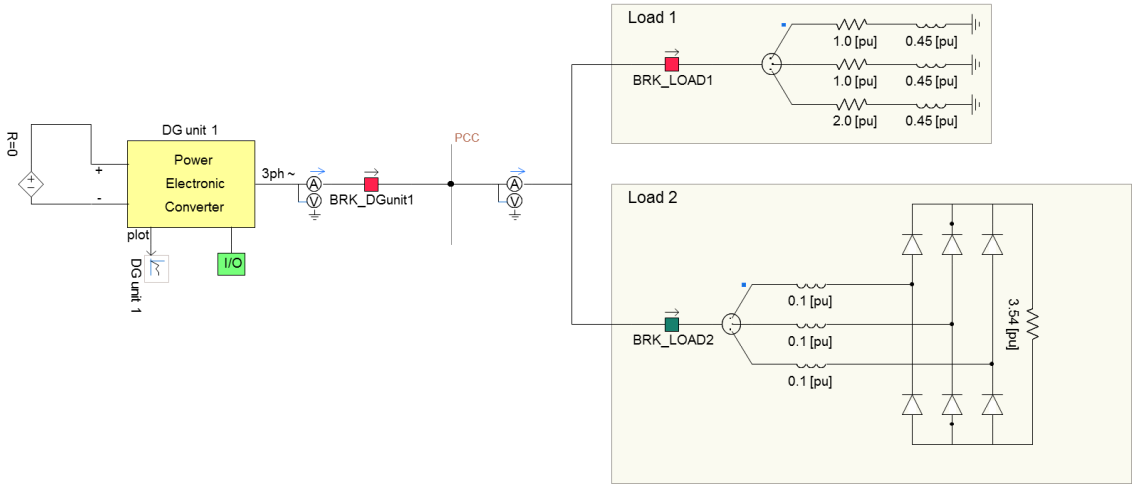

Fig. 40: SSG in stand-alone operation: scenario 3.

Fig. 41 shows the active and reactive powers. The instantaneous and average values are depicted since there is a high oscillating content in such powers. Although this oscillating content is present, during the period when only the unbalanced load is supplied, the SSG provides regulated voltage at the PCC with reduced unbalanced content. This can be seen in Fig. 42 and in detail in Fig. 46. Since there is not a peripheral controller specifically designed to ensure the mitigation of unbalanced content at the terminal voltage, this disturbance is not controlled in this simulation. The unbalanced content is thus dependent on the value of the series impedance of the switching filter and the unbalanced current drained by the load. Hence, for reduced values of inductances in the switching filter, acceptable unbalanced content at the terminal voltage is verified. If it is not sufficient, a peripheral controller has to be employed. The same situation can be verified regarding the harmonic load, as depicted in detail in Fig. 47.

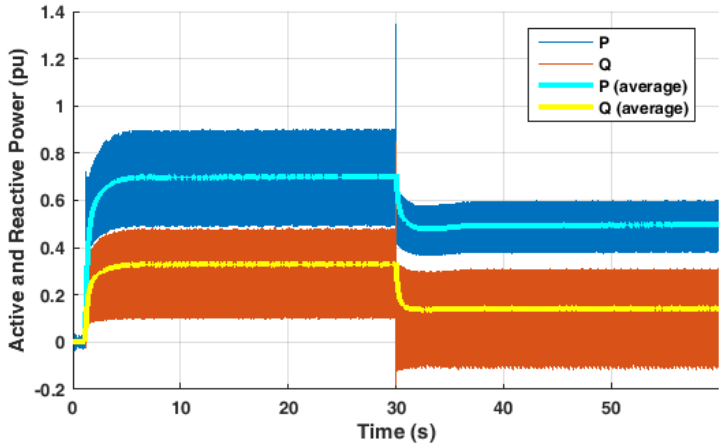

Fig. 41: Case 1, scenario 3: active and reactive power.

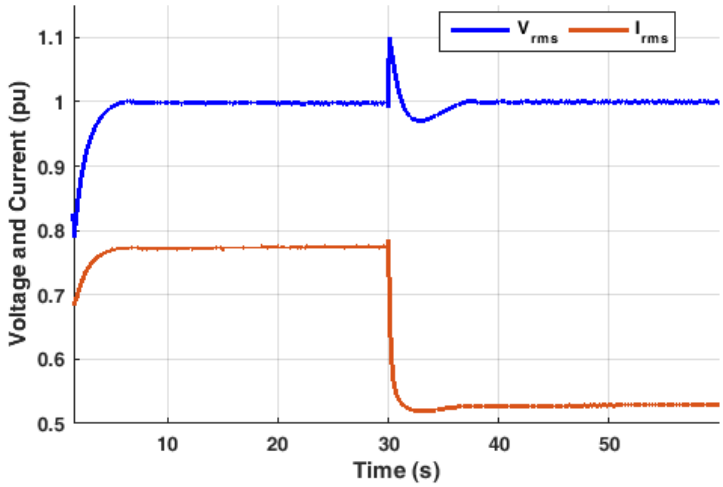

Fig. 42: Case 1, scenario 3: voltage and current.

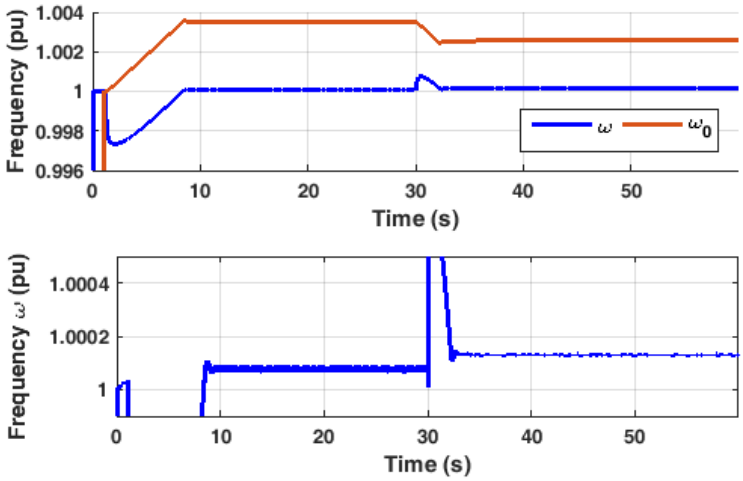

Fig. 43: Case 1, scenario 3: frequencies ω and ω_0.

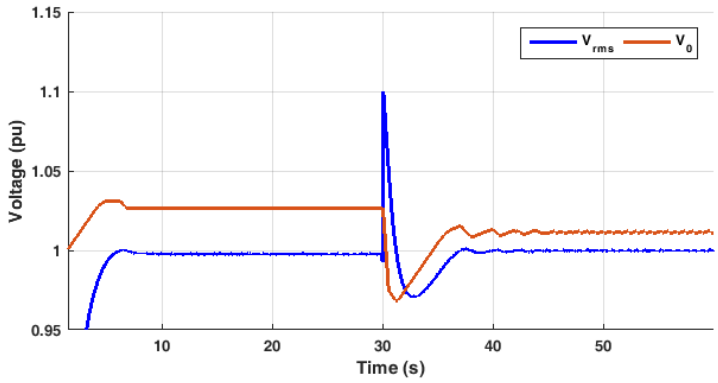

Fig. 44: Case 1, scenario 3: voltages V and V_0.

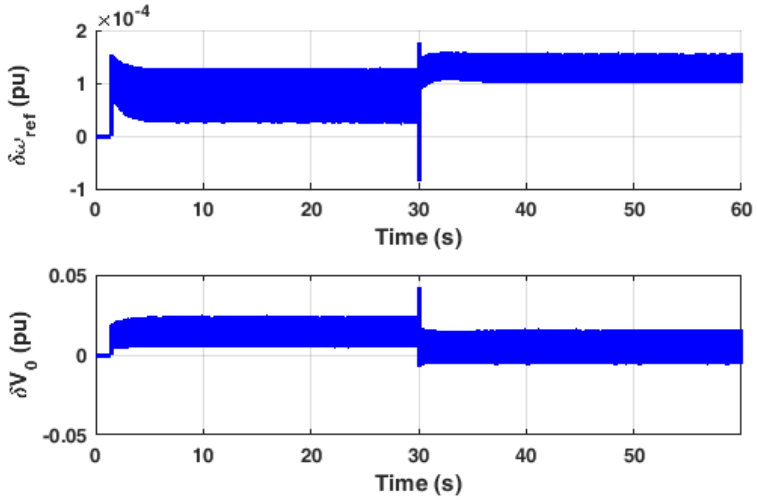

Fig. 45: Case 1, scenario 3: deviation functions δω_ref and δV_ref.

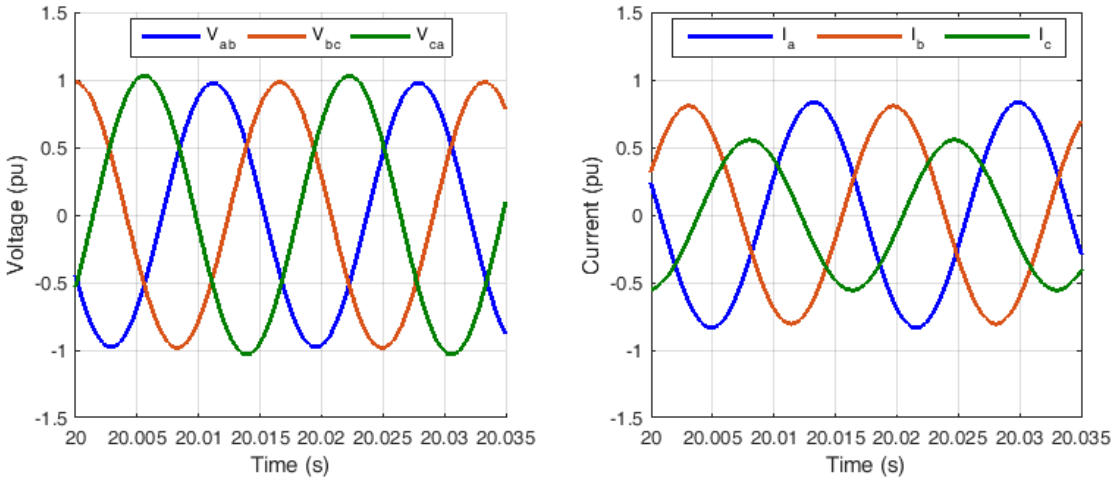

Fig. 46: Case 1, scenario 3: voltages and currents for unbalanced load.

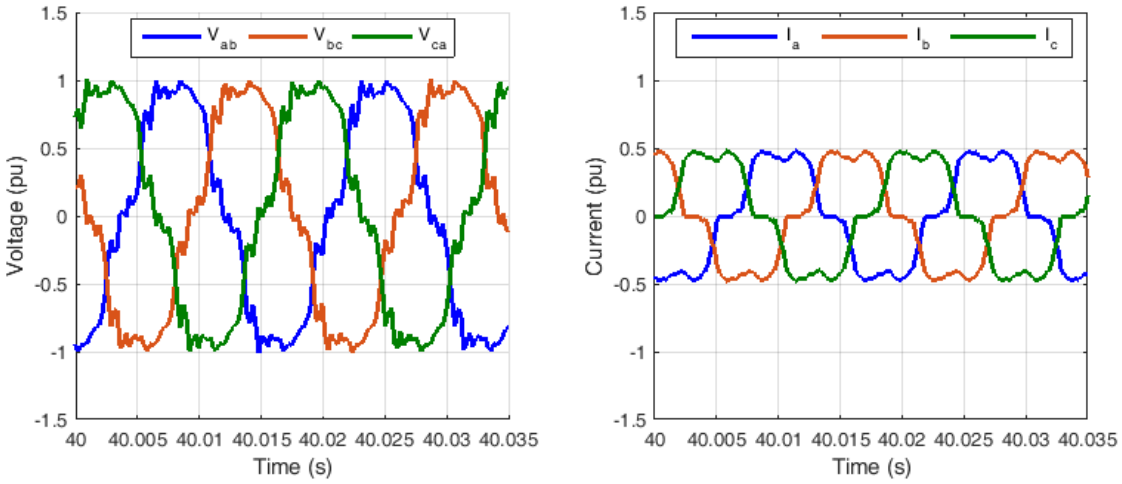

Fig. 47: Case 1, scenario 3: voltages and currents for harmonic load.

Despite the power quality drawbacks caused by the loads, the SSG was able to provide regulated frequency and voltage within the limits of $k_{S\omega}$ and k_{SV}. Note that in Fig. 45 the deviation functions have also an oscillating content, which was expected due to the presence of P and Q in the calculation of $\delta\omega_{ref}$ and δV_{ref}, respectively. However, as depicted in Fig. 43 and Fig. 44, the frequency and voltage amplitude are not affected by this oscillation as the integration gains k_{ω} and k_V are tuned with a slow dynamic and the oscillating frequencies do not interfere on the dynamic behavior of the sliding control.

- **Scenario 4: dynamic response, virtual inertia and the influence of the sliding droop control**

In this scenario, the dynamic of the SSG will be evaluated under changes in the virtual inertia. Moreover, the comparison between the dynamic operation of the SSG with and without the proposed sliding droop control will be provided. Two different disturbances are used to perform these studies: a load step change (load rejection) and a frequency oscillation. The power circuit for the load step change condition is depicted in Fig. 48. The load is connected at $t = 10.0\ s$ and disconnected at $t = 30.0\ s$ with full load rejection at this moment. The active-power setpoint is always $P_{set} = 1.0pu$.

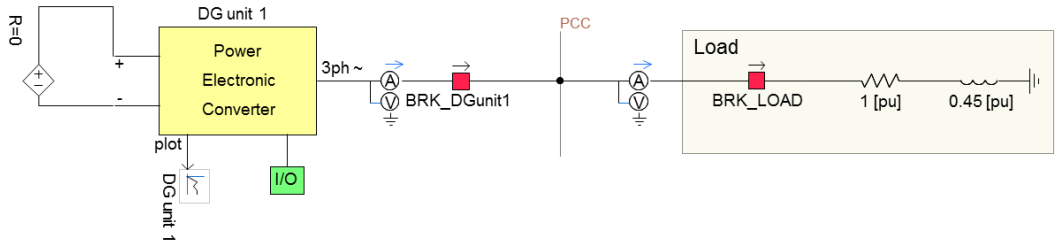

Fig. 48: SSG in stand-alone operation: scenario 4, load step change study (full load rejection).

The above scenario was simulated with three different virtual inertias. Fig. 49 shows the dynamic of the frequency for $H = 1.44, 14.4$, and $28.8\ s$. This figure shows the major influence of the virtual inertia in the dynamic behavior of the SSG during load step changes. This effect is highlighted by the bottom graph in Fig. 49. Moreover, the oscillation of the no-load frequency ω_0 is increased for higher virtual inertia values.

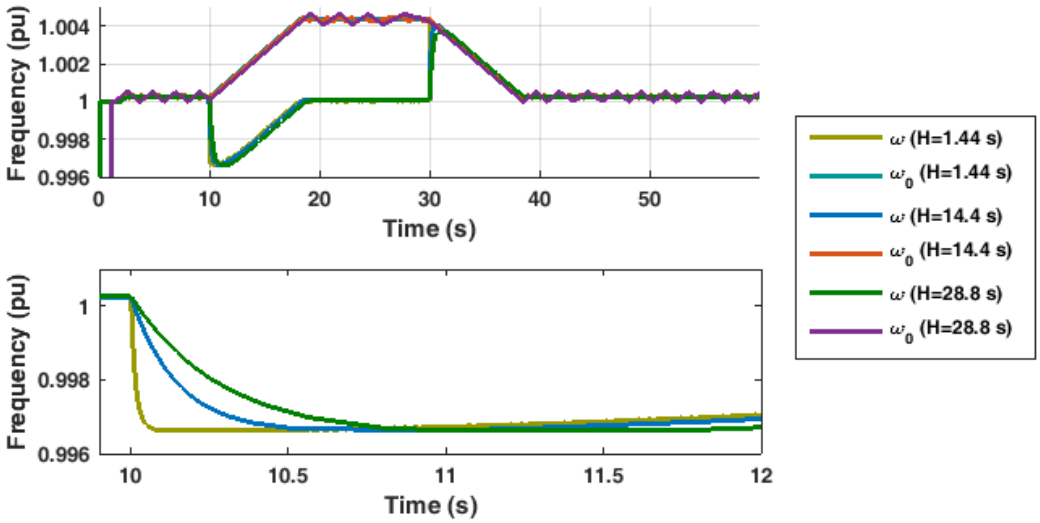

Fig. 49: Case 1, scenario 4: frequencies ω and ω_0 with sliding droop control.

When the virtual inertia is increased, the sensibility of the frequency ω is reduced. In other words, the higher the adopted virtual inertia, the slower the change in the frequency ω in response to a variation in the virtual electromagnetic torque in the SSG due to step changes in the load (step changes in the supplied active power). After the quick response effect in ω, in a similar way as that caused by the primary control level of a rotational synchronous machine, the upper graph in Fig. 49 shows the slower restoration of frequency provided by the sliding in the droop curve positioning, in a similar way as that of the secondary control level implemented in a real synchronous machine. Unfortunately, the effect of the sliding droop control is more significant and

undamped at higher virtual inertia values. One possible solution for reducing this oscillation is to tune the integration gain k_ω to slow down the speed of the sliding. This is similar to increasing the time response of a secondary controller applied to real generators with high inertia.

In Chapter 4 the drawback of increased magnitude of frequency deviation in a conventional (static) droop method was addressed. The adoption of high D_p gains can be considered as a solution to achieve reduced frequency deviation with static droop curves. However, in this case the dynamics of the SSG is severely impacted by the droop gain, and the ability of the virtual inertia to provide frequency stability in an area EPS is significantly reduced. This effect is observed in the example of Fig. 50, where the slope of the droop curve is defined as $D_p = 1/k_{S\omega} = 4000.0\,pu$ in order to achieve the same steady-state deviation of the sliding droop control.

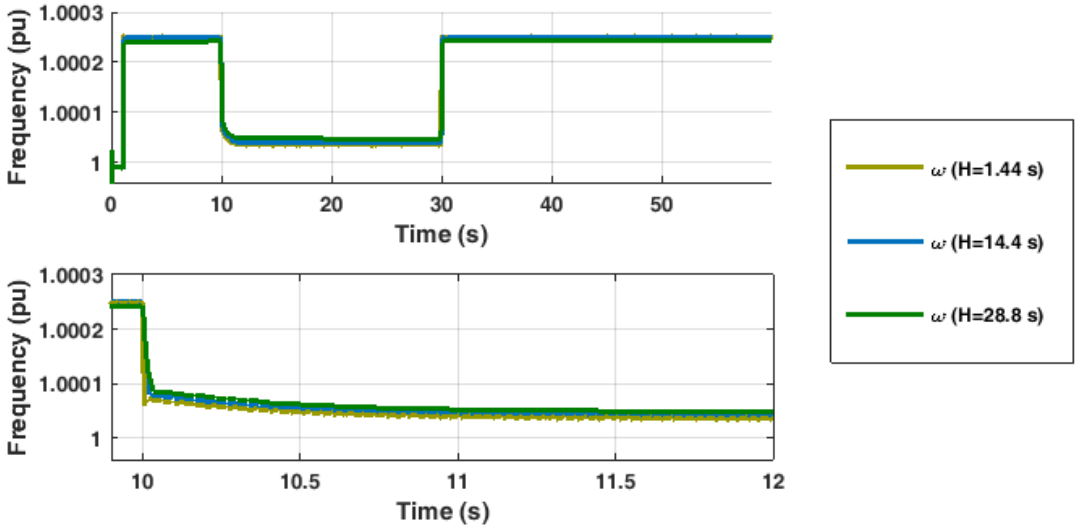

Fig. 50: Case 1, scenario 4: frequency ω with fixed droop curve and $D_p = 4000.0pu$.

If the slope of the static droop curve has the same value of that adopted in the proposed controller ($D_p = 200.0\,pu$), as depicted in Fig. 51, the dynamic performance of the SSG is again dictated by the virtual inertia, but the frequency deviation in steady state is compromised. Hence, for the SSG with static droop curve, if the slope of the droop curve is nearly flat (high values for D_p gain), then a reduced steady-state frequency deviation is achieved, but the major effect of the virtual inertia in the dynamic response is lost. On the other hand, if suitable slope of the droop curve is employed, then the major effect of the virtual inertia is ensured, but the frequency deviation in steady state is compromised.

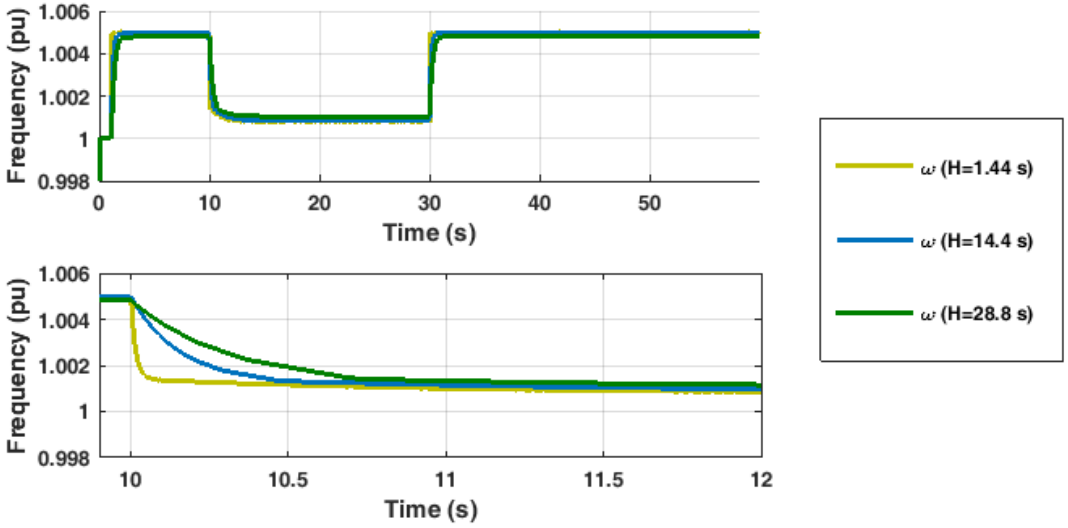

Fig. 51: Case 1, scenario 4: frequency ω with fixed droop curve and $D_p = 200.0pu$.

Once the analysis of the dynamic response of the SSG with the proposed controller for load step changes was made, the response to frequency oscillations was evaluated. The power-circuit used for the frequency-oscillation study is depicted in Fig. 52. The ideal source represents a strong bus ("infinite bus") of a large EPS compared to the rated power of the SSG. The voltage amplitude of this "infinite bus" is fixed at $1.0\,pu$, and the frequency is controlled to reproduce a undamped power frequency oscillation. The active-power setpoint of the SSG is fixed at $P_{set} = 0.5\,pu$.

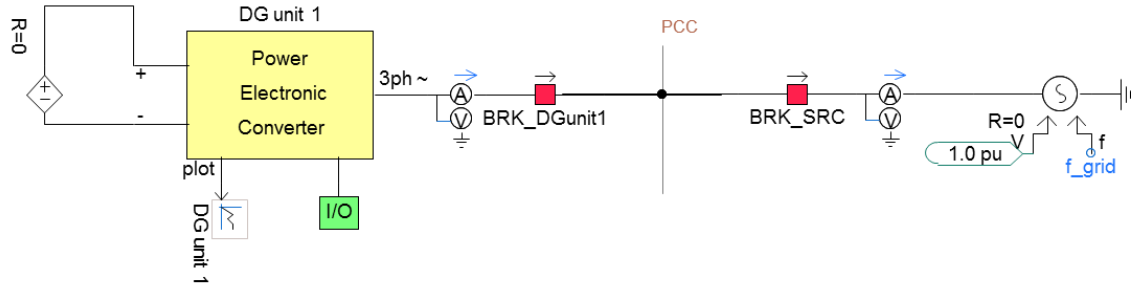

Fig. 52: SSG in stand-alone operation: scenario 4, frequency-oscillation study.

In order to evaluate the synchronous performance for the aforementioned disturbance, some operational restrictions have been neglected. In this simulation, the power electronic converter is considered as able to support increased overcurrent, thus no protection system was applied to avoid it. Moreover, the clearing-time for abnormal frequency oscillation is disregarded and the dc source that emulates an ideal GESS control is considered as able to provide any active-power demanded during the transient period.

In Fig. 53 the grid frequency, ω_{grid}, is depicted. This frequency oscillates with a sag of $0.0333\,pu$ in $2.0\,s$, followed by a recovery ramp of $30.0\,s$ to return to the nominal value. Fig. 54 shows in details the inner frequency ω of the SSG controller that varies in response to the ω_{grid} oscillation. The no-load frequency ω_0 decreases with a sliding speed given by k_ω until it reaches the minimum value allowed, according to $\omega_{0_{min}}$ determined in (4.25). The $\omega_{0_{min}}$ value is assumed until the instantaneous active power goes back within the P_{set} range (see Fig. 55), when ω_0 starts to increase again until it restores the steady-state condition.

Note that during the falling period of ω_{grid}, the sliding of ω_0 does not decrease in the same manner as that of ω_{grid}. As the sliding speed determined by k_ω is slower than the ω_{grid} negative ramping, the dynamic response of the SSG is predominantly dictated by the slope of the droop-curve (D_p gain) and the virtual inertia H. In conclusion, the above analysis shows that the proposed sliding droop control preserves the dynamic performance of the SSG by disaggregating the frequency deviation in steady state from the D_p gain.

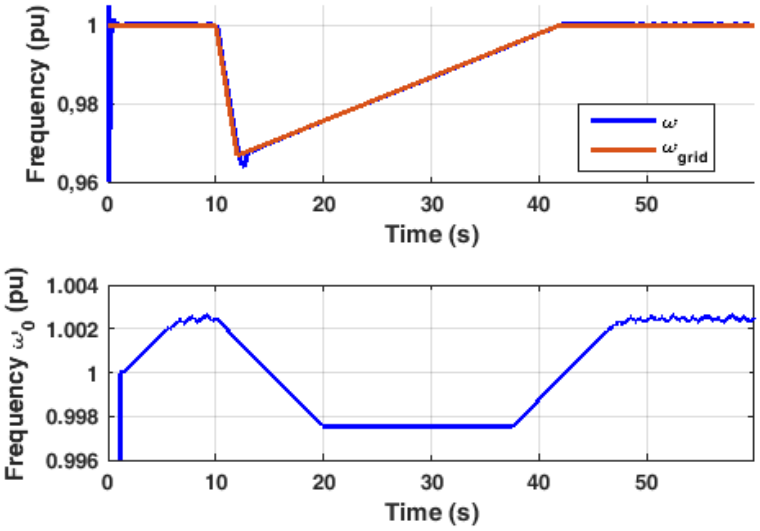

Fig. 53: Case 1, scenario 4: frequency-oscillation response, ω, ω_{grid} and ω_0.

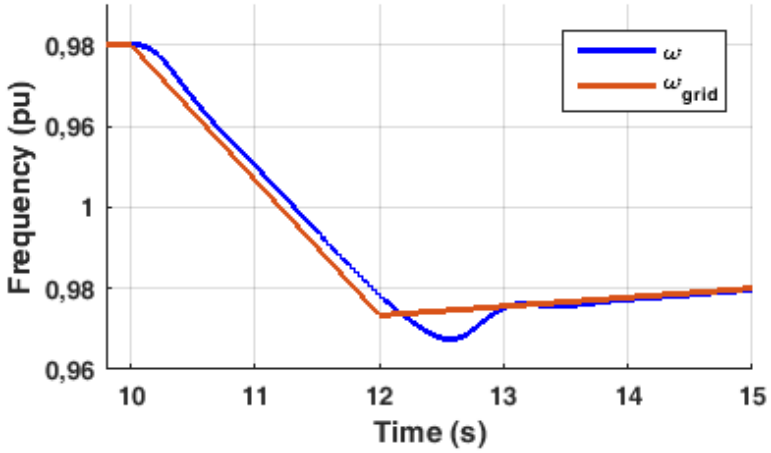

Fig. 54: Case 1, scenario 4: frequency-oscillation response, ω and ω_{grid} in detail.

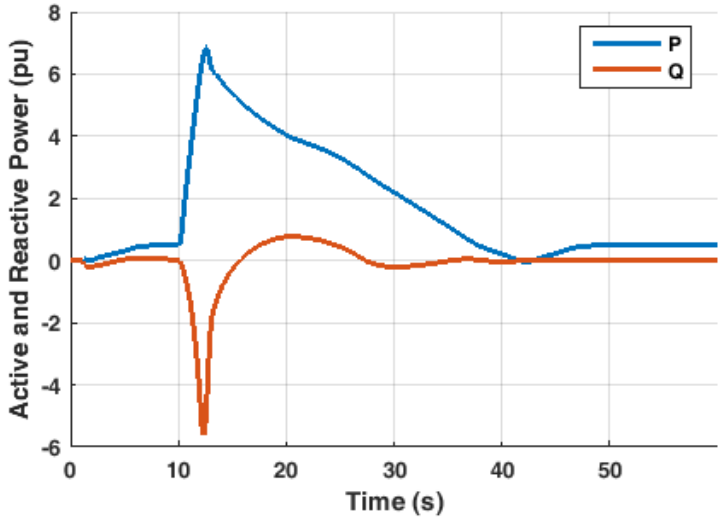

Fig. 55: Case 1, scenario 4: frequency-oscillation response, active and reactive power.

Case 2: microgrid scenario

This simulation scenario is presented to test the performance of multiple DG units controlled as an SSG with the proposed sliding droop control in a microgrid. Fig. 56 shows the microgrid arrangement. For DG units 1 and 4, $P_{set} = 1.0\,pu$, and for DG units 2, 3 and 5, $P_{set} = 0.5\,pu$ throughout the entire simulation. Thus, the total desired (available) power generation in the microgrid is far greater than the total load in the microgrid. In other words, the SSG control of the DG units cannot deliver the desired active power during isolated mode of operation. The reference values ω_{ref} and V_{ref} are set constant and equal to 1.0 pu, as neither communication channels between

DG units nor a tertiary control level was implemented. The system events are displayed in Table VII.

TABLE VII
SYSTEM EVENTS

Event	Time
Grid disconnected (islanded mode)	Initial condition
Load 1,2 connected	Initial condition
DG unit 1,2,3 and 4 startup (black-start operation)	1.0 s
Load 2 disconnection	50.0 *s*
Load 2 reconnection	100.0 s
DG unit 5 startup	151.0 s
Grid connection	200.5 s

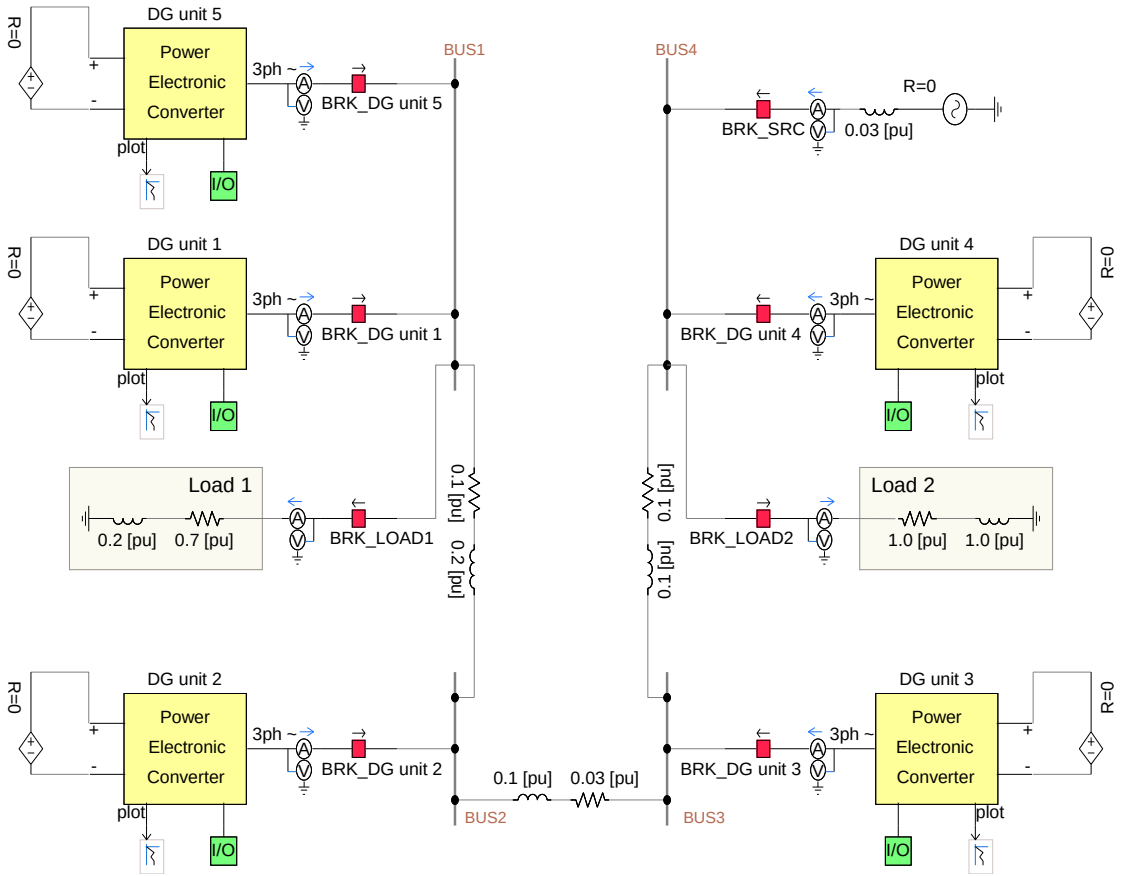

Fig. 56: SSG in microgrid scenario.

Fig. 57 to Fig. 60 present the simulation results with the proposed sliding droop control. In the initial condition the microgrid is in islanded mode, the loads 1 and 2 are connected (BRK_LOAD1 and BRK_LOAD2 are closed), and the microgrid is not

powered since all DG units are off. DG units 1 to 4 start operating from a black-start condition at $1.0\ s$. Fig. 57 shows that the active power is being shared proportionally to the available active power, P_{set}, in each DG unit. This situation is ensured even if the total load changes in the isolated microgrid, which occurs between 50.0 s and 100.0 s when load 2 is disconnected and reconnected. Moreover, in Fig. 58 the frequencies ω for all DG units, in steady state, are kept within the range given by $k_{S\omega}$.

The DG unit 5 starts at $\mathrm{t} = 150.0$ s. After this time, the system achieves a new operating point and the active-power sharing is maintained. Finally, at $\mathrm{t} = 200.5$ s, the microgrid is connected to the grid and then all units start to dispatch their (available) active-power setpoints to the grid. The results prove that the proposed sliding droop control enables the DG units to perform the desired goals for active-power dispatch in both islanded and grid-connected modes of operation.

The reactive-power goals are also satisfied. This can be verified in Fig. 59 through the reactive-power sharing between DG units 1 and 5, which are connected to the same bus. All DG units provide the reactive-power necessary to keep the voltage amplitudes within the range given by k_{SV} in steady state.

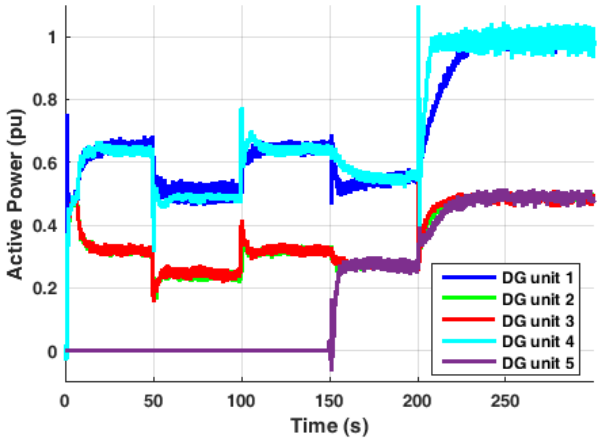

Fig. 57: Case 2, SSG with the proposed sliding droop control; active-power.

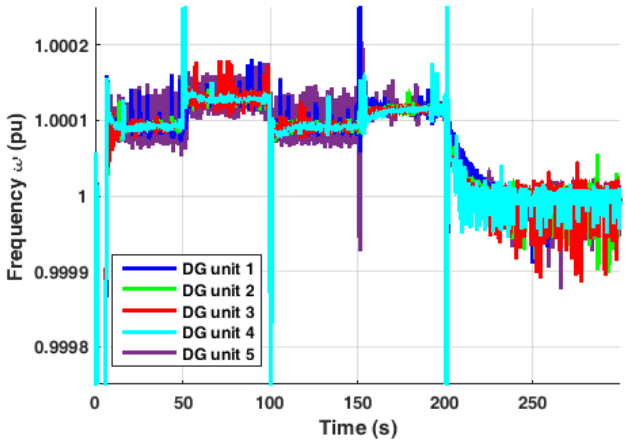

Fig. 58: Case 2, SSG with the proposed sliding droop control; frequency ω.

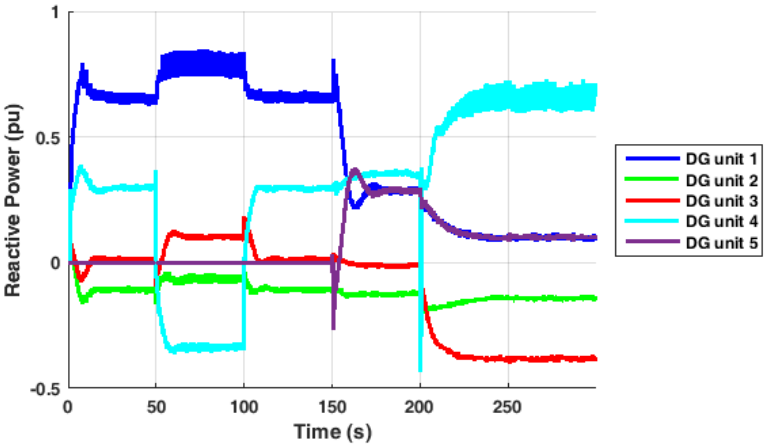

Fig. 59: Case 2, SSG with the proposed sliding droop control; reactive-power.

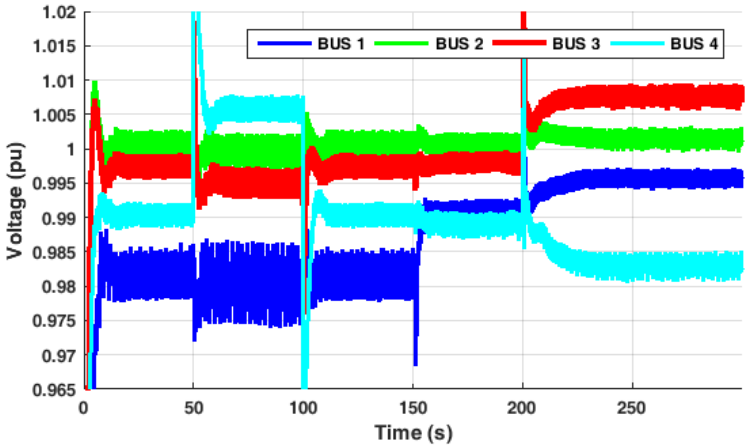

Fig. 60: Case 2, SSG with the proposed sliding droop control; voltage.

Fig. 61 shows in detail the currents of each DG unit during the grid-connection procedure. In this figure it is possible to verify that DG unit 4, which is connected to the same bus where the grid-connection was performed (BUS 4), has a significant

overcurrent, i.e. greater than 1.5 pu in the current of phase b. However, in less than ten cycles this overcurrent is reduced, and the synchronous behavior is maintained as verified in the frequency response (transitory oscillation in Fig. 58). The phase-angle difference between grid and microgrid voltages just before closure of the circuit breaker BRK_SRC was around 9°. It is important to highlight that no special controller was employed here to control the current overshoot. For instance, auxiliary control to realize the concept of virtual impedance could be implemented in each DG unit to avoid overcurrent during out of phase reclosing of the microgrid to the power grid. This auxiliary virtual-impedance control can be implemented without mischaracterizing the virtual synchronous machine behavior of the SSG controller. However, this should be investigated in future work.

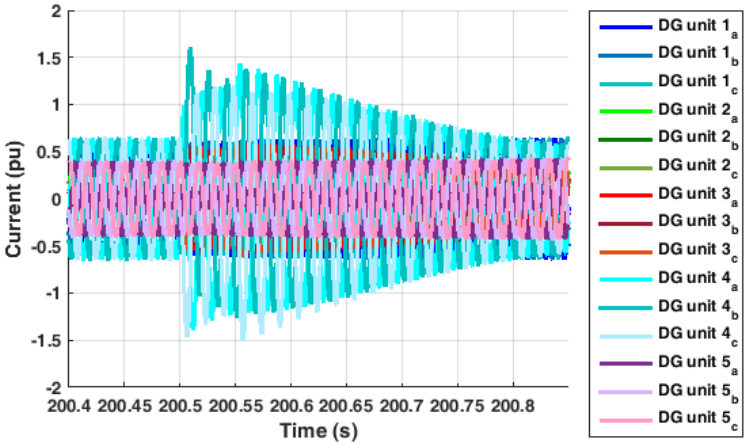

Fig. 61: Case 2, SSG with the proposed sliding droop control; currents at the grid connection.

For comparison, the same system was simulated again with the DG units being controlled as an SSG with conventional (static) droop-curves. The slopes of the curves were fixed with the maximum deviations, i.e. equal to $k_{S\omega}$ and k_{SV} as given in Table V ($D_p = 1 / k_{S\omega}$ and $D_q = 1/k_{SV}$). Fig. 62 shows that the DG units with different active-power setpoints are not able to perform active-power sharing proportionally to the available power. In other words, equation (4.13) and, consequently, equation (4.1), are not satisfied. The frequencies ω of each DG unit in steady state were kept within the limits of $k_{S\omega}$, as expected. This can be verified in Fig. 63. For the reactive-power, as the setpoint is always considered zero ($Q_{set} = 0\ pu$), similar results to those shown in Fig. 59 and Fig. 60 for the sliding droop control in steady state can be found in Fig. 64 and Fig. 65 for the fixed droop-curves. Note that the dynamics are different since the

operating point in the sliding droop control has the effect of restoring frequency, which is not verified by using the original concepts presented in [5].

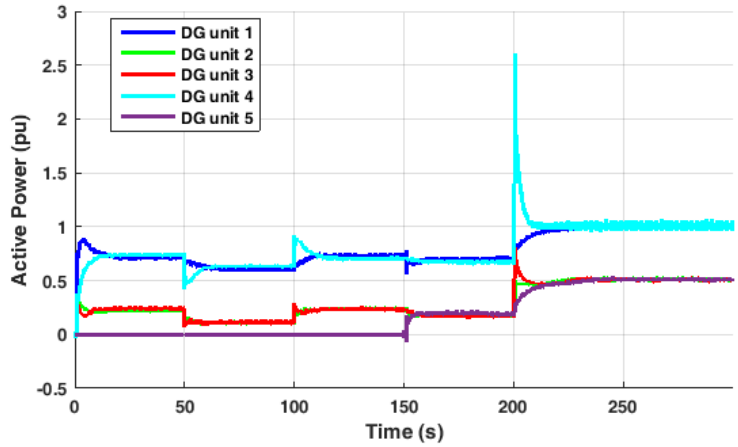

Fig. 62: Case 2, SSG with fixed droop curves; active power.

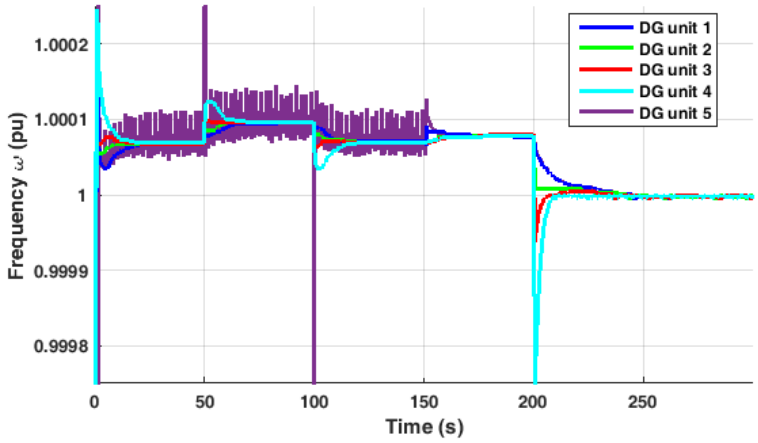

Fig. 63: Case 2, SSG with fixed droop curves; frequency ω.

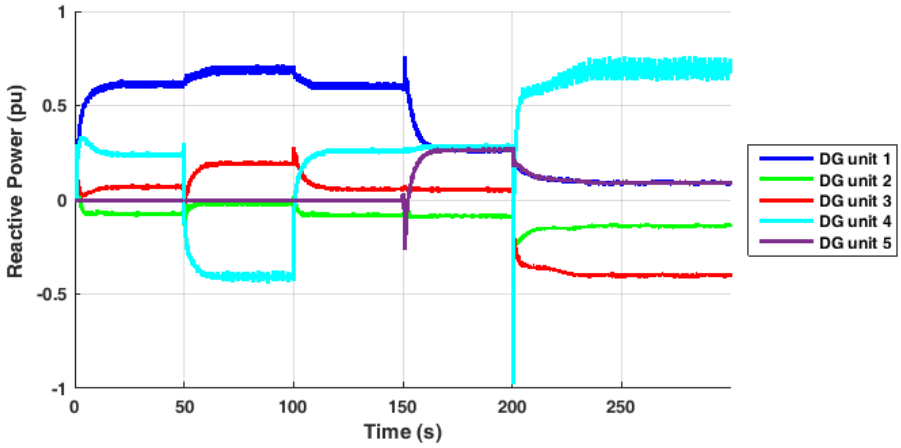

Fig. 64: Case 2, SSG with fixed droop curves; reactive-power.

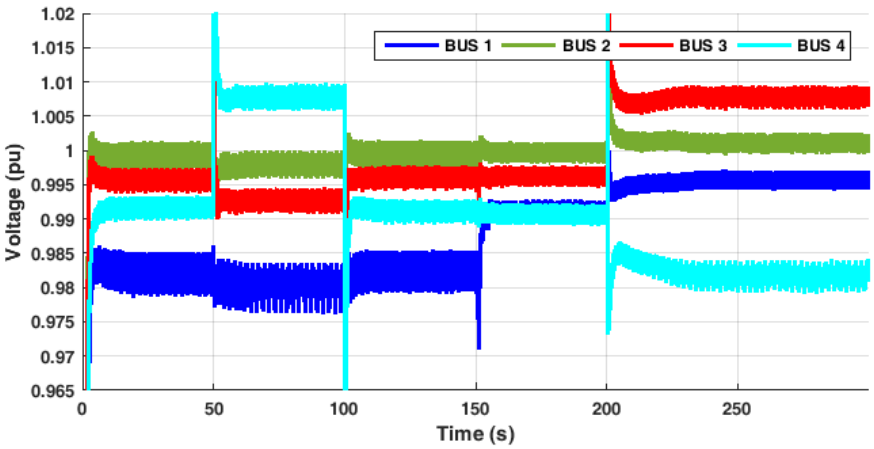

Fig. 65: Case 2, SSG with fixed droop curves; voltage.

Experimental analysis

The experimental test bench is composed of two DG units (DG unit 1 and 2) connected to the same bus, as shown in Fig. 66. The parameter values are the same as those presented in Table V except by the maximum deviations and sliding speeds. The base power is 3.5 kVA, the base ac-voltage is 220.0 V_{rms}, and the dc-link voltage of each DG unit is regulated at 450.0 V_{dc}. The switches S_{L1}, S_{L2}, S_{L3} and S_{GRID} connect load 1, load 2, load 3 to the grid, respectively. The power of the loads is given in pu, according to the base power of the DG units. The maximum deviations and sliding speeds were set as $k_{S\omega} = 1 \cdot 10^{-3} pu$ (0.06 Hz), $k_{SV} = 2 \cdot 10^{-2} pu$ (4.4 V), $k_{\omega} = 5 \cdot 10^{-4} pu/s$, and $k_V = 1 \cdot 10^{-3} pu/s$. An oscilloscope YOKOGAWA DL850EV was employed to measure simultaneously the voltages and currents of the DG units as well as to calculate the powers, frequency and voltage amplitude at the bus.

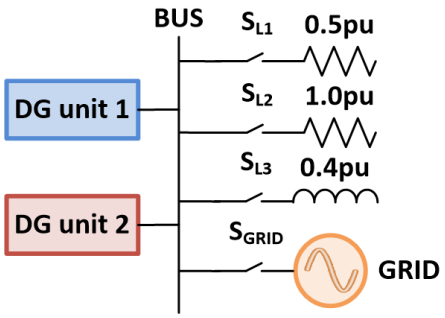

Fig. 66: Experimental bench.

Three different tests were performed. First, the active-power sharing and the frequency regulation were tested in islanded mode. In this test, details about the dynamics of voltage and current are provided during startup and load step changes. The reactive-power sharing and voltage regulation in islanded-mode are evaluated in test 2, and, finally, test 3 presents the performance of the DG units in grid-connected mode.

Test 1: Active-power sharing and frequency regulation in islanded-mode

In this test, the system is operating in islanded mode in order to evaluate the sharing performance and frequency/voltage regulation (S_{GRID} is open). Fig. 67 shows the test performed to evaluate the active-power sharing and the frequency regulation. In this case, only the resistive loads 1 and 2 were employed. Table VIII presents the system events.

TABLE VIII
SYSTEM EVENTS

Event	Time
Load 1 connected and Load 2 disconnected	Initial condition
DG unit 2 in steady state with $P_{set} = 1.0\ pu$	Initial condition
DG unit 1 startup with $P_{set} = 0.5\ pu$	20.0 s
DG unit 1 setpoint change to $P_{set} = 1.0\ pu$	60.0 s
DG unit 2 setpoint change to $P_{set} = 0.5\ pu$	100.0 s
DG unit 2 setpoint change to $P_{set} = 1.0\ pu$	140.0 s
Load 2 connection	160.0 s

It is verified in Fig. 67 that the active-power sharing is obtained with reduced error (1.6% for the worst case). Moreover, the power sharing is achieved independently of the setpoint of each unit, as well as independently from the amount of load. Although the frequency calculated by the oscilloscope is hardly affected by the harmonic contents of the synthesized voltages, the mean value (which represents the fundamental frequency) is kept within the maximum deviation stated by $k_{S\omega}$.

Fig. 68 shows the voltages and currents during the startup of DG unit 1. At this moment DG unit 2 was already in steady-state operation, feeding full-load of the

microgrid (just load 1 was connected at this time). It is possible to verify a smooth transition during the connection of DG unit 1, as a consequence of the well-determined start values (ω_{start} and V_{start}) provided by the auxiliary PLL control. After the connection, DG unit 1 gradually increases the active-power injection through the sliding droop control in order to take part of its power dispatch.

Fig. 69 and Fig. 70 show the response during load step changes caused by the connection of load 2. The currents are instantaneously shared equally between the units, which results in the maintenance of load sharing, as depicted also in Fig. 67. The frequency drop showed in detail in Fig. 70 indicates adequate response of the DG units as virtual synchronous machines.

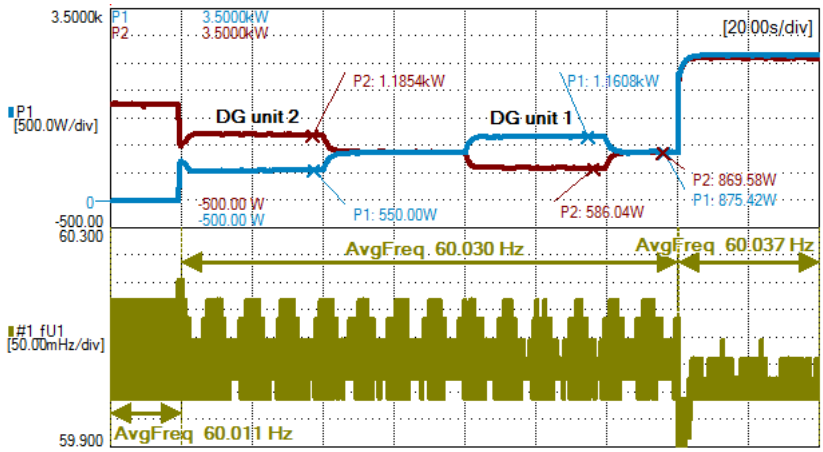

Fig. 67: Experimental results, test 1; active-power sharing and frequency.

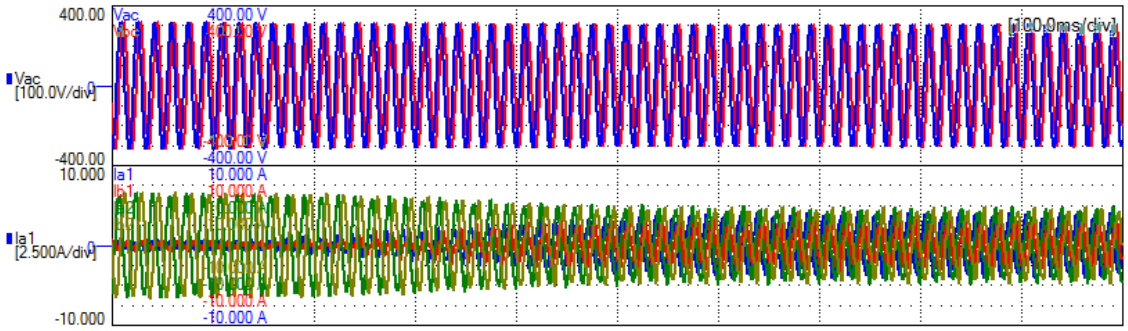

Fig. 68: Experimental results, test 1; voltages and currents during startup of DG unit 1.

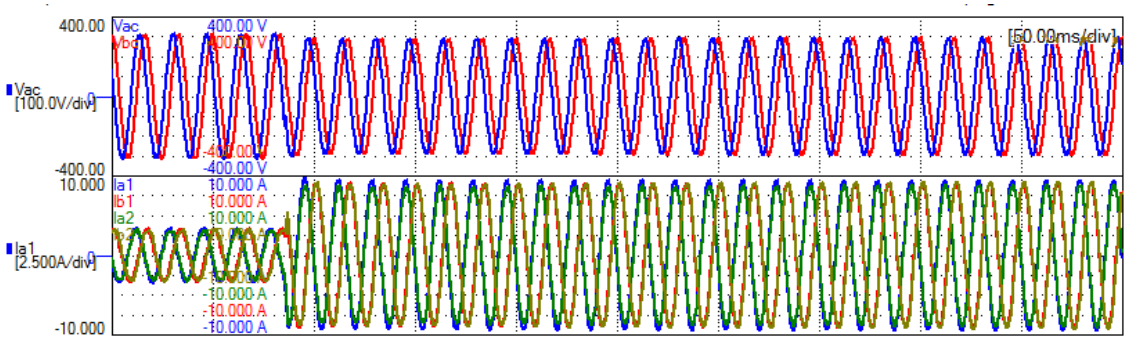

Fig. 69: Experimental results, test 1; voltages and currents during connection of Load 2.

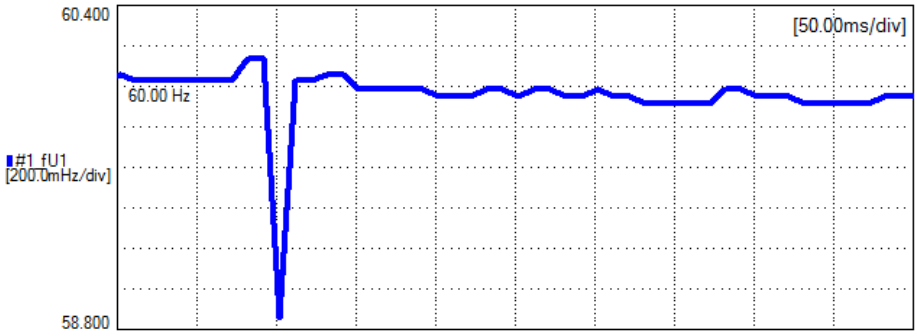

Fig. 70: Experimental results, test 1; frequency during connection of Load 2.

Test 2: Reactive-power sharing and voltage regulation in islanded mode of operation

Fig. 71 shows the test performed to evaluate the reactive-power sharing and the voltage regulation. In this case, load 1 and load 3 were connected during the entire test. In the initial condition, DG unit 1 is operating in steady state with $P_{set} = 1.0\,pu$ and after 15.0 seconds DG unit 2 starts with $P_{set} = 0.5\,pu$. It is verified that the reactive-power sharing was achieved with suitable accuracy, independently of the active-power setpoints, and the voltage was kept within the maximum deviation k_{SV} in steady state condition.

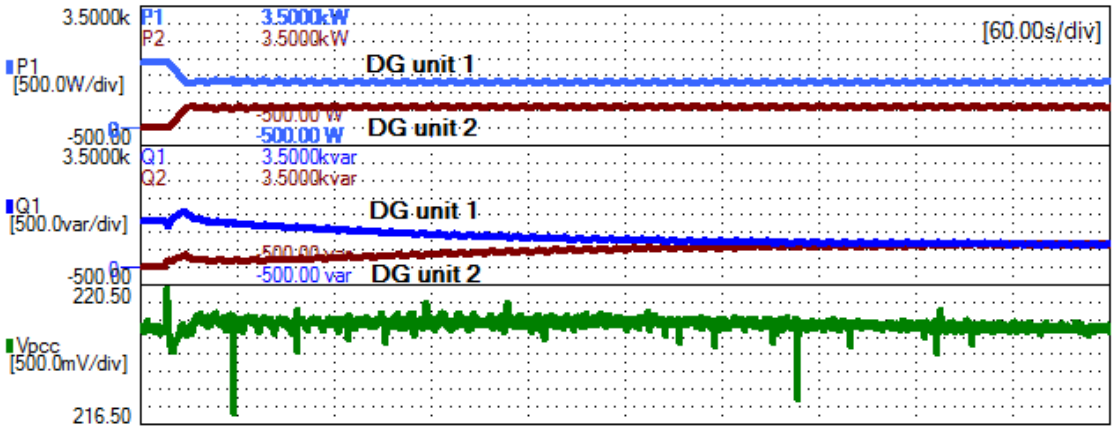

Fig. 71: Experimental results, test 2; active-power, reactive-power and voltage (rms).

Test 3: Active-power dispatch in grid-connected mode

This test is used to study the influence of $k_{S\omega}$ and ω_{ref} parameters in the performance of DG units in grid-connected mode. This is necessary due to the inherent oscillation of the frequency in real EPS, which can impact the performance of the power dispatch. The maximum frequency deviation $k_{S\omega}$ is kept the same as before, i.e. $k_{S\omega} = 1 \cdot 10^{-3} pu$ $(0.06\, Hz)$. As a first attempt, the frequency reference is set as $\omega_{ref} = 1.0\, pu$. The active-power setpoint of DG unit 1 and 2 were set as $P_{set} = 0.35$ and $0.7\, pu$, respectively. DG unit 2 started first and, after it reached the steady state, DG unit 1 was started.

Fig. 72 shows the active-power dispatch and the grid frequency. In this figure, a zone of frequency oscillation is highlighted, where the grid frequency increases significantly within the range where the sliding droop control places the droop curve to achieve sharing performance in islanded mode. As a result, the active-power dispatch is compromised since the DG units stop injecting the active-power equal to their setpoints. This effect is a consequence of the conflict between the frequency-regulation control, performed by the power-grid operator, and the tuning of the $k_{S\omega}$ and ω_{ref} parameters.

For instance, Fig. 73 shows the frequency of the Brazilian National Grid (SIN, in Portuguese) during a period of three days. It is possible to verify that the frequency is regulated most of time within 59.95 and $60.05\, Hz$. Therefore, one possible solution is suggested in Fig. 74 to avoid the ineffectiveness of power dispatch in the microgrid due to the inherent frequency oscillation of the large EPS. It is based on the SIN example of

Fig. 73. The frequency reference ω_{ref} is tuned above the normal operating zone of the SIN and the dead-band zone. This dead-band zone is used to guarantee that for most of the time, the grid frequency will not vary into the microgrid operating zone.

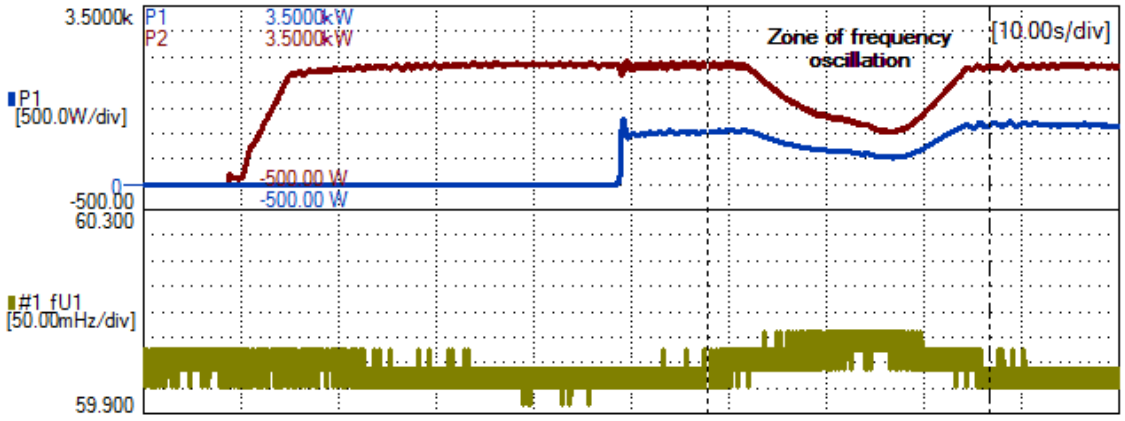

Fig. 72: Experimental results, test 3; active-power and frequency with $\omega_{ref} = 1.0\ pu$.

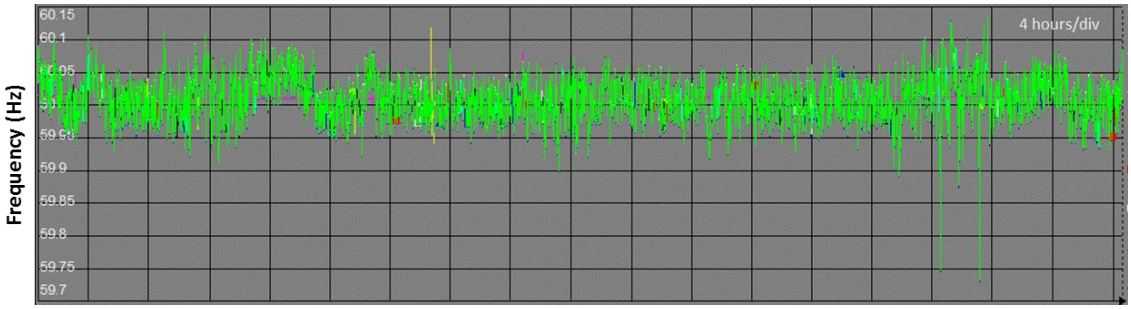

Fig. 73: Frequency in the Brazilian National Interconnected System (SIN, in Portuguese).

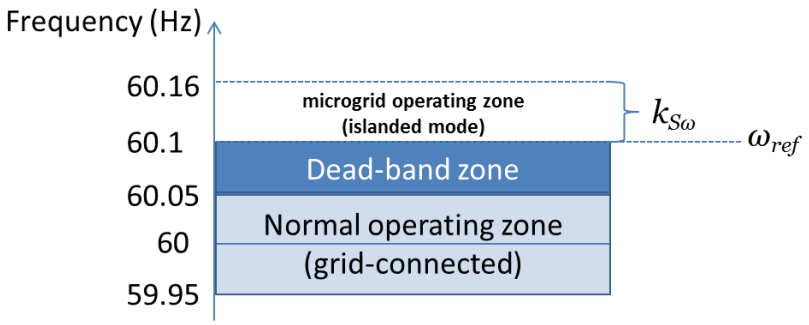

Fig. 74: Example of $k_{S\omega}$ and ω_{ref} tuning (related to the example of Fig. 73).

The aforementioned suggestion was tested and the result is depicted in Fig. 75. Note that the frequency deviation is, for most of time, within the normal operating range and in the dead-band zones. The power dispatch was ensured equal to the setpoints of each DG unit during the entire test.

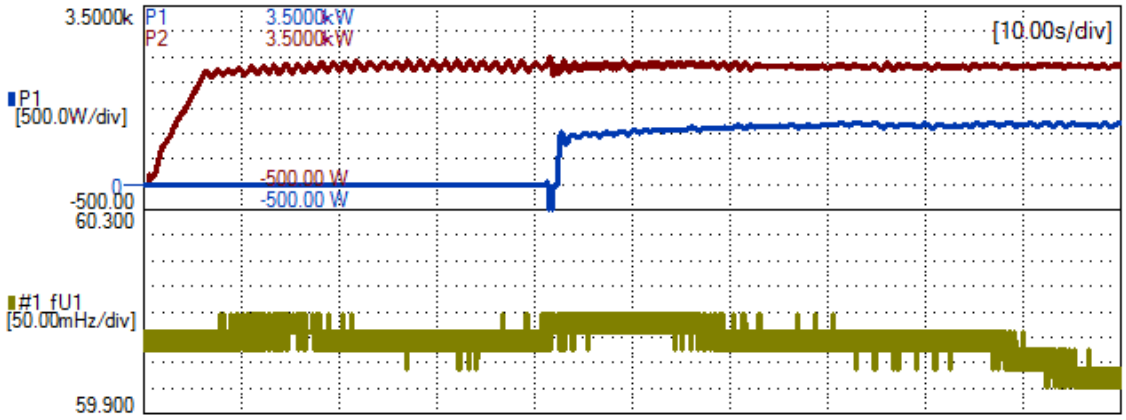

Fig. 75: Experimental results, test 3; active-power and frequency with $\omega_{ref} = 1.001667\ pu$.

Chapter 6 - Conclusion and future work

In this chapter the conclusions are provided and future works are suggested.

Conclusion

The growth of the distributed resources, led by advances in renewables and power-electronics technologies, is driving changes in the traditional Electric Power System model from a Centralized Power System to a Distributed Power System. These changes have also been driven by the advent of microgrids, the mischaracterization of the unidirectional power-flow, and the recent research which has resulted in new grid components, integration of smart technologies, adaptive power-grid architectures, and new standards.

The intrinsic characteristic of the DPS is to offer a variety of alternatives in terms of generation, consumption, power dispatch, control, protection, and integration with complementary technologies (forecasting, traffic monitoring, smart technologies, among others). In this sense, it is clear that there is no generalized profile which can be used for this type of EPS. Distinct DPS configurations will arise along with the availability of these alternatives in a given reality. Even so, a single unadjustable model of DPS would be inappropriate considering the plurality of possible DPS which can be implemented in the future to optimize energy usage, conserve resources and reduce energy waste.

The Static Synchronous Generator is a suitable controller for power electronics based power converters. The main functionalities of the synchronous machines are mimicked by the SSG allowing the power converters to be integrated into the power grid in the same way as rotating machines. Moreover, the flexibility of the digital controllers for the power converters can be used to enhance the entire performance and, consequently, achieve a better dynamic response, which would not be possible with actual rotating machines. The physical limitation of these machines in terms of constructive parameters, which are fixed and determine their behavior, is not a concern for the SSG approach. The SSG parameters can be adapted continuously to reach enhanced dynamic performance by means of adaptive control of the gains in the SSG model. This feature has been extensively used in recent studies to obtain enhanced performance. It is important to highlight that the SSG control method, when implemented in the front-end power converter of a DG unit, forces the DG unit to behave as a fast-controlled voltage source, with the desired value for virtual inertia, to contribute effectively to the frequency stability. This aggregates crucial operational

benefits that enhance the grid robustness, which is even more relevant when the contribution of DG units is significant compared to that of conventional power plants.

The proposed SSG functionalities were grouped according to the microgrid mode of operation. They were envisioned with the objective of obtaining "plug-and-play" equipment. Moreover, it was determined that the new approach of SSG has to work properly, whether a communication channel between DG units exists or not. Moreover it must also be capable of black-starting system recomposition.

In islanded mode of operation, these functionalities benefit the microgrid resilience, with special attention to the frequency and voltage control, and the power sharing among units. The active power is shared according to the P_{set} that is provided by the GESS controls of each DG unit. In other words, the active-power sharing occurs according to the currently available power of each DG unit. In grid-connected mode, the DG units contribute to feed power into the grid with an optimum power dispatch, equal to P_{set}. All the operational benefits of the synchronous machines are maintained, and quicker voltage regulation is also performed at the point of connection.

These functionalities were determined according to the trends that drive current research and standards. As it is known that these trends may vary along the development of the DPS, it was observed that the controller should be designed to be compatible with future changes in functionalities. This reinforces the intention of obtaining a flexible controller, i.e. in the same direction of the DPS profiles.

This work proposes an improvement in the classic control structure of the Static Synchronous Generator by adding a sliding droop control at the active- and reactive-power loops. This provides accurate performance in frequency/voltage regulation and power sharing between units in an islanded microgrid. In a grid-connected configuration, the units are able to inject the desired power orders imposed by P_{set} and also can operate complementarily as voltage regulators. These functionalities can be achieved also without the need of communication channels between the units. Therefore, the proposed controller fits with the proposed SSG functionalities.

A communication system is not needed since the proposed SSG functionalities are achieved independently of the microgrid operation mode and independently of any other component of the power grid. However, there are inputs in the controller that can be used to integrate it with a smart communication system if provided. Otherwise, these

inputs are substituted by constant values in the DG controllers, in case of the absence of a microgrid communication system.

The deviation functions of the sliding droop controls use mathematical expressions to obtain a frequency and voltage deviation according to the requirements of SSG functionalities. This permits the functionalities to be adapted or modified by simply changing the mathematical function that determines the respective deviations. In this way, the control structure of the sliding droop control is maintained.

The simulation results showed suitable performance in stand-alone operation, as well as in a multiple DG units in the microgrid scenario. The stand-alone operation ensured the synchronous performance and the basic functionalities of the SSG with the proposed sliding droop control for several conditions. The main drawback of the mismatch between inertia emulation and reduced frequency deviation in steady state was overcome with the sliding droop control, and a special scenario was simulated to verify this. Therefore, with the sliding droop control, the slopes of the droop-curves are not intrinsically related to the steady-state deviations of frequency and voltage amplitude.

In other scenarios, the transition between islanded and grid-connected modes was successfully achieved, as well as the synchronous performance with harmonic and unbalanced loads. Abnormal situations were also simulated to evaluate the dynamic response, virtual inertia effect and the influence of the sliding droop control. In the microgrid scenario, the proposed functionalities were ensured for step changes in power order P_{set} and relatively large load rejection and reclosing. These hard tests demonstrated the large stability margin of the proposed control method as a solution for DG units in Distributed Power Systems.

The experimental analysis testified the power sharing performance and frequency/voltage regulation. Finally, a specific test was performed to study the active-power dispatch in grid-connected mode regarding to the inherent frequency oscillations in actual power grids. In this test the sliding droop control demonstrated suitable flexibility to deal with these oscillations, providing viable alternatives for properly setting the controller parameters to ensure the desired power dispatch.

Future work

For future work, it is important to test the proposed controller together with peripheral controllers, such as those used to mitigate harmonic contents, variable virtual inertia controllers, virtual impedance, instantaneous and overload protections, etc. The tests have to confirm the maintenance of all functionalities, i.e. they have to ensure that the controllers do not interfere with each other's performances. It is important to highlight that some of these controllers are mandatory to enable the technology to be applied as a matured technology, because they are related to requirements stablished in the present standards and cannot be disregarded.

Different GESS controllers have to be investigated as well as the effectiveness of the whole system. Different kinds of resources, such as wind, photovoltaic and fuel cells should be tested in this environment. The proposed SSG functionalities may be modified, for instance, as a means of prioritizing the dispatch of one specific kind of resource according to economical, technical and/or political guidelines.

As the DPS is in constant development, the application of a specific technology is consolidated as it is employed in actual circumstances. Hence, a logical strategy to the development of the proposed controller is to implement it in large scale and identify the problems that will rise from the impact of this implementation. The task of consolidating a technology lies in its constant updating and its massive use, with the realization of the desired benefits.

References

[1] Renewable Energy Word Magazine, Jan/Feb 2015.

[2] J.M. Guerrero, "Connecting renewable energy sources into the smartgrid," in *Industrial Electronics (ISIE), 2011 IEEE International Symposium on*, 2011, pp. 2400-2566.

[3] Qing-Chang Zhong and G. Weiss, "Synchronverters: Inverters That Mimic Synchronous Generators," *Industrial Electronics, IEEE Transactions on*, vol. 58, no. 4, pp. 1259-1267, 2011.

[4] H.-P. Beck and R. Hesse, "Virtual synchronous machine," in *Electrical Power Quality and Utilisation, 2007. EPQU 2007. 9th International Conference on*, 2007, pp. 1-6.

[5] Qing-Chang Zhong and G. Weiss, "Static synchronous generators for distributed generation and renewable energy," in *Power Systems Conference and Exposition, 2009. PSCE '09. IEEE/PES*, 2009, pp. 1-6.

[6] B. W. França, A. R. de Castro, and M. Aredes, "Wind and photovoltaic power generation integrated to power grid through dc link and synchronverter," in *2015 IEEE 13th Brazilian Power Electronics Conference and 1st Southern Power Electronics Conference (COBEP/SPEC)*, Nov. 29 2015-Dec. 2 2015, pp. 1-6.

[7] E.L. van Emmerik, B.W. Franca, and M. Aredes, "A synchronverter to damp electromechanical oscillations in the Brazilian transmission grid," in *Industrial Electronics (ISIE), 2015 IEEE 24th International Symposium on*, 3-5 June 2015, pp. 221-226.

[8] EL van Emmerik et al., "Synchronverter to damp multiple electromechanical oscillations," in *Advances in Power and Energy Engineering*.: CRC Press, #mar# 2016, pp. 617-622--. [Online]. http://dx.doi.org/10.1201/b20131-102

[9] B.W. Franca, L.F. da Silva, M.A. Aredes, and M. Aredes, "An Improved iUPQC Controller to Provide Additional Grid-Voltage Regulation as a STATCOM," *Industrial Electronics, IEEE Transactions on*, vol. 62, no. 3, pp. 1345-1352, 2015.

[10] J.A.M. Neto, L. Lovisolo, B.W. Franca, and M. Aredes, "Robust positive-

sequence detector algorithm," in *Industrial Electronics, 2009. IECON '09. 35th Annual Conference of IEEE*, 2009, pp. 788-793.

[11] Bruno W França et al., "Performance analysis and technical feasibility of an iUPQC in industrial grids," *Journal of Power and Energy Engineering*, vol. 2, no. 04, p. 500, 2014.

[12] Maynara A Aredes, Bruno W França, and Maurício Aredes, "Fuzzy adaptive P&O control for MPPT of a photovoltaic module," *Journal of Power and Energy Engineering*, vol. 2, no. 04, p. 120, 2014. [Online]. http://www.scirp.org/journal/PaperInformation.aspx?PaperID=44866

[13] Grzegorz Benysek Ryszard Strzelecki, *Power Electronics in Smart Electrical Energy Networks*, Grzegorz Benysek Ryszard Strzelecki, Ed.: Springer, January 2008.

[14] Hirofumi Akagi, Edson Hirokazu Watanabe, and Mauricio Aredes, *Instantaneous Power Theory and Applications to Power Conditioning*.: Wiley-IEEE Press, 2007.

[15] F. Luo, Y.M. Lai, C.K. Tse, and K.H. Loo, "A triple-droop control scheme for inverter-based microgrids," in *IECON 2012 - 38th Annual Conference on IEEE Industrial Electronics Society*, 25-28 Oct. 2012, pp. 3368-3375.

[16] J. M. Guerrero, P. C. Loh, T. L. Lee, and M. Chandorkar, "Advanced Control Architectures for Intelligent Microgrids-Part II: Power Quality, Energy Storage, and AC/DC Microgrids," *IEEE Transactions on Industrial Electronics*, vol. 60, no. 4, pp. 1263-1270, April 2013.

[17] H.H. Abdeltawab and Y.A.I. Mohamed, "Market-Oriented Energy Management of a Hybrid Wind-Battery Energy Storage System Via Model Predictive Control With Constraint Optimizer," *Industrial Electronics, IEEE Transactions on*, vol. 62, no. 11, pp. 6658-6670, Nov. 2015.

[18] P. Li, R. Dargaville, F. Liu, J. Xia, and Y. Song, "Data-Based Statistical Property Analyzing and Storage Sizing for Hybrid Renewable Energy Systems," *Industrial Electronics, IEEE Transactions on*, vol. 62, no. 11, pp. 6996-7008, Nov. 2015.

[19] "IEEE Standard for Interconnecting Distributed Resources with Electric Power Systems," *IEEE Std 1547-2003*, pp. 1-28, July 2003.

[20] João Abel Peças Lopes, André Guimarães Madureira, and Carlos Coelho Leal Monteiro Moreira, "A view of microgrids," *Wiley Interdisciplinary Reviews: Energy and Environment*, vol. 2, no. 1, pp. 86-103, Jul 2012. [Online]. http://dx.doi.org/10.1002/wene.34

[21] G. Pepermans, J. Driesen, D. Haeseldonckx, R. Belmans, and W. D'haeseleer, "Distributed generation: definition, benefits and issues," *Energy Policy*, vol. 33, no. 6, pp. 787-798, Apr 2005. [Online]. http://dx.doi.org/10.1016/j.enpol.2003.10.004

[22] Dan T. Ton and Merrill A. Smith, "The U.S. Department of Energy's Microgrid Initiative," *The Electricity Journal*, vol. 25, no. 8, pp. 84-94, Oct 2012. [Online]. http://dx.doi.org/10.1016/j.tej.2012.09.013

[23] Robert Lasseter et al., "The CERTS microgrid concept," *White paper for Transmission Reliability Program, Office of Power Technologies, US Department of Energy*, 2002.

[24] Nikos Hatziargyriou et al., "Microgrids--large scale integration of microgeneration to low voltage grids," *CIGRE C6-309*, 2006.

[25] U.S. Depatment of Energy, The Role of Microgrids in Helping to Advance the Nation's Energy System.

[26] A.P.N. Tahim, D.J. Pagano, E. Lenz, and V. Stramosk, "Modeling and Stability Analysis of Islanded DC Microgrids Under Droop Control," *Power Electronics, IEEE Transactions on*, vol. 30, no. 8, pp. 4597-4607, 2015.

[27] J. Xiao, P. Wang, and L. Setyawan, "Hierarchical Control of Hybrid Energy Storage System in DC Microgrids," *Industrial Electronics, IEEE Transactions on*, vol. 62, no. 8, pp. 4915-4924, 2015.

[28] J.M. Guerrero, J.C. Vasquez, J. Matas, L.a, L.G. de Vicuna, and M. Castilla, "Hierarchical Control of Droop-Controlled AC and DC Microgrids-A General Approach Toward Standardization," *Industrial Electronics, IEEE Transactions on*, vol. 58, no. 1, pp. 158-172, 2011.

[29] K. W. Hu and C. M. Liaw, "On the flywheel/battery hybrid energy storage system for DC microgrid," in *Future Energy Electronics Conference (IFEEC), 2013 1st International*, 3-6 Nov. 2013, pp. 119-125.

[30] E. Barklund, N. Pogaku, M. Prodanovic, C. Hernandez-Aramburo, and T.C. Green, "Energy Management in Autonomous Microgrid Using Stability-Constrained Droop Control of Inverters," *Power Electronics, IEEE Transactions on*, vol. 23, no. 5, pp. 2346-2352, Sept. 2008.

[31] D. M. Bui et al., "Review on protection coordination strategies and development of an effective protection coordination system for DC microgrid," in *Power and Energy Engineering Conference (APPEEC), 2014 IEEE PES Asia-Pacific*, 7-10 Dec. 2014, pp. 1-10.

[32] A. Meghwani, S. C. Srivastava, and S. Chakrabarti, "A new protection scheme for DC microgrid using line current derivative," in *Power \& Energy Society General Meeting, 2015 IEEE*, 26-30 July 2015, pp. 1-5.

[33] J. D. Park, J. Candelaria, L. Ma, and K. Dunn, "DC Ring-Bus Microgrid Fault Protection and Identification of Fault Location," *IEEE Transactions on Power Delivery*, vol. 28, no. 4, pp. 2574-2584, Oct. 2013.

[34] K. P. K. Vineeth and M. K. Sreenivasan, "Hardware implementation of high efficient and high voltage gain dc-dc converter for dc microgrid applications," in *Electrical, Computer and Communication Technologies (ICECCT), 2015 IEEE International Conference on*, 5-7 March 2015, pp. 1-5.

[35] F. Nejabatkhah and Y. W. Li, "Overview of Power Management Strategies of Hybrid AC/DC Microgrid," *IEEE Transactions on Power Electronics*, vol. 30, no. 12, pp. 7072-7089, Dec. 2015.

[36] V. K. Hema and R. Dhanalakshmi, "Analysis of power sharing on hybrid AC-DC microgrid," in *Emerging Research Areas: Magnetics, Machines and Drives (AICERA/iCMMD), 2014 Annual International Conference on*, 24-26 July 2014, pp. 1-6.

[37] P. C. Loh, D. Li, Y. K. Chai, and F. Blaabjerg, "Autonomous Control of Interlinking Converter With Energy Storage in Hybrid AC/DC Microgrid," *IEEE Transactions on Industry Applications*, vol. 49, no. 3, pp. 1374-1382, May-June 2013.

[38] N. Eghtedarpour and E. Farjah, "Power Control and Management in a Hybrid AC/DC Microgrid," *IEEE Transactions on Smart Grid*, vol. 5, no. 3, pp. 1494-1505, May 2014.

[39] P. J. Hart, T. M. Jahns, and R. H. Lasseter, "Performance characteristics of a hybrid CERTS microgrid electric vehicle charging station," in *Energy Conversion Congress and Exposition (ECCE), 2014 IEEE*, 14-18 Sept. 2014, pp. 3309-3316.

[40] Sung-Hwan Park, Jin-Young Choi, and Dong-Jun Won, "Cooperative control between the distributed energy resources in AC/DC hybrid microgrid," in *Innovative Smart Grid Technologies Conference (ISGT), 2014 IEEE PES*, 19-22 Feb. 2014, pp. 1-5.

[41] Tam Harbert, "Microgrids for a post-Fukushima Japan," *Spectrum, IEEE*, vol. 52, no. 3, pp. 16-17, March 2015.

[42] Estefanía Planas, Asier Gil-de-Muro, Jon Andreu, Iñigo Kortabarria, and Iñigo Martínez de Alegría, "General aspects, hierarchical controls and droop methods in microgrids: A review," *Renewable and Sustainable Energy Reviews*, vol. 17, pp. 147-159, Jan 2013. [Online]. http://dx.doi.org/10.1016/j.rser.2012.09.032

[43] "IEEE Standard for Interconnecting Distributed Resources with Electric Power Systems - Amendment 1," *IEEE Std 1547a-2014 (Amendment to IEEE Std 1547-2003)*, pp. 1-16, May 2014.

[44] "IEEE Standard Conformance Test Procedures for Equipment Interconnecting Distributed Resources with Electric Power Systems," *IEEE Std 1547.1-2005*, pp. 1-62, July 2005.

[45] "IEEE Application Guide for IEEE Std 1547(TM), IEEE Standard for Interconnecting Distributed Resources with Electric Power Systems," *IEEE Std 1547.2-2008*, pp. 1-217, April 2009.

[46] "IEEE Guide for Monitoring, Information Exchange, and Control of Distributed Resources Interconnected with Electric Power Systems," *IEEE Std 1547.3-2007*, pp. 1-160, Nov 2007.

[47] "IEEE Guide for Design, Operation, and Integration of Distributed Resource Island Systems with Electric Power Systems," *IEEE Std 1547.4-2011*, pp. 1-54, July 2011.

[48] "IEEE Recommended Practice for Interconnecting Distributed Resources with Electric Power Systems Distribution Secondary Networks," *IEEE Std 1547.6-2011*, pp. 1-38, Sept 2011.

[49] "IEEE Guide for Conducting Distribution Impact Studies for Distributed Resource Interconnection," *IEEE Std 1547.7-2013*, pp. 1-137, Feb 2014.

[50] American National Standard for Electric Power Systems and Equipment—Voltage Ratings (60 Hertz), 2011.

[51] Wang Haiyun et al., "A hierarchical control of microgrid based on droop controlled voltage source converter," in *Power and Energy Engineering Conference (APPEEC), 2013 IEEE PES Asia-Pacific*, 8-11 Dec. 2013, pp. 1-4.

[52] Hongbin Sun, Boming Zhang, Wenchuan Wu, and Qinglai Guo, "Family of energy management system for smart grid," in *Innovative Smart Grid Technologies (ISGT Europe), 2012 3rd IEEE PES International Conference and Exhibition on*, 2012, pp. 1-5.

[53] Baris Baykant Alagoz, Cemal Keles, and Asim Kaygusuz, "Towards energy webs: Hierarchical tree topology for future smart grids," in *Smart Grid Congress and Fair (ICSG), 2015 3rd International Istanbul*, 29-30 April 2015, pp. 1-4.

[54] Omid Palizban, Kimmo Kauhaniemi, and Josep M Guerrero, "Microgrids in active network management—Part I: Hierarchical control, energy storage, virtual power plants, and market participation," *Renewable and Sustainable Energy Reviews*, vol. 36, pp. 428-439, 2014.

[55] Omid Palizban, Kimmo Kauhaniemi, and Josep M Guerrero, "Microgrids in active network management--part II: System operation, power quality and protection," *Renewable and Sustainable Energy Reviews*, vol. 36, pp. 440-451, 2014.

[56] J. Wang, N.C.P. Chang, X. Feng, and A. Monti, "Design of a Generalized Control Algorithm for Parallel Inverters for Smooth Microgrid Transition Operation," *Industrial Electronics, IEEE Transactions on*, vol. 62, no. 8, pp. 4900-4914, 2015.

[57] J. M. Guerrero, M. Chandorkar, T. L. Lee, and P. C. Loh, "Advanced Control Architectures for Intelligent Microgrids-Part I: Decentralized and Hierarchical Control," *IEEE Transactions on Industrial Electronics*, vol. 60, no. 4, pp. 1254-1262, April 2013.

[58] T.L. Vandoorn, J.D.M. De Kooning, B. Meersman, and L. Vandevelde, "Review of primary control strategies for islanded microgrids with power-electronic

interfaces," *Renewable and Sustainable Energy Reviews*, vol. 19, p. 613â€“628, Mar 2013. [Online]. http://dx.doi.org/10.1016/j.rser.2012.11.062

[59] Zeng Liu, Jinjun Liu, Yalin Zhao, Weihan Bao, and Yan Zhang, "Output impedance modeling and stability criterion for parallel inverters with master-slave sharing scheme in AC distributed power system," in *Applied Power Electronics Conference and Exposition (APEC), 2012 Twenty-Seventh Annual IEEE*, 2012, pp. 1907-1913.

[60] Yunqing Pei, Guibin Jiang, Xu Yang, and Zhaoan Wang, "Auto-master-slave control technique of parallel inverters in distributed AC power systems and UPS," in *Power Electronics Specialists Conference, 2004. PESC 04. 2004 IEEE 35th Annual*, vol. 3, 2004, pp. 2050--2053 Vol.3.

[61] Zeng Liu, Jinjun Liu, and Hao Wang, "Output impedance modeling and stability criterion for parallel inverters with average load sharing scheme in AC distributed power system," in *Applied Power Electronics Conference and Exposition (APEC), 2012 Twenty-Seventh Annual IEEE*, 2012, pp. 1921-1926.

[62] T.-F. Wu, Y.-H. Huang, Y.K. Chen, and Z.-R. Liu, "A 3C strategy for multi-module inverters in parallel operation to achieve an equal current distribution," in *Power Electronics Specialists Conference, 1998. PESC 98 Record. 29th Annual IEEE*, vol. 1, 17-22 May 1998, pp. 186--192 vol.1.

[63] R. Ramos, D. Biel, F. Guinjoan, and E. Fossas, "Distributed control strategy for parallel-connected inverters. Sliding mode control approach and FPGA-based implementation," in *IECON 02 [Industrial Electronics Society, IEEE 2002 28th Annual Conference of the]*, vol. 1, 2002, pp. 111--116 vol.1.

[64] J. Liu, Y. Miura, and T. Ise, "Comparison of Dynamic Characteristics Between Virtual Synchronous Generator and Droop Control in Inverter-Based Distributed Generators," *Power Electronics, IEEE Transactions on*, vol. 31, no. 5, pp. 3600-3611, May 2016.

[65] E. Serban, C. Pondiche, and M. Ordonez, "Islanding Detection Search Sequence for Distributed Power Generators Under AC Grid Faults," *Power Electronics, IEEE Transactions on*, vol. 30, no. 6, pp. 3106-3121, 2015.

[66] H. Laaksonen, "Advanced Islanding Detection Functionality for Future Electricity Distribution Networks," *Power Delivery, IEEE Transactions on*, vol. 28, no. 4,

pp. 2056-2064, 2013.

[67] J.W. Simpson-Porco et al., "Secondary Frequency and Voltage Control of Islanded Microgrids via Distributed Averaging," *Industrial Electronics, IEEE Transactions on*, vol. 62, no. 11, pp. 7025-7038, Nov. 2015.

[68] A. L. Dimeas and N. D. Hatziargyriou, "Operation of a Multiagent System for Microgrid Control," *IEEE Transactions on Power Systems*, vol. 20, no. 3, pp. 1447-1455, Aug. 2005.

[69] "Dispersed Generation Impact on Continental Europe Region Security -," european network of transmission system operators for electricity - entsoe, Tech. rep. November 2014. [Online]. https://www.entsoe.eu/Documents/Publications/SOC/Continental_Europe/141113_Dispersed_Generation_Impact_on_Continental_Europe_Region_Security.pdf

[70] J. Driesen and K. Visscher, "Virtual synchronous generators," in *Power and Energy Society General Meeting - Conversion and Delivery of Electrical Energy in the 21st Century, 2008 IEEE*, 2008, pp. 1-3.

[71] Lennart Harnefors, "Control of a voltage source converter using synchronous machine emulation," aug, 26 2008.

[72] George; Zhong, Qing-Chang Weiss, "Static Synchronous Generators," 2010.

[73] Zhenyu Ma, Qing-Chang Zhong, and J.D. Yan, "Synchronverter-based control strategies for three-phase PWM rectifiers," in *Industrial Electronics and Applications (ICIEA), 2012 7th IEEE Conference on*, 2012, pp. 225-230.

[74] Phi-Long Nguyen, Qing-Chang Zhong, F. Blaabjerg, and J.M. Guerrero, "Synchronverter-based operation of STATCOM to Mimic Synchronous Condensers," in *Industrial Electronics and Applications (ICIEA), 2012 7th IEEE Conference on*, 2012, pp. 942-947.

[75] Chang hua Zhang et al., "An improved synchronverter model and its dynamic behaviour comparison with synchronous generator," in *Renewable Power Generation Conference (RPG 2013), 2nd IET*, 2013, pp. 1-4.

[76] Qing-Chang Zhong, Zhenyu Ma, Wen-Long Ming, and George C. Konstantopoulos, "Grid-friendly wind power systems based on the synchronverter technology," *Energy Conversion and Management*, vol. 89, pp. 719-726, Jan

2015. [Online]. http://dx.doi.org/10.1016/j.enconman.2014.10.027

[77] J.C. Vasquez, J.M. Guerrero, A. Luna, P. Rodriguez, and R. Teodorescu, "Adaptive Droop Control Applied to Voltage-Source Inverters Operating in Grid-Connected and Islanded Modes," *Industrial Electronics, IEEE Transactions on*, vol. 56, no. 10, pp. 4088-4096, 2009.

[78] P.L. Villenueve, "Concerns generated by islanding [electric power generation]," *Power and Energy Magazine, IEEE*, vol. 2, no. 3, pp. 49-53, 2004.

[79] Qing-Chang Zhong and D. Boroyevich, "A droop controller is intrinsically a phase-locked loop," in *Industrial Electronics Society, IECON 2013 - 39th Annual Conference of the IEEE*, 2013, pp. 5916-5921.

[80] Stephen Chapman, *Electric Machinery Fundamentals*, 5th ed. Ney York: McGraw-Hill Science/Engineering/Math, Feb. 2011.

[81] Qing-Chang Zhong, "Robust Droop Controller for Accurate Proportional Load Sharing Among Inverters Operated in Parallel," *Industrial Electronics, IEEE Transactions on*, vol. 60, no. 4, pp. 1281-1290, April 2013.

[82] Theodor S. Borsche, Göran Andersson Andreas Ulbig, "Impact of Low Rotational Inertia on Power System Stability and Operation," 2014. [Online]. http://arxiv.org/abs/1312.6435v4

[83] M. Benidris and J. Mitra, "Enhancing stability performance of renewable energy generators by utilizing virtual inertia," in *Power and Energy Society General Meeting, 2012 IEEE*, 2012, pp. 1-6.

[84] F.M. Uriarte, C. Smith, S. VanBroekhoven, and R.E. Hebner, Microgrid Ramp Rates and the Inertial Stability Margin, 2015.

[85] John Grainger and William Stevenson Jr., *Power System Analysis*.: McGraw-Hill Science/Engineering/Math, 1994.

[86] A. E. Fitzgerald, *Electric machinery*. Boston, Mass: McGraw-Hill, 2003.

[87] Prabha Kundur, *Power System Stability and Control*.: McGraw-Hill Professional, 1994.

[88] D. Pan, X. Ruan, C. Bao, W. Li, and X. Wang, "Optimized Controller Design for LCL Type Grid-Connected Inverter to Achieve High Robustness Against Grid-Impedance Variation," *Industrial Electronics, IEEE Transactions on*, vol. 62, no.

3, pp. 1537-1547, 2015.

[89] M. Liserre, F. Blaabjerg, and S. Hansen, "Design and control of an LCL-filter-based three-phase active rectifier," *IEEE Transactions on Industry Applications*, vol. 41, no. 5, pp. 1281-1291, Sept.-Oct. 2005.

[90] M.A. Torres L, L.A.C. Lopes, L.A. Moran T, and J.R. Espinoza C, "Self-Tuning Virtual Synchronous Machine: A Control Strategy for Energy Storage Systems to Support Dynamic Frequency Control," *Energy Conversion, IEEE Transactions on*, vol. 29, no. 4, pp. 833-840, 2014.

[91] J. Alipoor, Y. Miura, and T. Ise, "Distributed generation grid integration using virtual synchronous generator with adoptive virtual inertia," in *Energy Conversion Congress and Exposition (ECCE), 2013 IEEE*, 2013, pp. 4546-4552.

[92] D. Remon, A. M. Cantarellas, E. Rakhshani, I. Candela, and P. Rodriguez, "An active power self-synchronizing controller for grid-connected converters emulating inertia," in *Renewable Energy Research and Application (ICRERA), 2014 International Conference on*, 19-22 Oct. 2014, pp. 424-429.

[93] Xiaorong Zhu, Yi Wang, Lie Xu, Xiangyu Zhang, and Heming Li, "Virtual inertia control of DFIG-based wind turbines for dynamic grid frequency support," in *Renewable Power Generation (RPG 2011), IET Conference on*, 2011, pp. 1-6.

[94] J. Alipoor, Y. Miura, and T. Ise, "Power System Stabilization Using Virtual Synchronous Generator With Alternating Moment of Inertia," *Emerging and Selected Topics in Power Electronics, IEEE Journal of*, vol. 3, no. 2, pp. 451-458, June 2015.

[95] John W. Simpson-Porco, Florian Dörfler, and Francesco Bullo, "Synchronization and power sharing for droop-controlled inverters in islanded microgrids," *Automatica*, vol. 49, no. 9, pp. 2603-2611, Sep 2013. [Online]. http://dx.doi.org/10.1016/j.automatica.2013.05.018

[96] J.M. Guerrero, L. Garcia De Vicuna, J. Matas, M. Castilla, and J. Miret, "Output Impedance Design of Parallel-Connected UPS Inverters With Wireless Load-Sharing Control," *Industrial Electronics, IEEE Transactions on*, vol. 52, no. 4, pp. 1126-1135, 2005.

[97] Jinwei He and Yun Wei Li, "Analysis, Design, and Implementation of Virtual Impedance for Power Electronics Interfaced Distributed Generation," *Industry*

Applications, IEEE Transactions on, vol. 47, no. 6, pp. 2525-2538, Nov.-Dec. 2011.

[98] Xiongfei Wang, Yun Wei Li, F. Blaabjerg, and Poh Chiang Loh, "Virtual-Impedance-Based Control for Voltage-Source and Current-Source Converters," *Power Electronics, IEEE Transactions on*, vol. 30, no. 12, pp. 7019-7037, Dec. 2015.

[99] R. Aouini, B. Marinescu, K. Ben Kilani, and M. Elleuch, "Synchronverter-Based Emulation and Control of HVDC Transmission," *Power Systems, IEEE Transactions on*, vol. 31, no. 1, pp. 278-286, Jan 2016.

[100] J.M. Guerrero, J.C. Vasquez, J. Matas, M. Castilla, and L.G. de Vicuna, "Control Strategy for Flexible Microgrid Based on Parallel Line-Interactive UPS Systems," *Industrial Electronics, IEEE Transactions on*, vol. 56, no. 3, pp. 726-736, 2009.

[101] Chia-Tse Lee, Chia-Chi Chu, and Po-Tai Cheng, "A new droop control method for the autonomous operation of distributed energy resource interface converters," in *Energy Conversion Congress and Exposition (ECCE), 2010 IEEE*, 2010, pp. 702-709.

[102] Hua Han, Yao Liu, Yao Sun, Mei Su, and J.M. Guerrero, "An Improved Droop Control Strategy for Reactive Power Sharing in Islanded Microgrid," *Power Electronics, IEEE Transactions on*, vol. 30, no. 6, pp. 3133-3141, 2015.

[103] G. Chen, F.L. Lewis, E.N. Feng, and Y. Song, "Distributed Optimal Active Power Control of Multiple Generation Systems," *Industrial Electronics, IEEE Transactions on*, vol. 62, no. 11, pp. 7079-7090, Nov. 2015.

[104] Xibo Yuan, Fei Wang, D. Boroyevich, Yongdong Li, and R. Burgos, "DC-link Voltage Control of a Full Power Converter for Wind Generator Operating in Weak-Grid Systems," *Power Electronics, IEEE Transactions on*, vol. 24, no. 9, pp. 2178-2192, Sept. 2009.

[105] E. Robles et al., "Frequency-Adaptive Stationary-Reference-Frame Grid Voltage Sequence Detector for Distributed Generation Systems," *Industrial Electronics, IEEE Transactions on*, vol. 58, no. 9, pp. 4275-4287, 2011.